MECHANISM OF MITOCHONDRIAL DYNAMIN ADAPTOR BINDING AND MEMBRANE RECRUITMENT

by

Huyen T Bui

A dissertation submitted to the faculty of
The University of Utah
in partial fulfillment of the requirements for the degree of

Doctor of Philosophy

Department of Biochemistry

The University of Utah

May 2013

The University of Utah Graduate School

STATEMENT OF DISSERTATION APPROVAL

The dissertation of **Huyen T Bui**

has been approved by the following supervisory committee members:

Janet Shaw	, Chair	**11/28/2012** Date Approved
Dana Carroll	, Member	**11/28/2012** Date Approved
Tim Formosa	, Member	**11/28/2012** Date Approved
David Grunwald	, Member	**11/28/2012** Date Approved
Dennis Winge	, Member	**11/28/2012** Date Approved

and by **Wesley Sundquist & Christopher Hill**, Chair of the Department of **Biochemistry**

and by Donna M. White, Interim Dean of The Graduate School.

ABSTRACT

Many cellular membrane fission events are mediated by dynamin-related proteins (DRP), which self-assemble into spirals encircling the lipid tubes at their sites of action. DRPs are GTPases whose activities are dramatically stimulated upon assembly. Rapid GTP hydrolysis causes constriction of DRP spirals and leads to membrane fission. DRP-mediated membrane fission is initiated by the recruitment of a certain DRP to the specific cellular membrane via adaptor proteins. The adaptors also co-assemble with DRPs to form active fission complexes. The molecular mechanism for this important recruitment step is poorly understood, as is the function of adaptor proteins during fission complex formation and membrane severing.

In this thesis, we studied DRP membrane recruitment and adaptor functions using the yeast mitochondrial fission machinery including the DRP Dnm1, the adaptor Mdv1, and the membrane anchor Fis1. To initiate mitochondrial fission, Dnm1 is recruited to the mitochondria via a direct interaction with Mdv1, which binds Fis1 on the mitochondrial outer membrane. As described in Chapter 2, we identified a novel motif in the Dnm1 Insert B domain that is essential for the interaction of Dnm1 with Mdv1. Mutations in this conserved motif severely impaired Dnm1-Mdv1 interaction and mitochondrial fission. Suppressor mutations in the Mdv1 β-propeller domain rescued defects caused by the Insert B mutations. The positions of these suppressor mutations define potential binding sites for Insert B on the Mdv1 β-propeller. In Chapter 3, we demonstrated that Mdv1

plays dual functions, as an adaptor and in scaffolding, during fission complex formation. Mdv1 dimerizes via a 92Å coiled-coil, which determines the optimal architecture of fission complexes. Together, these studies provide mechanistic insights regarding DRP membrane recruitment and the functions of adaptors in DRP-mediated membrane fission. Although the sequence of Insert B and the adaptors are varied among DRPs, we believe that they are functionally conserved and may have co-evolved to meet the requirements of specific fission events in different tissues and cell types.

CONTENTS

ABSTRACT iii

LIST OF FIGURES vii

LIST OF TABLES ix

CHAPTERS

1. INTRODUCTION 1

    Classical dynamin (Dyn) 2
    Dynamin-related proteins (DRPs) 4
    Dynamin structure 7
    DRP assembly and GTPase stimulation 8
    DRP membrane recruitment – Open questions 11
    Mitochondria 12
    DRP-mediated mitochondrial fission 15
    Model of fission complex formation 18
    Thesis overview 18
    References 20

2. A NOVEL MOTIF IN THE YEAST MITOCHONDRIAL DYNAMIN Dnm1 IS ESSENTIAL FOR ADAPTOR BINDING AND MEMBRANE RECRUITMENT 25

    Introduction 26
    Results 27
    Discussion 31
    Materials and methods 33
    Acknowledgements 34
    References 34
    Supplemental materials 36

3. MOLECULAR ARCHITECTURE OF A DYNAMIN ADAPTOR: IMPLICATIONS FOR ASSEMBLY OF MITOCHONDRIAL FISSION COMPLEXES 38

Introduction 39
Results 40
Discussion 46
Materials and methods 49
Acknowledgements 50
References 50
Supplemental materials 52

4. DISCUSSION 58

Dnm1 biochemical properties are optimized for yeast mitochondrial fission 59
Adaptors are required for mitochondrial dynamin membrane recruitment 60
Understanding the InsB-β-propeller interaction 62
Dynamin-adaptor interactions in the mammalian mitochondrial fission machinery 67
Conclusion 70
References 70

APPENDIX 73

LIST OF FIGURES

Figure		Page
1.1.	Classical dynamin structure and assembly	5
1.2.	A tubular mitochondrial network in wildtype yeast cells is maintained by the balance of fusion and fission events	14
1.3.	Domain structures of yeast and mammalian mitochondrial fission proteins	16
1.4.	Model for step-wise assembly of fission complexes	19
2.1.	Dnm1 InsB contains a sequence of 8 strictly conserved residues (F610-K613) predicted to be solvent inaccessible	27
2.2.	Dnm1 InsB conserved residues are important for Dnm1 function in mitochondrial fission	28
2.3.	InsB conserved residues are critical for Dnm1-Mdv1 interaction	29
2.4.	Suppressors of a *dnm1*^{InsB} mutation cluster in the Mdv1 β-propeller	30
2.5.	Suppressor mutations in the Mdv1 β-propeller rescue mitochondrial fission defects caused by Dnm1^{F610A}	31
2.6.	Comparison of InsB domains and mitochondrial fission adaptors in different organisms	32
2.S1.	Expression, interaction and assembly properties of Dnm1 and Mdv1 variants	36
3.1.	Mdv1 self-assembles via a dimeric, antiparallel coiled-coil	40
3.2.	Disruption of Mdv1 coiled-coil formation blocks mitochondrial fission	41
3.3.	Coiled coil formation promotes mitochondrial recruitment and assembly of the Mdv1 fission adaptor	42

3.4. Efficient Dnm1-Mdv1 interaction and Dnm1 assembly into functional mitochondrial fission complexes requires Mdv1 coiled-coil formation 44

3.5. Dimerization via a heterologous antiparallel coiled-coil partially restores Mdv1 adaptor function 45

3.6. The Mdv1 coiled-coil sequence contributes to efficient Fis1 binding 46

3.7. Effect of coiled-coil shortening on Mdv1 function 47

3.8. Molecular architecture of the mitochondrial dynamin-related receptor 48

3.S1. Additional analysis of $mdv1^{HR2}$ localization and function 52

3.S2. Glu250 is exposed on one face of the dimeric antiparallel coiled coil 53

3.S3. Additional analysis of $mdv1^{D2HR}$ and $mdv1^{D4HR}$ proteins 54

3.S4. Dominant negative effects of WT and mutant Mdv1 protein 55

4.1. Biochemical analysis of Dnm1 InsB 64

LIST OF TABLES

Table		Page
1.1.	Members of the dynamin superfamily mediate cellular membrane remodeling	3
2.1.	Characterization of Mdv1 suppressors of the *dnm1*^{F610A} allele	30
2.S1.	Screen for *mdv1* suppressors of *dnm1*^{F610A}	37
2.S2.	Plasmids used in Chapter 2	37
3.S1.	Plasmids used in Chapter 3	56
3.S2.	X-ray data and model statistics	56

CHAPTER 1

INTRODUCTION

At any one time, a typical eukaryotic cell carries out thousands of chemical reactions, many of which are mutually incompatible. In order for the cell to operate effectively, these intracellular processes must be segregated. One strategy is to confine different metabolic processes and the enzymes required to perform them within membrane-enclosed organelles. Each organelle is responsible for a specialized set of functions. They have unique ultra-structure, morphology, as well as membrane lipid and protein compositions. Many organelle membranes are constantly remodeled by fusion and fission events, which help define the morphology and distribution of the organelle population. This dynamic behavior of cellular membranes is essential for function of the cell and its organelles.

The eukaryotic dynamin superfamily contains large GTPases that regulate cellular membrane remodeling (summarized in Table 1.1). Certain dynamins participate in membrane fusion events. In particular, mitofusin and OPA1/Mgm1 act in mitochondrial fusion, and atlastin is implicated in ER membrane fusion. However, the majority of dynamin family members mediate cellular membrane fission. Their domain structure and activity are closely related to those of classical dynamin (Dyn), which functions in vesicle budding during endocytosis. This thesis is focused on fission-mediating dynamins (including Dyn), and hereafter will refer to them as dynamins or dynamin-related proteins (DRPs).

Classical dynamin (Dyn)

Dyn is the first dynamin to be identified and characterized. Initially identified as a GTPase co-purified with brain microtubules, Dyn is now known to play roles in the scission of vesicles during endocytosis. In cells carrying a mutant dynamin,

Table 1.1. **Members of the dynamin superfamily mediate cellular membrane remodeling.**

Dynamins	Organisms	Sites of action	Functions
Dyn	Animals	Endocytic sites at the plasma membrane	Endocytic vesicle budding
Dynamin-related proteins (DRPs)			
Drp1 DRP3A/3B Dnm1	Animals Plants Yeast	Mitochondria Peroxisomes	Mitochondrial fission Peroxisomal fission
ARC5	Plants	Chloroplast	Chloroplast fission
MX	Animals	ER	Antiviral
Vps1	Fungi	Endosomes Plasma membrane	Membrane fission
Other Dynamins			
Mitofusin	Animals/yeast	Mitochondrial outer membrane	Mitochondrial fusion
OPA1/Mgm1	Animals/yeast	Mitochondrial inner membrane	Mitochondrial fusion
Atlastin	Animals	ER	ER membrane fusion
Guanylate-binding proteins	Animals	Intracellular vesicles	Defense against viral and bacterial pathogens
Phragmoplastin	Plants	Cell plate	Cell division
Bacterial Dlp	Cyanobacteria	Intergral membrane	Membrane fusion

Dyn, Classical dynamin; ARC5, ACCUMULATION AND REPLICATION OF CHLOROPLAST; Drp1, Dynamin-related protein; Dnm1, Dynamin-related; ER, Endoplasmic reticulum; OPA1, Optic atrophy; Mgm1, Mitochondrial genome maintenance; Vps1, Vacuolar protein sorting-associated ; MX, Myxovirus resistance proteins; Dlp, Dynamin-like protein.

endocytic vesicles are depleted because the endocytic pits are not pinched off (Suzuki et al., 1971; Grigliatti et al., 1973; Chen et al., 1991; van der Bliek and Meyerowitz, 1991). Instead, endocytic pits are arrested and accumulated at the plasma membrane. Similar arrested endocytic pits are also observed in mammalian cells upon exposure to GTP-γS, a nonhydrolyzable GTP analogue (Takei et al., 1995), or upon expression of a GTPase dominant-negative mutation (Herskovits et al., 1993; van der Bliek et al., 1993; Damke et al., 1994; Marks et al., 2001). These observations emphasize that the Dyn GTPase activity is required for vesicle budding.

Dyn consists of five domains: GTPase, Middle, Pleckstrin Homology (PH), GTPase Effector (GED) and Proline-Rich (PRD) Domains (Fig. 1.1A) (van der Bliek, 1999). The Middle and GED domains mediate Dyn self-assembly and modulate its GTPase activity, the PH domain is responsible for Dyn-membrane interaction, and the PRD facilitates Dyn binding to SH3-proteins. In vivo, Dyn forms a "collar" at the endocytic pit neck. In vitro, it self-assembles into rings and spirals, whose diameter is similar to that of the pit neck (Hinshaw and Schmid, 1995; Takei et al., 1995). The in vitro Dyn structures likely resemble the in vivo complexes. Upon assembly, Dyn GTPase activity is stimulated up to 100 fold (Barylko et al., 1998; Stowell et al., 1999). GTP hydrolysis leads to membrane constriction and fission, thereby releasing endocytic vesicles from the plasma membrane.

Dynamin-related proteins (DRPs)

DRPs contain three highly conserved dynamin domains, GTPase, Middle, and GED, but not the PH and PRD domains (Fig. 1.1A) (van der Bliek, 1999). In place of the PH domain, the DRPs harbor a region called Insert B (InsB), which has variable sequence

Figure 1.1. **Classical dynamin structure and assembly.** (A) Linear domain organization of classical dynamin (Dyn) and dynamin-related proteins (DRPs). (B) Crystal structure of nucleotide free Dyn1ΔPRD (PDB code 3SNH) (Faelber et al., 2011; Ford et al., 2011). (A and B) Regions that belong to the same structural domain are shown in the same color. (C) Model of dynamin dimer interacting with lipid membrane (side and top views) (D) Interfaces in the stalk region mediate dynamin dimerization (interface 2) and polymerization (interface 1 and 3). (E) Model of rings in dynamin assembly, adopted from the 3D reconstruction of dynamin assembled on liposome in vitro (Mears et al., 2011). (F) The dimerization of GTPase domains (in GTP-bound state) between adjacent rungs of the dynamin spiral is thought to stimulate GTPase hydrolysis, resulting in conformational changes that constrict and sever the membrane. PH, Pleckstrin homology; GED, GTPase effector domain; PRD, proline-rich domain; BSE, Bundle signaling element. Adapted from by author with permission from Shawn M. Ferguson and Pietro De Camilli, Department of Cell Biology, Yale University School of Medicine, USA. (Ferguson and De Camilli, 2012)

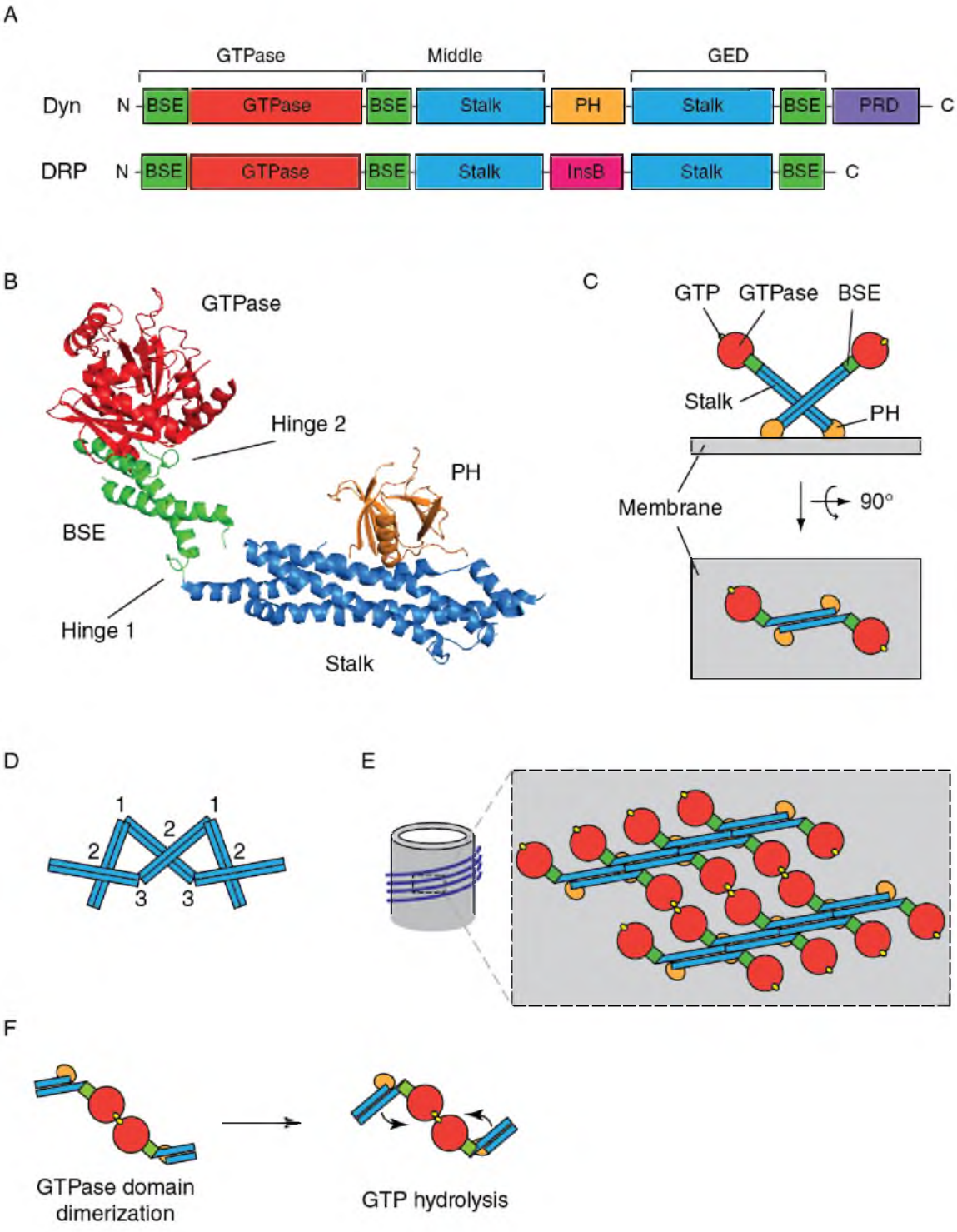
A
GTPase
Middle
GED
Dyn
N
BSE
GTPase
BSE
Stalk
PH
Stalk
BSE
PRD
C
DRP
N
BSE
GTPase
BSE
Stalk
InsB
Stalk
BSE
C
B
GTPase
Hinge 2
PH
BSE
Hinge 1
Stalk
C
GTP
GTPase
BSE
Stalk
PH
Membrane
90°
D
1
1
2
2
2
3
3
E
F
GTPase domain
dimerization
GTP hydrolysis

of undefined structure. It is still unclear whether InsB has a functional role in DRP-mediated membrane fission.

Like Dyn, DRPs self-assemble into fission complexes surrounding the fission site, and sever the membrane by a process involving assembly-stimulated GTP hydrolysis. However, the precise action of DRPs during membrane fission is poorly understood. In vitro membrane fission assays using purified Dyn on liposomes have suggested several models. It is still controversial which model reflects the behavior and activity of dynamin in vivo. However, the most popular model suggests that DRP-mediated membrane fission requires (1) the assembly of DRP into spirals around the lipid tubules at the fission sites, (2) stimulated GTPase activity upon assembly, (3) dramatic conformational changes of the DRP spiral upon GTP hydrolysis resulting in lipid constriction, and (4) severing of the lipid tube in a controlled manner to prevent leakage of the lumen contents (Schmid and Frolov, 2011).

Dynamin structure

Our understanding of dynamin GTPases has been advanced significantly by structural studies on dynamin (Zhang and Hinshaw, 2001; Faelber et al., 2011; Ford et al., 2011) and MxA (Daumke et al., 2010; Gao et al., 2010). Because of the high degree of conservation of the domain structure, all DRPs are predicted to adopt a four domain architecture similar to that of DynΔPRD, including GTPase, Bundle Signaling Element (BSE), stalk, and PH/InsB (Fig. 1.1B-C). This structural architecture does not follow the linear sequence of the domains. The GTPase domain, which contains a curved central β-sheet surrounded by α-helices at both sides, is connected to the BSE by a flexible loop region called hinge 2. The BSE is formed by three helices contributed by the N-terminus

of the GTPase domain, the N-terminus of the Middle domain, and the C-terminus of GED domain. These three helices form a bundle, burying a highly conserved hydrophobic surface. The BSE is linked to the stalk by hinge 1. The stalk is a bundle of four helices, three of which are provided by the Middle domain. The last stalk helix is from the GED domain. In DynΔPRD, the PH domain is at the bottom of the stalk and is connected to the last two stalk helices. The dynamin PH domain consists of seven antiparallel β-strands and a C-terminus amphipathic helix. The β-strands are arranged into two β-sheets. Flexible loops in the PH domain mediate direct interaction with the lipid bilayer. All crystal structures of dynamin lack the PRD, which is C-terminal to the GED domain. The PRD is predicted to emerge near the BSE and project away from the membrane, where it could be accessed by Dyn binding proteins. This general architecture appears to be conserved among DRPs. However, in DRPs, the dynamin PH domain is replaced by the InsB region, and the PRD is missing.

DRP assembly and GTPase stimulation

Dynamin conformations

Structural studies and in vitro assays using purified dynamin reported three distinct dynamin conformations depending on its nucleotide association status. The conformational changes are likely induced by GTP binding and GTP hydrolysis.

Conformation 1 represents dynamin in solution in the absence of nucleotide. The dynamin crystal structure was solved in this state (Faelber et al., 2011; Ford et al., 2011). However, it is believed that in vivo dynamin exists only transiently in the free nucleotide state because of its high association and dissociation rates for guanine nucleotides, and the high intracellular GTP concentration (1mM) (Damke et al., 1994).

Conformation 2 represents GTP-bound dynamin. This conformation was reconstituted in cryo-EM studies using purified Dyn in the presence of the non-hydrolyzable GTP analog GMPPCP (Zhang and Hinshaw, 2001). Although dynamin can assemble into spirals in the absence of nucleotide in vitro (Hinshaw and Schmid, 1995), it has been shown to be recruited to the membrane in the GTP-bound form (Sever et al., 1999; Fish et al., 2000; Sever et al., 2000). Therefore, binding of GTP may induce the switching from conformation 1 to conformation 2, which may be more favorable for membrane binding.

Conformation 3 represents dynamin during the transition state of the GTP hydrolysis reaction. This conformation was solved for dynamin GTPase-GED fusion (GG) in the presence of GDP•AlF^{4-} (Chappie et al., 2010). The GG crystal structure suggested that GTP hydrolysis causes dramatic conformational changes that lead to the constriction of the dynamin-lipid tubes (Fig. 1.1F).

Dynamin assembles by interaction interfaces in the stalk

The crystal structure of the DRP MxA stalk suggests that DRPs self-assemble via three interfaces in the stalk region (Fig. 1.1C-D) (Gao et al., 2010). Interface 1 is at the top of the stalk, right below the BSE. Interface 2 is located in the center of the stalk. Interface 3 is at the bottom of the stalk, right above the PH domain. The stalk dimerizes in a cross-like manner at interface 2, forming the dynamin building blocks. Interactions at interfaces 1 and 3 are established only during assembly of dynamin dimers into rings and spirals, linking the neighboring dimers in the same ring. In the structure of the MxA stalk region, the stalk interactions result in one-ring assembly. In the DynΔPRD nucleotide-free crystal structure (Faelber et al., 2011; Ford et al., 2011), there is no direct interaction

between the stalks at predicted interface 1. Instead, the dynamin stalks are tilted by 5° relative to the stalk axis. However, because this surface is hydrophobic and its residues are highly conserved, it is likely to have a similar role in Dyn as in MxA assembly. It is predicted that the closure of interface 1 during Dyn assembly could induce a pitch that favors the spiral complexes in dynamin instead of the ring-like structure as in MxA. Indeed, the direct interactions at all stalk interfaces fit into the cryo-EM reconstruction of GMPPCP-bound Dyn on liposomes (conformation 2). This reflects the conformational changes induced by GTP binding, and is consistent with the model that Dyn is recruited to the membrane in the GTP-bound form (Sever et al., 1999; Fish et al., 2000; Sever et al., 2000).

GTPase activity is stimulated by cross-ring GTPase domain dimerization

In a Dyn spiral, Dyn molecules interact via three stalk interfaces, forming the "spiral back-bone." GTPase domains project from the back-bone in opposite directions (Fig. 1.1E) (Faelber et al., 2011; Ford et al., 2011). The GTPase domains of molecules in two adjacent rings dimerize via a fourth self-interacting interface. This interaction was discovered in the crystal structure of Dyn GG (Chappie et al., 2010). GG is a monomer in the absence of nucleotides, but dimerizes in the presence of GTP or GDP•AlF^{4-}. This suggests that GTPase domain dimerization occurs only during GTP hydrolysis. Dimerization of the GTPase domain in Dyn assemblies puts the components of the GTPase active site in the optimal conformation, leading to a dramatic stimulation of GTPase activity (>100 fold) (Barylko et al., 1998; Stowell et al., 1999). GTP hydrolysis induces conformation changes (Fig. 1.1E), causing membrane constriction and fission.

These conformational changes are also predicted to disrupt the interaction at stalk interface 1 and lead to dynamin disassembly.

DRP membrane recruitment – Open questions

Which DRP domain is essential for membrane recruitment?

In order to mediate fission at a certain cellular membrane, DRPs first need to be targeted to the right organelle. While Dyn binds directly to the lipid bilayer via the PH domain, DRPs require membrane adaptor proteins to bind a specific membrane. The molecular mechanism for the recruitment step is poorly understood. To understand this key step, it is crucial to identify the domain responsible for the interaction of DRPs with their membrane adaptors.

How do adaptor(s) regulate DRP assembly and stimulate GTPase activity?

In the current model of DRP-mediated membrane fission, the DRP only starts assembling once it is associated with the membrane via interaction with the adaptor molecule. Moreover, the exact position of each monomer is extremely important for the formation of functional dynamin complex, where GTPase domains can dimerize properly across the rings. This raises the question whether the adaptor plays a regulatory role in DRP assembly.

To address these questions, we chose to study the interaction between budding yeast mitochondrial dynamin Dnm1 and its membrane adaptor Mdv1, the essential components of the yeast mitochondrial fission complex.

Mitochondria

Mitochondrial function and ultrastructure

Mitochondria are complex double-membrane organelles in eukaryotic cells. The most prominent role for mitochondria is to generate ATP for diverse cellular functions. However, mitochondria are indispensable for life, even in cells that do not depend on respiration, because they are required for essential cellular processes including the assembly of iron–sulphur clusters, the citric acid cycle, fatty acid β-oxidation, heme and phospholipid biosynthesis. In addition, mitochondria are key regulators of developmental processes, aging and apoptosis.

Mitochondria are bound by two membranes. The mitochondrial outer membrane contains porin "pores" and offers little resistance to the movement of small molecules into and out of the mitochondrion. The inner membrane provides more control over what enters and leaves the mitochondrion compared to the outer membrane. The inner membrane folds inward to form cristae, which house the electron transport chain complexes that participate in cellular respiration and the production of ATP. Between the two membranes is the intermembrane space, and the region enclosed by the inner membrane is called the matrix. The matrix contains the mitochondrial genome and independent protein-synthetic machinery, which synthesize proteins needed for cellular respiration.

Mitochondrial dynamics

In many eukaryotic cells, mitochondria are elongated, branched and distributed throughout the cytoplasm (Fig. 1.2, middle panel). Mitochondria constantly fuse, divide

and move along cytoskeletal tracks. These dynamic activities control their morphology and intracellular distribution and determine their cell type-specific appearance.

The number and shape of mitochondria are governed by the balance of fusion and fission events. Fusion generates the network, which is important for the dissipation of metabolic energy along the mitochondrial tubules. Fusion of individual organelles back to the network also prevents the aging process caused by mtDNA mutations. The healthy mitochondrial network provides mtDNA copies to complement or repair mutations from the individual mitochondrion. By contrast, fission generates small and transportable compartments, which can be easily transferred to the daughter cells, transported along cytoskeletal tracks and turned over by mitophagy (Westermann, 2010).

Budding yeast is the optimal model to study mitochondrial membrane dynamics because mutations impairing these processes lead to clear morphological and growth phenotypes. In wildtype yeast cells, mitochondria form a tubular network distributed evenly around the cell cortex. This network is maintained by a balance between fusion and fission events (Fig. 1.2) (Okamoto and Shaw, 2005). When fusion is blocked, ongoing fission results in fragmented mitochondria. By contrast, fission defects lead to formation of net-like mitochondria due to ongoing fusion. Moreover, budding yeast can survive without mitochondrial DNA if provided with a fermentable carbon source (dextrose). Therefore, the membrane dynamics defects that cause mitochondrial DNA loss can still be studied in live yeast cells. In this thesis, we use mitochondrial fission machinery in yeast as a model to address questions about DRP adaptor binding and membrane recruitment.

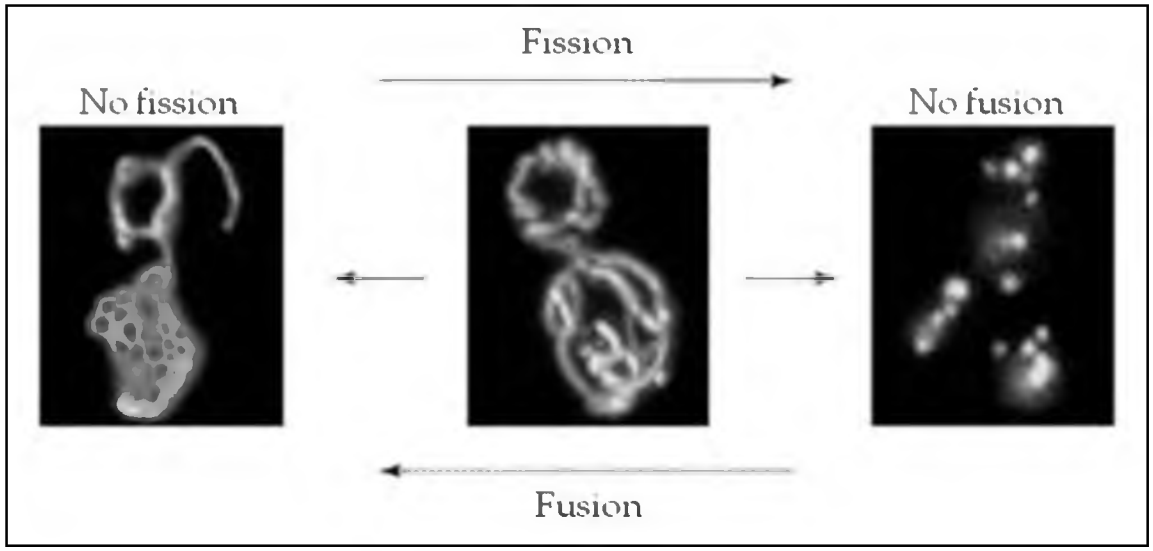

Figure 1.2. **A tubular mitochondrial network in wildtype yeast cells is maintained by the balance of fusion and fission events.** Fission defects lead to formation of net-like mitochondria due to ongoing fusion. By contrast, when fusion is blocked, ongoing fission results in fragmented mitochondria. Image courtesy of J. Shaw, University of Utah, USA and J. Nunnari, University of California, Davis, USA (Shaw and Nunnari, 2002).

DRP-mediated mitochondrial fission

Mitochondrial fission is best understood in budding yeast. Three essential components of the yeast fission machinery are Dnm1 (the dynamin, Drp1 in mammals), Mdv1 (the adaptor) and Fis1 (the membrane anchoring molecule, hFis1 in human) (Fig. 1.3). Knocking out any of these genes causes fission defects, in which unopposed fusion of mitochondrial tubules causes a net-like or collapsed mitochondrial morphology (Okamoto and Shaw, 2005). Yeast also encodes a second adaptor, Caf4, which is an Mdv1 paralog (Fig. 1.3) (Griffin et al., 2005). Although Caf4 is capable of facilitating fission (Qian Guo thesis), it is not essential for fission. While Dnm1 and Fis1 are conserved in mammals, the mammalian adaptors (Mff and MiD49/51) share no conservation with Mdv1 and Caf4 (Fig. 1.3).

The yeast mitochondrial fission dynamin Dnm1 contains three dynamin conserved domains GTPase, Middle, and GED as well as the less conserved InsB region. In vivo, Dnm1 forms punctate structures encircling mitochondrial tubules at the fission sites (Otsuga et al., 1998; Bleazard et al., 1999). When *DNM1* is disrupted, the formation of fission complexes is blocked despite normal expression and mitochondrial localization of Fis1 and Mdv1 (Tieu and Nunnari, 2000). The *dnm1*Δ yeast strain survives and propagates normally during vegetative growth. However, the collapsing of mitochondria into a single net prevents the proper segregation of mitochondria into four spores during sporulation, reducing the viability of yeast spores (Gorsich and Shaw, 2004). In mammalian cell lines, Drp1 knock down or mutation also causes morphology defects, where mitochondria are interconnected and cluster around the nucleus (Smirnova et al., 1998). In *C. elegans* (Labrousse et al., 1999) and mouse (Wakabayashi et al., 2009),

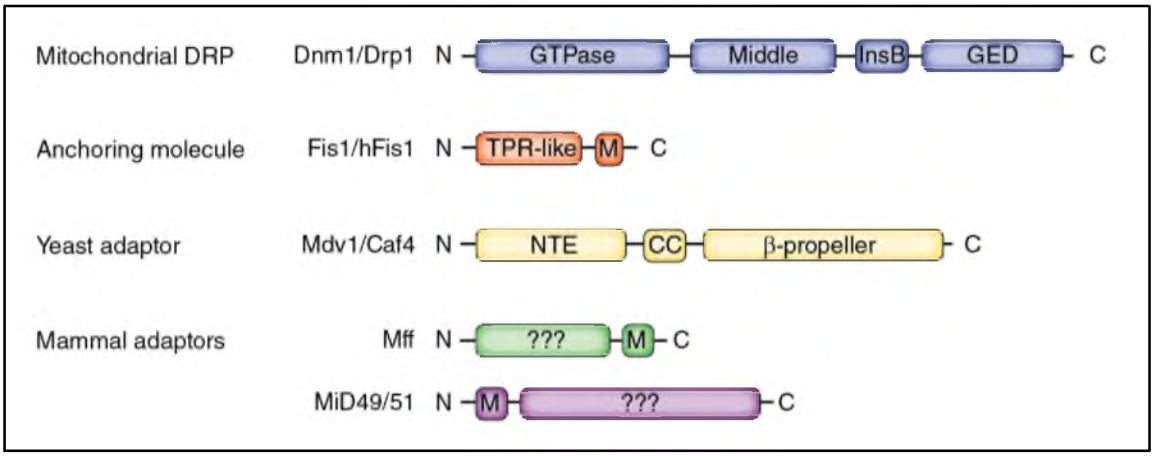

Figure 1.3. **Domain structures of yeast and mammalian mitochondrial fission proteins.** Abbreviations: Fis1, Fission1; TPR, Tetratricopeptide repeat; M, transmembrane; Dnm1, Dynamin-related 1; Drp1, Dynamin-related protein 1; InsB, Insert B; GED, GTPase effector domain; Mdv1, Mitochondrial division 1; Caf4, CCR4 associated factor 4; NTE, N- terminal extension; CC, Coiled-coil; Mff, Mitochondrial fission factor; MiD; Mitochondrial dynamics; ???, Unknown.

disruption of Drp1 causes embryonic lethality. A human Drp1 mutation was reported in a baby who died 37 days after birth with abnormal brain development and optic atrophy (Waterham et al., 2007).

Fis1 is a tail-anchored mitochondrial outer membrane protein with a single tetratricopeptide repeat-like (TPR-like) fold facing the cytoplasm. GFP-Fis1 is distributed evenly on the mitochondrial outer membrane. Depletion of Fis1 in yeast results in cytoplasmic localization of Dnm1 and Mdv1 and impaired mitochondrial fission (Mozdy et al., 2000). Reports on the role of mammalian Fis1 (hFis1) in fission differ, depending on the cell line used. Fis1 RNAi knockdown in COS-7 cells causes a defect in fission (James et al., 2003). Conversely, Fis1 overexpression promotes fission and causes mitochondrial fragmentation (Stojanovski et al., 2004). By contrast, Fis1 RNAi knockdown in HeLa cells has no significant effect on mitochondrial morphology (Otera et al., 2010). It is possible that these disparate phenotypes are cell-type specific. Fis1 is found in the same complex with Dnm1/Drp1 (Yu et al., 2005), but a direct interaction between Fis1 and Dnm1/Drp1 is unlikely.

Mdv1 is a WD-repeat protein, which contains an N-terminal extension (NTE), a predicted coiled-coil domain, and eight WD repeats predicted to form a β-propeller domain. Mdv1 acts as an adaptor to bridge Dnm1 and Fis1 in mitochondrial fission complexes (Tieu and Nunnari, 2000; Cerveny et al., 2001). Its NTE domain interacts with Fis1, and the β-propeller domain interacts with Dnm1 (Cerveny and Jensen, 2003). GFP-Mdv1 colocalizes with both Fis1 and Dnm1. It uniformly labels the mitochondrial tubule like Fis1, and forms foci that colocalize with Dnm1 puncta. Fission occurs at sites where Mdv1 and Dnm1 colocalize (Naylor et al., 2006). Disruption of *MDV1* blocks

mitochondrial localization of Dnm1 (Cerveny and Jensen, 2003). Conversely, Mdv1 fails to form puncta in the absence of Dnm1 (Tieu and Nunnari, 2000).

Model of fission complex formation

Combined findings on the fission machinery in yeast allow us to propose a working model for fission complex assembly (Fig. 1.4). Mitochondrial fission complexes are observed at sites where an ER tubule crosses and induce a constriction of the mitochondrial tubule (Friedman et al., 2011). The assembly of mitochondrial fission complexes is initiated by recruitment of Dnm1 from the cytoplasm to pre-existing Fis1-Mdv1 complexes on the mitochondrial outer membrane (Mozdy et al., 2000; Tieu and Nunnari, 2000; Cerveny et al., 2001). Once on the membrane, Dnm1 further assembles to form multimeric complexes. The polymerization of dynamin molecules drives the reorganization and multimerization of the receptors, leading to the formation of fission complexes (Bhar et al., 2006; Naylor et al., 2006). These fission complexes are further activated by an unknown mechanism to carry out mitochondrial division. In this model, recruitment of cytoplasmic Dnm1/Drp1 to the membrane receptor on the membrane is a key step in regulating the formation of fission complexes and subsequent mitochondrial division.

Thesis overview

This thesis focuses on elucidating the DRP recruitment step by investigating: (1) the molecular basis of the Dnm1-Mdv1 interaction required for recruitment, and (2) the role of the adaptor protein in regulating dynamin assembly.

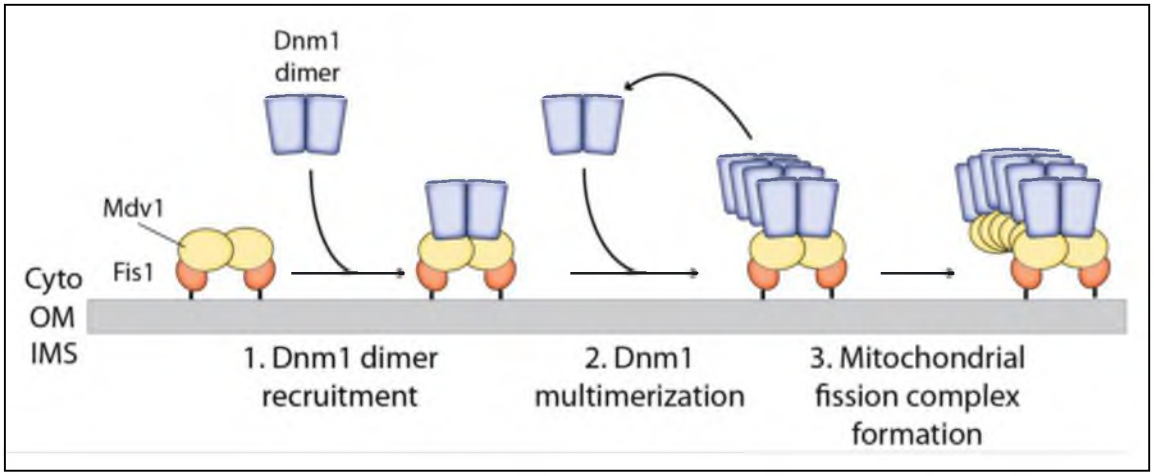

Figure 1.4. **Model for step-wise assembly of fission complexes.** (1) cytoplasmic Dnm1 dimers (blue) are recruited to pre-existing Fis1-Mdv1 (orange-yellow) on the mitochondrial outer membrane (grey). (2) Dnm1 oligomers assemble into multimeric complexes. (3) Dnm1 polymerization drives the formation of fission complexes containing Dnm1, Fis1 and Mdv1. These fission complexes are further activated to carry out mitochondrial division.

Dyn binds directly to the lipid bilayer via the PH domain. However, the PH domain is replaced by InsB domain in DRPs. In Chapter 2, we identified a conserved motif in InsB that essential for Dnm1 recruitment. This is the first study to show a functional role for InsB in dynamin membrane recruitment. We also identified potential binding sites on Mdv1 that may participate in interaction with Dnm1 InsB. Interestingly, mitochondrial dynamin InsB sequences may have coevolved with the adaptor proteins to meet the unique requirements of mitochondrial fission in different organisms.

In addition to its role in Dnm1 recruitment, Mdv1 co-assembles with Dnm1 in the final fission complex. This suggests that Mdv1 may play more substantial roles in fission. In vitro, Mdv1 has been shown to co-assemble with Dnm1 on liposomes, and contribute to the stimulation of Dnm1 GTPase activity (Lackner et al., 2009). In Chapter 3, we solved the structure of 92Å long coiled-coil in Mdv1, and demonstrated that the dimerization of Mdv1 helps determine the optimal architecture of the functional fission complexes.

References

Barylko, B., D. Binns, K.M. Lin, M.A. Atkinson, D.M. Jameson, H.L. Yin, and J.P. Albanesi. 1998. Synergistic activation of dynamin GTPase by Grb2 and phosphoinositides. *J Biol Chem*. 273:3791-3797.

Bhar, D., M.A. Karren, M. Babst, and J.M. Shaw. 2006. Dimeric Dnm1-G385D Interacts with Mdv1 on Mitochondria and Can Be Stimulated to Assemble into Fission Complexes Containing Mdv1 and Fis1. *J Biol Chem*. 281:17312-17320.

Bleazard, W., J.M. McCaffery, E.J. King, S. Bale, A. Mozdy, Q. Tieu, J. Nunnari, and J.M. Shaw. 1999. The dynamin-related GTPase Dnm1 regulates mitochondrial fission in yeast. *Nat Cell Biol*. 1:298-304.

Cerveny, K.L., and R.E. Jensen. 2003. The WD-repeats of Net2p interact with Dnm1p and Fis1p to regulate division of mitochondria. *Mol Biol Cell*. 14:4126-4139.

Cerveny, K.L., J.M. McCaffery, and R.E. Jensen. 2001. Division of mitochondria requires a novel DMN1-interacting protein, Net2p. *Mol Biol Cell*. 12:309-321.

Chappie, J.S., S. Acharya, M. Leonard, S.L. Schmid, and F. Dyda. 2010. G domain dimerization controls dynamin's assembly-stimulated GTPase activity. *Nature*. 465:435-440.

Chen, M.S., R.A. Obar, C.C. Schroeder, T.W. Austin, C.A. Poodry, S.C. Wadsworth, and R.B. Vallee. 1991. Multiple forms of dynamin are encoded by shibire, a Drosophila gene involved in endocytosis. *Nature*. 351:583-586.

Damke, H., T. Baba, D.E. Warnock, and S.L. Schmid. 1994. Induction of mutant dynamin specifically blocks endocytic coated vesicle formation. *J Cell Biol*. 127:915-934.

Daumke, O., S. Gao, A. von der Malsburg, O. Haller, and G. Kochs. 2010. Structure of the MxA stalk elucidates the assembly of ring-like units of an antiviral module. *Small GTPases*. 1:62-64.

Faelber, K., Y. Posor, S. Gao, M. Held, Y. Roske, D. Schulze, V. Haucke, F. Noe, and O. Daumke. 2011. Crystal structure of nucleotide-free dynamin. *Nature*. 477:556-560.

Ferguson, S.M., and P. De Camilli. 2012. Dynamin, a membrane-remodelling GTPase. *Nat Rev Mol Cell Biol*. 13:75-88.

Fish, K.N., S.L. Schmid, and H. Damke. 2000. Evidence that dynamin-2 functions as a signal-transducing GTPase. *J Cell Biol*. 150:145-154.

Ford, M.G., S. Jenni, and J. Nunnari. 2011. The crystal structure of dynamin. *Nature*. 477:561-566.

Friedman, J.R., L.L. Lackner, M. West, J.R. DiBenedetto, J. Nunnari, and G.K. Voeltz. 2011. ER Tubules Mark Sites of Mitochondrial Division. *Science*. 334:358-362.

Gao, S., A. von der Malsburg, S. Paeschke, J. Behlke, O. Haller, G. Kochs, and O. Daumke. 2010. Structural basis of oligomerization in the stalk region of dynamin-like MxA. *Nature*. 465:502-506.

Gorsich, S.W., and J.M. Shaw. 2004. Importance of mitochondrial dynamics during meiosis and sporulation. *Mol Biol Cell*. 15:4369-4381.

Griffin, E.E., J. Graumann, and D.C. Chan. 2005. The WD40 protein Caf4p is a component of the mitochondrial fission machinery and recruits Dnm1p to mitochondria. *J Cell Biol*. 170:237-248.

Grigliatti, T.A., L. Hall, R. Rosenbluth, and D.T. Suzuki. 1973. Temperature-sensitive mutations in Drosophila melanogaster. XIV. A selection of immobile adults. *Mol Gen Genet*. 120:107-114.

Herskovits, J.S., C.C. Burgess, R.A. Obar, and R.B. Vallee. 1993. Effects of mutant rat dynamin on endocytosis. *J Cell Biol*. 122:565-578.

Hinshaw, J.E., and S.L. Schmid. 1995. Dynamin self-assembles into rings suggesting a mechanism for coated vesicle budding. *Nature*. 374:190-192.

James, D.I., P.A. Parone, Y. Mattenberger, and J.C. Martinou. 2003. hFis1, a novel component of the mammalian mitochondrial fission machinery. *J Biol Chem*. 278:36373-36379.

Labrousse, A.M., M.D. Zappaterra, D.A. Rube, and A.M. van der Bliek. 1999. C. elegans dynamin-related protein DRP-1 controls severing of the mitochondrial outer membrane. *Mol Cell*. 4:815-826.

Lackner, L.L., J.S. Horner, and J. Nunnari. 2009. Mechanistic analysis of a dynamin effector. *Science*. 325:874-877.

Marks, B., M.H. Stowell, Y. Vallis, I.G. Mills, A. Gibson, C.R. Hopkins, and H.T. McMahon. 2001. GTPase activity of dynamin and resulting conformation change are essential for endocytosis. *Nature*. 410:231-235.

Mears, J.A., L.L. Lackner, S. Fang, E. Ingerman, J. Nunnari, and J.E. Hinshaw. 2011. Conformational changes in Dnm1 support a contractile mechanism for mitochondrial fission. *Nat Struct Mol Biol*. 18:20-26.

Mozdy, A.D., J.M. McCaffery, and J.M. Shaw. 2000. Dnm1p GTPase-mediated mitochondrial fission is a multi-step process requiring the novel integral membrane component Fis1p. *J Cell Biol*. 151:367-380.

Naylor, K., E. Ingerman, V. Okreglak, M. Marino, J.E. Hinshaw, and J. Nunnari. 2006. Mdv1 interacts with assembled dnm1 to promote mitochondrial division. *J Biol Chem*. 281:2177-2183.

Okamoto, K., and J.M. Shaw. 2005. Mitochondrial morphology and dynamics in yeast and multicellular eukaryotes. *Annu Rev Genet*. 39:503-536.

Otera, H., C. Wang, M.M. Cleland, K. Setoguchi, S. Yokota, R.J. Youle, and K. Mihara. 2010. Mff is an essential factor for mitochondrial recruitment of Drp1 during mitochondrial fission in mammalian cells. *J Cell Biol*. 191:1141-1158.

Otsuga, D., B.R. Keegan, E. Brisch, J.W. Thatcher, G.J. Hermann, W. Bleazard, and J.M. Shaw. 1998. The dynamin-related GTPase, Dnm1p, controls mitochondrial morphology in yeast. *J Cell Biol*. 143:333-349.

Schmid, S.L., and V.A. Frolov. 2011. Dynamin: functional design of a membrane fission catalyst. *Annu Rev Cell Dev Biol*. 27:79-105.

Sever, S., H. Damke, and S.L. Schmid. 2000. Dynamin:GTP controls the formation of constricted coated pits, the rate limiting step in clathrin-mediated endocytosis. *J Cell Biol*. 150:1137-1148.

Sever, S., A.B. Muhlberg, and S.L. Schmid. 1999. Impairment of dynamin's GAP domain stimulates receptor-mediated endocytosis. *Nature*. 398:481-486.

Shaw, J.M., and J. Nunnari. 2002. Mitochondrial dynamics and division in budding yeast. *Trends Cell Biol*. 12:178-184.

Smirnova, E., D.L. Shurland, S.N. Ryazantsev, and A.M. van der Bliek. 1998. A human dynamin-related protein controls the distribution of mitochondria. *J Cell Biol*. 143:351-358.

Stojanovski, D., O.S. Koutsopoulos, K. Okamoto, and M.T. Ryan. 2004. Levels of human Fis1 at the mitochondrial outer membrane regulate mitochondrial morphology. *J Cell Sci*. 117:1201-1210.

Stowell, M.H., B. Marks, P. Wigge, and H.T. McMahon. 1999. Nucleotide-dependent conformational changes in dynamin: evidence for a mechanochemical molecular spring. *Nat Cell Biol*. 1:27-32.

Suzuki, D.T., T. Grigliatti, and R. Williamson. 1971. Temperature-sensitive mutations in Drosophila melanogaster. VII. A mutation (para-ts) causing reversible adult paralysis. *Proc Natl Acad Sci U S A*. 68:890-893.

Takei, K., P.S. McPherson, S.L. Schmid, and P. De Camilli. 1995. Tubular membrane invaginations coated by dynamin rings are induced by GTP-gamma S in nerve terminals. *Nature*. 374:186-190.

Tieu, Q., and J. Nunnari. 2000. Mdv1p Is a WD Repeat Protein that Interacts with the Dynamin-related GTPase, Dnm1p, to Trigger Mitochondrial Division. *J Cell Biol*. 151:353-366.

van der Bliek, A.M. 1999. Functional diversity in the dynamin family. *Trends Cell Biol*. 9:96-102.

van der Bliek, A.M., and E.M. Meyerowitz. 1991. Dynamin-like protein encoded by the Drosophila shibire gene associated with vesicular traffic. *Nature*. 351:411-414.

van der Bliek, A.M., T.E. Redelmeier, H. Damke, E.J. Tisdale, E.M. Meyerowitz, and S.L. Schmid. 1993. Mutations in human dynamin block an intermediate stage in coated vesicle formation. *J Cell Biol*. 122:553-563.

Wakabayashi, J., Z. Zhang, N. Wakabayashi, Y. Tamura, M. Fukaya, T.W. Kensler, M. Iijima, and H. Sesaki. 2009. The dynamin-related GTPase Drp1 is required for embryonic and brain development in mice. *J Cell Biol*. 186:805-816.

Waterham, H.R., J. Koster, C.W. van Roermund, P.A. Mooyer, R.J. Wanders, and J.V. Leonard. 2007. A lethal defect of mitochondrial and peroxisomal fission. *N Engl J Med*. 356:1736-1741.

Westermann, B. 2010. Mitochondrial fusion and fission in cell life and death. *Nat Rev Mol Cell Biol*. 11:872-884.

Yu, T., R.J. Fox, L.S. Burwell, and Y. Yoon. 2005. Regulation of mitochondrial fission and apoptosis by the mitochondrial outer membrane protein hFis1. *J Cell Sci*. 118:4141-4151.

Zhang, P., and J.E. Hinshaw. 2001. Three-dimensional reconstruction of dynamin in the constricted state. *Nat Cell Biol*. 3:922-926.

CHAPTER 2

A NOVEL MOTIF IN THE YEAST MITOCHONDRIAL DYNAMIN Dnm1 IS ESSENTIAL FOR ADAPTOR BINDING AND MEMBRANE RECRUITMENT

Authors

Huyen T. Bui, Mary A. Karren, Debjani Bhar, and Janet M. Shaw

A novel motif in the yeast mitochondrial dynamin Dnm1 is essential for adaptor binding and membrane recruitment

Huyen T. Bui, Mary A. Karren, Debjani Bhar, and Janet M. Shaw

Department of Biochemistry, University of Utah School of Medicine, Salt Lake City, UT 84112

To initiate mitochondrial fission, dynamin-related proteins (DRPs) must bind specific adaptors on the outer mitochondrial membrane. The structural features underlying this interaction are poorly understood. Using yeast as a model, we show that the Insert B domain of the Dnm1 guanosine triphosphatase (a DRP) contains a novel motif required for association with the mitochondrial adaptor Mdv1. Mutation of this conserved motif specifically disrupted Dnm1–Mdv1 interactions, blocking Dnm1 recruitment and mitochondrial fission. Suppressor mutations in Mdv1 that restored Dnm1–Mdv1 interactions and fission identified potential protein-binding interfaces on the Mdv1 β-propeller domain. These results define the first known function for Insert B in DRP adaptor interactions. Based on the variability of Insert B sequences and adaptor proteins, we propose that Insert B domains and mitochondrial adaptors have coevolved to meet the unique requirements for mitochondrial fission of different organisms.

Introduction

Eukaryotic cells possess a family of dynamin-related proteins (DRPs), each of which is responsible for a specific cellular membrane-remodeling event. For example, the dynamin-related GTPase Drp1 (Dnm1 in yeast) mediates mitochondrial (Bleazard et al., 1999; Labrousse et al., 1999; Sesaki and Jensen, 1999) and peroxisomal fission (Koch et al., 2003; Li and Gould, 2003; Kuravi et al., 2006), Atlastin (Hu et al., 2009; Orso et al., 2009; Moss et al., 2011) and Mitofusins (Hales and Fuller, 1997; Hermann et al., 1998; Rapaport et al., 1998; Chen et al., 2003; Eura et al., 2003) play roles in ER and mitochondrial membrane fusion, respectively, and ARC5 (Gao et al., 2003) facilitates chloroplast membrane division. Like classical dynamin, DRPs self-assemble into highly ordered oligomers that use the energy of GTP hydrolysis to remodel lipid bilayers (Praefcke and McMahon, 2004).

Dynamin and DRPs have conserved GTPase, middle, and GTPase effector domains (see Fig. 1 A; van der Bliek, 1999). These domains mediate self-assembly and modulate GTPase activity. Dynamin and DRPs also contain nonconserved domains that, in some cases, have been shown to determine their cellular distribution and heterotypic interactions. For example, a proline-rich domain at the C terminus of dynamin facilitates its binding to a variety of actin-binding proteins. Dynamin also harbors a pleckstrin homology (PH) domain between its GTPase and GTPase effector domain, which is essential for interactions with the plasma membrane. In place of the PH domain, DRPs contain a region called Insert B (InsB) whose length and sequence varies. Whether or not there is a conserved function for InsB is not clear.

Although dynamin interacts directly with the lipid bilayer via its PH domain, DRPs do not initially interact with the lipid bilayers they remodel. Instead, they are recruited to specific cellular sites via interactions with membrane-associated adaptor proteins. In most cases, the DRP domains necessary for adaptor interactions have not been identified. However, structural studies of dynamin and several DRPs (Mears et al., 2007, 2011; Faelber et al., 2011; Ford et al., 2011) suggest that InsB is a likely candidate because it is predicted to reside at the base of the DRP oligomer, closest to the membrane.

Correspondence to Janet M. Shaw: shaw@biochem.utah.edu

Abbreviations used in this paper: coIP, coimmunoprecipitation; DRP, dynamin-related protein; DSP, dithiobis(succinimidyl propionate); InsB, Insert B; mt-ffRFP, mitochondrial-targeted fast-folding RFP; PH, pleckstrin homology; WT, wild-type.

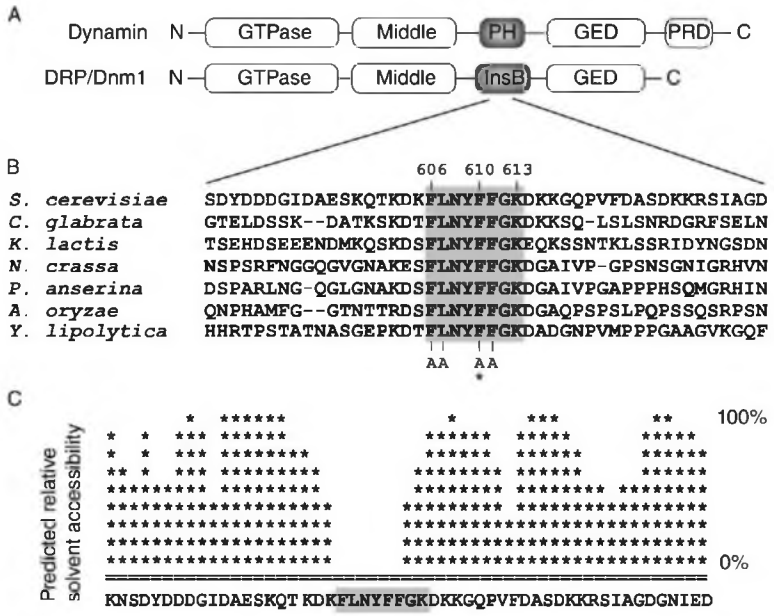

Figure 1. **Dnm1 InsB contains a sequence of eight strictly conserved residues (F610–K613) predicted to be solvent inaccessible.** (A) Domain structures of Dynamin and the DRP/Dnm1. GED, GTPase effector domain; PRD, proline-rich domain. (B) Alignment of a segment of InsB from the indicated fungal Dnm1 homologues. The asterisk marks the position of the *dnm1*^{F610A} mutation. (C) Plot showing the predicted relative solvent accessibility of a section of Dnm1 InsB (PredictProtein server). Shaded boxes indicate residues that are conserved in fungi.

We used the yeast mitochondrial fission machinery as a model to directly test the function of InsB in DRP adaptor interactions and DRP1 membrane recruitment. In vivo, Dnm1 (the yeast DRP) is recruited to the mitochondrial outer membrane by Mdv1 (the adaptor; Tieu and Nunnari, 2000; Cerveny et al., 2001), which in turn associates with membrane-anchored Fis1 (Mozdy et al., 2000). Once on the membrane, Dnm1 coassembles with Mdv1 into spirals that encircle and divide the mitochondrial tubule (Bhar et al., 2006; Naylor et al., 2006). We identified a motif in the Dnm1 InsB domain that is required to recruit Dnm1 to mitochondria. The amino acid sequence of this motif is strictly conserved among fungi and is predicted to form a solvent-inaccessible helix (PSIPRED v2.6). Amino acid substitutions in this InsB helix inhibit the recruitment of Dnm1 to mitochondria and block fission. Importantly, these mutations do not impair Dnm1 self-assembly. Instead, they specifically disrupt the Dnm1–Mdv1 interaction. The disrupted interaction is rescued by suppressor mutations in the Mdv1 β-propeller domain to which Dnm1 binds. These findings identify a new functional motif in the Dnm1 InsB domain required for Mdv1 binding and recruitment of Dnm1 from the cytoplasm to its site of action on mitochondria.

Results

Dnm1 InsB contains a conserved sequence motif predicted to be solvent inaccessible

In a previous genetic screen (Bhar et al., 2006), we identified an InsB mutation (F610L) that interfered with Dnm1 function in mitochondrial fission. Alignment of *Saccharomyces cerevisiae* Dnm1 InsB with its fungal homologues revealed a motif of eight strictly conserved residues encompassing F610 (Fig. 1, A and B). These residues are predicted to form a short helix (PSIPRED v2.6) that is less accessible to solvent than surrounding residues (Fig. 1 C), suggesting that they are part of an interaction interface.

InsB motif residues are important for Dnm1 function in mitochondrial fission

Yeast mitochondria form multiple tubular and branched structures that are continually remodeled by fission and fusion events. When fission is disrupted or blocked, mitochondria fuse to form netlike structures or a single interconnected tubule that often collapses to one side of the cell (Bleazard et al., 1999). To evaluate Dnm1 InsB motif function, we individually replaced the eight conserved residues with alanine and quantified the ability of each mutant protein to rescue fission defects in cells lacking the wild-type (WT) Dnm1 protein (*dnm1Δ*). As shown in Fig. 2 A, expression of WT Dnm1 rescued fission in up to 90% of *dnm1Δ* cells. In contrast, four Dnm1 mutant proteins (F606A, L607A, F610A, and F611A) failed to rescue mitochondrial morphology in this strain. Hereafter, these four loss-of-function proteins will be collectively referred to as Dnm1^{InsBmut}. Western blotting of whole cell extracts indicated that the Dnm1^{InsBmut} proteins were expressed at levels similar to WT Dnm1 (Fig. S1 A). Thus, mutations in conserved residues of InsB block Dnm1 function in mitochondrial fission but do not affect protein stability.

In the absence of WT Dnm1, the inability of Dnm1^{InsBmut} proteins to support fission could be caused by their failure to self-assemble. To test this possibility, we coexpressed HA- and Myc-tagged versions of the same InsB mutant proteins in *dnm1Δ* cells and performed coimmunoprecipitation (coIP) assays. As shown in Fig. 2 B, each form of the HA-tagged Dnm1^{InsBmut} pro-

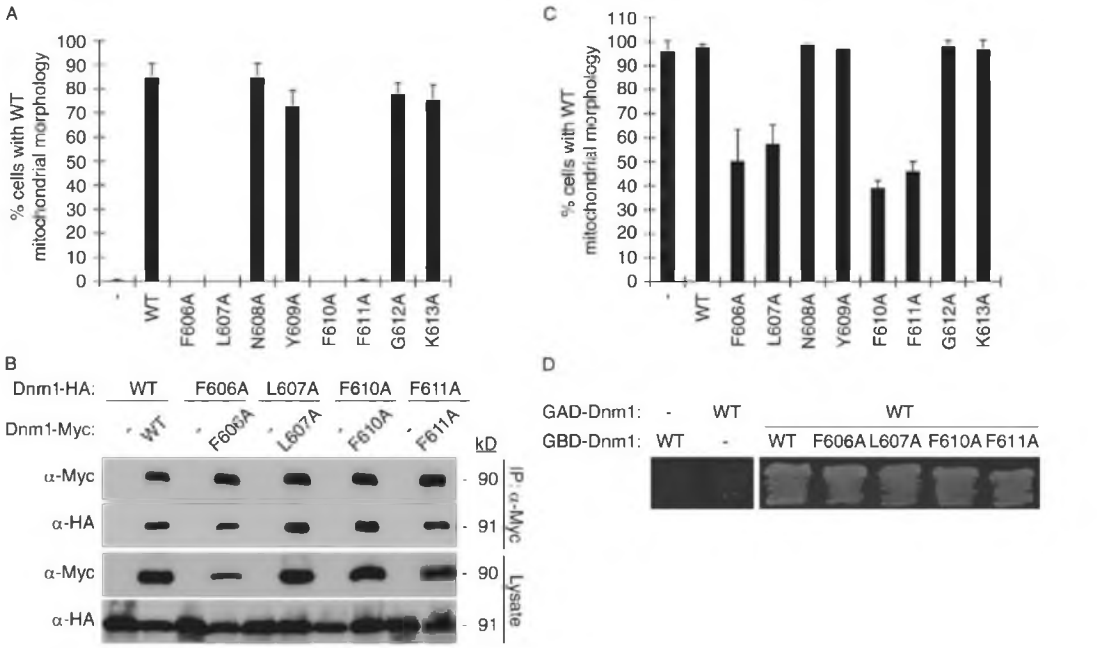

Figure 2. **Dnm1 InsB conserved residues are important for Dnm1 function in mitochondrial fission.** (A) Quantification of mitochondrial morphology in *dnm1Δ* cells expressing indicated Dnm1 variants. (B) Lysates from cells expressing the indicated C-terminal HA- or Myc-tagged Dnm1 proteins were used for immunoprecipitation with anti-Myc agarose beads. Immunoprecipitated fractions (top) and lysates (bottom) were analyzed by SDS-PAGE and Western blotting with anti-Myc and anti-HA antibodies. (C) Quantification of mitochondrial morphology in WT cells expressing indicated Dnm1 variants. (A and C) Black columns and error bars represent the mean and standard deviation of at least three independent experiments ($n = 100$). (D) pGBD and pGAD plasmids expressing the indicated fusion proteins were cotransformed into the Y187 yeast two-hybrid reporter strain and grown on S-Dextrose minus adenine plates at 30°C for 3 d.

tein was efficiently coprecipitated with the Myc-tagged version of itself. Thus, the F606, L607, F610, and F611 residues in InsB are not essential for Dnm1 self-assembly.

We also observed that coexpression of WT and Dnm1^{InsBmut} proteins caused dominant-negative fission defects (Fig. 2 C). Although expression of a second copy of WT *DNM1* in WT cells did not cause significant changes in mitochondrial morphology, expression of Dnm1^{InsBmut} proteins in WT cells blocked fission in up to 60% of the population. One explanation for these dominant-negative fission phenotypes is that Dnm1^{InsBmut} proteins are able to assemble with WT Dnm1. Consistent with this idea, we observed an interaction between WT Dnm1 and Dnm1^{InsBmut} proteins in a two-hybrid assay (Fig. 2 D). The interaction of Dnm1^{InsBmut} with WT Dnm1 could interfere with multiple steps in mitochondrial fission including fission complex formation and Dnm1 adaptor interactions.

The InsB motif is essential for Dnm1 binding to the Mdv1 adaptor

After mitochondrial membrane recruitment and self-assembly, the majority of GFP-tagged Dnm1 can be visualized as puncta on mitochondrial tubules (Fig. 3 A; Otsuga et al., 1998). In contrast, all of the GFP-Dnm1^{InsBmut} proteins failed to associate with mitochondria (Fig. 3 A, a representative cell is shown). Instead, GFP-Dnm1^{InsBmut} proteins assembled into punctuate structures that moved rapidly through the cytoplasm and could not be captured by digital imaging. In a few cells, GFP-Dnm1^{InsBmut} also formed larger, immobile aggregates in the cytoplasm (Fig. 3 A). Importantly, this localization of GFP-Dnm1^{InsBmut} proteins is indistinguishable from that observed for GFP-Dnm1 in cells lacking Fis1 or fission adaptor proteins (Mozdy et al., 2000; Griffin et al., 2005). This observation raised the possibility that mutations in Dnm1^{InsBmut} proteins were disrupting interactions with the Mdv1 adaptor.

In vitro pull-down assays using purified GST-Mdv1 β-propeller and His-tagged Dnm1 showed that the Mdv1 β-propeller domain binds directly to Dnm1 (Fig. S1 B). To determine whether InsB mutations affected the Dnm1–Mdv1 interaction, we performed coIP experiments from *dnm1Δ* cells expressing Myc-tagged Dnm1^{InsBmut} proteins. Although full-length Mdv1 was efficiently coprecipitated by WT Dnm1-Myc, Mdv1 interaction with all of the Dnm1^{InsBmut}-Myc proteins was dramatically reduced (Fig. 3 B). These combined results identify a novel motif in InsB essential for Dnm1–Mdv1 interaction and Dnm1 recruitment to mitochondria.

Suppressors of a *dnm1*^{InsBmut} mutation cluster in the Mdv1 β-propeller

Using an integrated form of the *dnm1*^{F610A} mutation, we performed a suppressor screen to identify residues in Mdv1 important for Dnm1–Mdv1 interaction (see Materials and methods and Table S1). Although the screen covered 84% of the *MDV1*

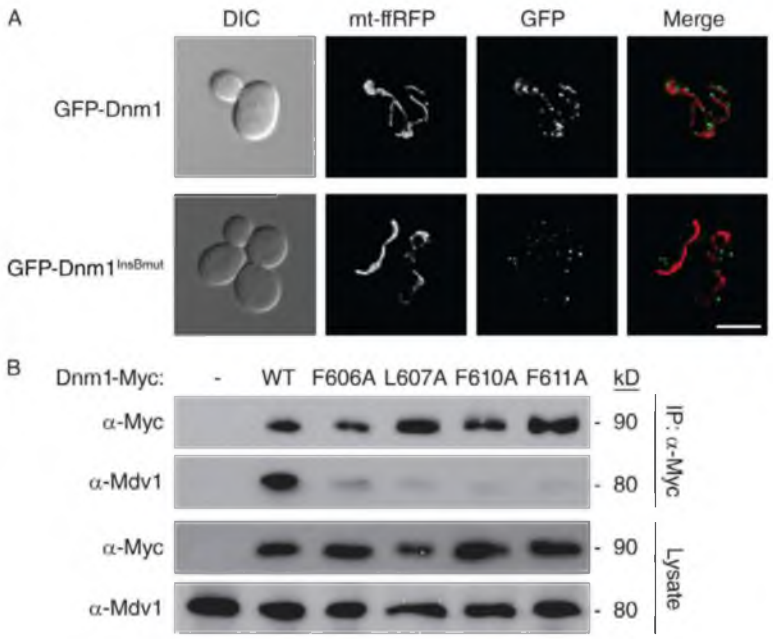

Figure 3. **InsB conserved residues are critical for Dnm1–Mdv1 interaction.** (A) Representative images of GFP-Dnm1 and GFP-Dnm1^{InsBmut} (F606A, L607A, F610A, or F611A) localization in *dnm1Δ* cells. Differential interference contrast microscopy (DIC), mitochondrial matrix-targeted dsRed (mt-ffRFP), GFP, and merged images are shown. Bar, 5 µm. (B) Lysates from cells expressing the indicated C-terminal Myc-tagged Dnm1 were used for immunoprecipitation with anti-Myc agarose beads. Immunoprecipitated fractions (top) and lysates (bottom) were analyzed by SDS-PAGE and Western blotting with anti-Myc and anti-Mdv1 antibodies.

coding sequence, all but one suppressor mutation fell in the Mdv1 β-propeller domain (Fig. 4 A). Most of the affected residues localized to the top of the Mdv1 β-propeller model (Fig. 4 B, right), suggesting that they are part of an interaction interface. Suppressors affecting residues on the bottom of the structure may define an additional binding interface. Two additional mutations, S557C and T558I, lay in a short sequence that was eliminated during homology modeling. These results are consistent with our finding that the Mdv1 β-propeller is sufficient for direct interaction with Dnm1 (Fig. S1 B). The final suppressor mutation altered residue Q288 in the Mdv1 coiled-coil domain. This suppressor was not analyzed further, as the structure and function of the coiled-coil domain has been extensively studied (Koirala et al., 2010; Zhang et al., 2012).

In addition to Mdv1, yeast encodes a second fission adaptor protein called Caf4 (Griffin et al., 2005). Although these two adaptors are paralogues and have similar domain structures, Caf4 is not essential for mitochondrial fission. Sequence alignment revealed that most of the suppressor mutations affected conserved or similar amino acids in the Mdv1 and Caf4 β-propeller domains (Fig. 4 C). This conservation is consistent with an important functional role for these amino acids in vivo.

All but one of the residues (S541) identified in our suppressor screen differ from those reported by others (Cerveny and Jensen, 2003; Naylor et al., 2006). The mutations in these previous studies were selected based on homology modeling with known β-propeller structures, whereas the mutations we identified here were selected by the organism in a suppressor screen and are specifically relevant to defects caused by InsB mutations. The exception, S541, was reported not to have a phenotype when replaced by glutamine (Q) in the full-length Mdv1 protein (Naylor et al., 2006). In contrast, we found that an Mdv1 S541G mutant protein was unable to rescue mitochondrial fission defects in an *mdv1Δ* strain (Table 1). This difference may be because of the different yeast strain backgrounds used in these two studies. It is also possible that mutation to glycine has a more significant effect on local protein structure and flexibility than mutation to glutamine.

Suppressor mutations in the Mdv1 β-propeller rescue mitochondrial fission defects caused by Dnm1^{F610A}

In control studies, the Mdv1 suppressor proteins were all stably expressed in vivo (Fig. S1 C). To verify that the Mdv1 suppressor proteins were capable of rescuing fission, we expressed them from a plasmid in cells lacking WT Mdv1 and expressing Dnm1^{F610A} protein from the genome. All of the Mdv1 suppressors rescued mitochondrial fission defects in this strain (up to 70% rescue). Representative results are shown in Fig. 5 A for the five best rescuing Mdv1 suppressors (Y418C, D539G, D539Y, L540P, and D576G). The same Mdv1 suppressors also rescued mitochondrial morphology defects caused by other Dnm1^{InsBmut} proteins (F606A, L607A, and F611A; Fig. 5 B).

To test whether Mdv1 suppressors could rescue the mitochondrial recruitment of Dnm1^{F610A}, Mdv1 suppressors and GFP-Dnm1^{F610A} were coexpressed in an *mdv1Δdnm1Δ* strain. GFP mitochondrial puncta were visible in up to 70% of these cells (Fig. 5 C). The mitochondrial recruitment and puncta formation by GFP-Dnm1^{F610A} suggested that Dnm1 interaction with the Mdv1 suppressor proteins had been restored. However, this interaction could not be detected in coIP assays, even after chemical cross-linking (unpublished data). Thus, the restored interaction between Dnm1^{F610A} and Mdv1 suppressors is less robust than WT.

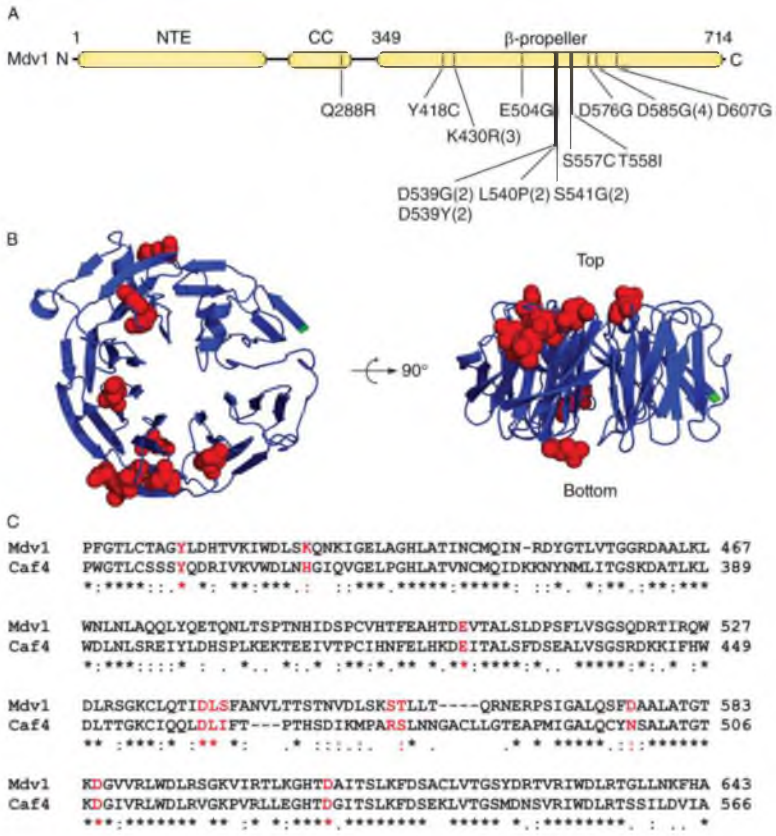

Figure 4. **Suppressors of a *dnm1*^{ins8} mutation cluster in the Mdv1 β-propeller.** (A) Domain structure of Mdv1 with indicated Dnm1^{F610A} suppressor mutations (the number of mutations obtained for each allele is in parentheses). NTE, N-terminal Extension; CC, coiled coil. (B) Top and side views of the Mdv1 β-propeller model (blue). Red indicates residues changed by suppressor mutations. The N terminus is in green. (C) Alignment of the portions of the Mdv1 (aa 408–643) and Caf4 (aa 329–566) β-propeller sequences. Residues affected by suppressor mutations are shown in red. Symbols below the sequence alignment indicate identity (*), strong similarity (:), and weak similarity (.) of amino acids.

Table 1. **Characterization of Mdv1 suppressors of the *dnm1*^{F610A} allele**

Mutations	WT mitochondrial morphology[a]		GFP mitochondrial puncta[b]		Interaction with Dnm1[c]	
	DNM1 mdv1Δ	*dnm1*^{F610A} *mdv1Δ*	Dnm1	Dnm1^{F610A}	Dnm1	Dnm1^{F610A}
	%	%				
Mdv1	67 ± 7	0 ± 0	+	+	+	–
Y418C	6 ± 3	41 ± 16	+	+	++	+
K430R	9 ± 8	28 ± 4	+	+	+	–
E504G	19 ± 8	32 ± 16	+	+	++	–
D539G	9 ± 2	68 ± 11	+	+	++	+
D539Y	11 ± 1	61 ± 14	+	+	++	+
L540P	12 ± 5	58 ± 14	+	+	++	+
S541G	8 ± 4	38 ± 12	+	+	++	+
S557C	9 ± 8	45 ± 8	+	+	++	+
T558I	10 ± 8	34 ± 6	+	+	++	+
D576G	68 ± 17	53 ± 9	+	+	–	–
D585G	45 ± 3	30 ± 8	+	+	–	–
D607G	15 ± 6	31 ± 12	+	+	++	–

[a]Numbers are the mean and standard deviation of at least three independent experiments, $n = 300$.
[b]+, GFP puncta localized to mitochondrial tubules.
[c]Yeast two-hybrid assays. –, No growth on His or Ade minus medium; +, growth on His but not Ade minus medium; ++, growth on both His and Ade minus media. Growth on Ade minus medium is the more stringent indicator of protein–protein interaction.

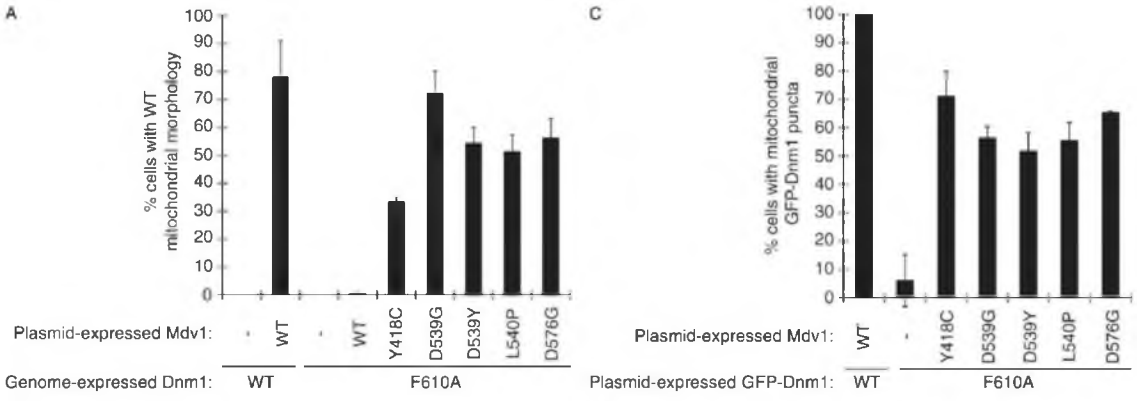

B

Mdv1 suppressors rescue mitochondrial morphology defects caused by Dnm1 InsB mutant proteins

Plasmid-expressed Mdv1	Plasmid-expressed Dnm1		
	F606A	L607A	F611A
WT	7±4	27±3*	1±1
Y418C	56±9	59±2	50±5
D539G	53±13	60±2	53±7
D539Y	55±3	62±8	43±10
L540P	45±3	52±6	41±6
D576G	42±2	51±6	34±6

Numbers are the mean and standard deviation of at least three independent experiments, $n = 300$.

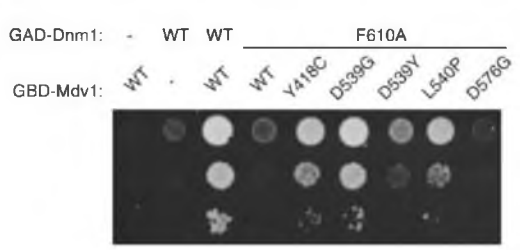

Figure 5. **Suppressor mutations in the Mdv1 β-propeller rescue mitochondrial fission defects caused by Dnm1^{F610A}.** (A) Quantification of mitochondrial morphology in *mdv1Δ DNM1* and *mdv1Δ dnm1::dnm1^{F610A}* strains expressing the indicated Mdv1 suppressor proteins. (B) Quantification of mitochondrial morphology in *mdv1Δdnm1Δ* strains expressing indicated Mdv1 and Dnm1 proteins from plasmids. The mitochondria were visualized with MitoFluor Red 589 (Molecular Probes). (*) Plasmid-expressed WT Mdv1 rescued Dnm1^{L607A} better than genome-expressed WT Mdv1 (Fig. 2 A). This is likely because of the higher steady-state abundance of the plasmid-expressed protein. (C) Quantification of GFP-Dnm1 localization in *mdv1Δ dnm1Δ* cells expressing the indicated Mdv1 and GFP-Dnm1 variants. (A and C) Black columns and error bars represent the mean and standard deviation of at least three independent experiments (A, $n = 300$; C, $n = 150$). (D) pGBD and pGAD plasmids expressing the indicated fusion proteins were cotransformed into the Y187 yeast two-hybrid reporter strain and grown on S-Dextrose minus histidine plates at 30°C for 3 d.

As an alternative, we evaluated Dnm1^{F610A}–Mdv1 suppressor interactions using the yeast two-hybrid growth assay. Previous studies established that WT Dnm1 and WT Mdv1 interact in this assay (Fig. 5 D; Tieu and Nunnari, 2000; Cerveny and Jensen, 2003; Karren et al., 2005). Although the interaction was severely disrupted when Dnm1^{F610A} was paired with WT Mdv1, the interaction was partially (D539Y and L540P) or completely (Y418C and D539G) restored by substituting an Mdv1 suppressor protein for WT Mdv1 (Fig. 5 D). Surprisingly, the Mdv1^{D576G} suppressor protein reproducibly rescued both mitochondrial morphology and GFP-Dnm1^{F610A} localization (Fig. 5, A–C), but was unable to restore growth in the two-hybrid assay (Fig. 5 D). In the morphology rescue and localization studies, binding of Dnm1^{F610A} to this Mdv1 suppressor may be sufficient to recruit Dnm1^{F610A} to the membrane, after which cooligomerization of both proteins into mitochondrial fission complexes could further stabilize the interaction. Such stabilizing forces may be compromised by the spheroplasting/lysis required for coIP studies or by the fusion of both proteins to nuclear targeting sequences used in the two-hybrid assay. This interpretation is supported by our finding that GFP-Mdv1^{D576G} assembled into punctate fission complexes in the presence of Dnm1^{F610A} (Fig. S1 D).

Discussion

Although Dnm1 binding to Mdv1 and recruitment to the mitochondrial membrane is essential for fission, the Dnm1 domains required for this interaction were not known. Here we identify a novel motif in Dnm1 InsB that is specifically required for interaction with the Mdv1 β-propeller. Second-site suppression studies and cell-based assays confirm that the InsB–β-propeller interaction is critical for Dnm1–Mdv1 binding and Dnm1 membrane recruitment. The Dnm1 InsB motif and Mdv1 adaptor sequences required for this interaction are conserved in fungi but not in mammals or plants (Fig. 6). Thus, different InsB domains and adaptors may have coevolved in different organisms to mediate membrane targeting of mitochondrial dynamin-related GTPases.

Our mutational analysis demonstrates that four hydrophobic residues in the Dnm1 InsB motif are necessary for interaction with Mdv1. However, the purified Dnm1 InsB domain (aa

A

Organism	Mitochondrial dynamin adaptor protein (Predicted structural domain)	Ref.
Yeast	Mdv1 (β-propeller)	Tieu et al., 2000 Cerveny et al., 2001
	Caf4 (β-propeller)	Griffin et al., 2005
Mammal	Mff (unknown)	Gandre-Babbe and van der Bliek, 2008 Otera et al., 2010
	MID49/51 (unknown)	Palmer et al., 2011 Zhao et al., 2011
Plant	ELM1 (DUF1022)	Arimura et al., 2008
Red Algae	Mda1 (β-propeller)	Nishida et al., 2007

B

```
ScInsB   NFLSATE----AMDDIMKTRRKRNQELLKSKLSQQENGQTNGINGTSSISSNIDQDSAKN 588
CmInsB   DFIGGNK----AMSQLVRARMEEEERRTRSAKAANSTDNAANSAPKESNANDNRILQPRR 583
AtInsB   NFIGGTKAVEAAMHQVKSSRIPHPVARPKDTVEPDRTSSSTSQVKSRSFLG--RQANGIV 586
HsInsB   DFADACGLMNNNIEEQRRNRLARELPSAVSRDKSSKVPSALAPASQEPSPAASAEADGKL 560

ScInsB   SDYDDDGIDAESKQTKDKFLNYFFGKDKKGQPVFDASDKKRSIAGDGNIEDFRNLQISDF 648
CmInsB   RNQDENAKKNDDARRKDDKSPNKTDASN----AEKDARSDRNPRGDPTMDNFFNEADEDE 639
AtInsB   TDQGVVSADAEKAQPAANASDTRWGIPS----IFRGG-DTRAVTKDSLLNKPFSEAVEDM 641
HsInsB   IQDSRRETKNVASGGGGVGDGVQEPTTGNWRGMLKTSKAEELLAEEKSKPIPIMPASPQK 620

ScInsB   S---------LGDIDDLENAEPP--- 662
CmInsB   EDGNERRNRGLHTLPSVPEHLKAGEV 665
AtInsB   S-----HNLSMIYLKEPPAVLRPTET 662
HsInsB   G--------HAVNLLDVPVPVARK-- 636
```

C

Sequence 1	Sequence 2	% Identity
HsInsB	ScInsB	9
MmInsB	ScInsB	6
HsInsB	MmInsB	94
ScInsB	Fungal InsB	17-39

Figure 6. **Comparison of InsB domains and mitochondrial fission adaptors in different organisms.** (A) Mitochondrial fission adaptors and their predicted structural domains are listed for the indicated organisms. (B) Alignment of Dnm1 InsB sequences from *Saccharomyces cerevisiae* (Sc), *Cyanidioschyzon merolae* (Cm), Arabidopsis *thaliana* (At), and *Homo sapiens* (Hs). The conserved motif in *S. cerevisae* Dnm1 InsB is underlined. Symbols below the sequence alignment indicate identity (*), strong similarity (:), and weak similarity (.) of amino acids. (C) The percentage of amino acid identity between the pairs of InsB sequences in each row is indicated. mM, *Mus musculus*. The range of identities for the fungal homologues includes pairwise comparisons of ScInsB with InsB from all the fungal species listed in Fig. 1 B.

535–639) is not sufficient to bind the Mdv1 β-propeller in vitro (unpublished data). Because the conserved motif in InsB is hydrophobic, it may not adopt a functional conformation when InsB is expressed on its own. In full-length Dnm1, the InsB motif may normally be buried in the interior of the protein. In this case, a conformational change in Dnm1 would be required to expose critical residues in InsB for adaptor binding. A conformational change of this type could be stimulated by GTP binding to Dnm1. This scenario would be consistent with the previous finding that Mdv1 preferentially binds to the GTP-bound form of Dnm1 (Cerveny and Jensen, 2003; Naylor et al., 2006; Lackner et al., 2009).

Our GFP localization and two-hybrid studies established that suppressor mutations in the Mdv1 β-propeller partially restore the interaction of the adaptor with Dnm1^{F610A}. However, this suppression is not allele specific because the suppressor mutations also rescue defects caused by *dnm1*^{F606A}, *dnm1*^{L607A}, and *dnm1*^{F611A} (Fig. 5 B). These results suggest that suppression is not occurring by a classical "lock and key" model. It is possible that the suppressor mutations in the Mdv1 β-propeller increase protein flexibility, allowing them to bind the mutant Dnm1 proteins more efficiently. An alternative explanation is that the suppressor mutations establish new contacts that enhance the interaction between the Mdv1 β-propeller and Dnm1^{F610A}. Although all twelve of the Mdv1 suppressor mutations in the β-propeller were able to recruit and assemble GFP-tagged WT Dnm1 into mitochondrial puncta, ten failed to rescue mitochondrial fission (Table 1, <20% rescue in a *DNM1 mdv1Δ* strain). Interestingly, these ten Mdv1 suppressor proteins exhibit more robust interaction with WT Dnm1 in a two-hybrid assay (Table 1), likely because of the new contacts. When WT Dnm1 is substituted for Dnm1^{F610A}, these new interactions may interfere with post-recruitment and/or assembly steps of mitochondrial fission. The substituted amino acids in the Mdv1 suppressors must be physically close enough to Dnm1 to establish contacts. Thus, the residues affected by the suppressor mutations likely delineate regions of the Mdv1 β-propeller in close proximity to Dnm1.

As new mitochondrial fission components were identified, it became clear that different organisms express unrelated adaptor proteins (Fig. 6 A; Tieu and Nunnari, 2000; Cerveny et al., 2001; Griffin et al., 2005; Nishida et al., 2007; Arimura et al., 2008; Gandre-Babbe and van der Bliek, 2008; Otera et al., 2010; Palmer et al., 2011; Zhao et al., 2011). We propose that the InsB domain provides some of the variability needed to mediate these diverse DRP adaptor interactions. As shown in Fig.

6 (B and C), sequence alignments reveal little identity between InsB domains of fungi, algae, plants, and mammals. Conversely, high identity is observed among InsB sequences of representative mammals (Fig. 6 C, 94%). The functional interaction we observe between Dnm1 InsB and the Mdv1 β-propeller in yeast may be recapitulated for DRP adaptor interactions in other organisms. However, there are almost certainly additional DRP adaptor interfaces that remain to be identified, especially in mammals, where a single DRP is able to interact with several structurally distinct adaptors (Fig. 6 A; Gandre-Babbe and van der Bliek, 2008; Otera et al., 2010; Palmer et al., 2011; Zhao et al., 2011). A recent study showed that mutation of a conserved residue in the Drp1 middle domain disrupts interaction with a mitochondrial adaptor called Mff (Strack and Cribbs, 2012). The model that InsB domains mediate DRP interactions in other organisms can be directly tested in genetic and cellular studies, as well as structural studies of DRPs bound to their cognate adaptor proteins.

Materials and methods

Yeast strains and plasmids

Yeast strains used in this study include JSY5740 (*MATa leu2Δ1 his3Δ200 trp1Δ63 ura3-52 lys2Δ202*), JSY1361 (*MATα leu2Δ1 his3Δ200 trp1Δ63 ura3-52 lys2Δ202 dnm1::HIS3*), JSY9134 (*MATα leu2Δ1 his3Δ200 trp1Δ63 ura3-52 lys2Δ202 mdv1::HIS3 dnm1::HIS3*), JSY9744 (MATα *leu2Δ1 his3Δ200 trp1Δ63 ura3-52 lys2Δ202 mdv1::HIS3 dnm1::dnm1^{F610A} fzo1-1*), JSY9983 (*MATα leu2Δ1 his3Δ200 trp1Δ63 ura3-52 lys2Δ202 mdv1::HIS3 dnm1::dnm1^{F610A}*), JSY3903 (*MATα leu2Δ1 his3Δ200 trp1Δ63 ura3-52 lys2Δ202 mdv1::HIS3*), and JSY5148 (*MATα trp1-901 leu2-3, 112 ura3-52 his3-200 gal4Δ gal80Δ LYS2::GAL1-HIS3, GAL2-ADE2 met2::GAL7-lacZ*).

A list of plasmids used in this study is provided in Table S2. For *pRS415-dnm1^{InsBmut}*, site-directed mutagenesis of a *pRS415-DNM1* template was used to introduce sequences encoding single substitutions F606A, L607A, N608A, Y609A, F610A, F611A, G612A, and K613A. Similar methods were used to generate *pRS415MET25-GFP-dnm1^{InsBmut}*, *pRS425-dnm1^{InsBmut}-MYC*, and *pRS426- dnm1^{InsBmut}-3xHA*. To create *pGAD-C1-DNM1* and *pGAD-C1-dnm1^{F610A}*, BamHI-*DNM1*-SalI and BamHI-*dnm1^{F610A}*-SalI fragments were cloned between the BamHI and SalI sites of the *pGAD-C1* vector. Similarly, BamHI-*MDV1*-SalI and BamHI-*mdv1^{suppressor}*-SalI fragments were cloned between the BamHI and SalI sites of the *pGBD-C1* vector to generate *pGBD-C1-MDV1* and *pGBD-C1-mdv1^{suppressor}*.

Fluorescence microscopy

Mitochondrial morphologies were quantified in WT, *dnm1Δ*, and *dnm1Δmdv1Δ* strains expressing the indicated proteins. The WT morphology category includes unbudded or budded cells with more than two free tubule ends in the mother cell. The formation of GFP-Dnm1 mitochondrial puncta was quantified by analysis of deconvolved epifluorescence images of random fields of cells. Phenotypic quantification is reported as the mean and standard deviation of three independent experiments (total $n \geq 300$ cells unless noted). Unless specified in the figure legend, the mitochondria were visualized by expressing mitochondrial-targeted fast-folding RFP (mt-ffRFP). Dnm1 InsB variants were expressed from the *DNM1* promoter in the *pRS415* vector. GFP-tagged Dnm1 variants were expressed from the *pRS415-MET25* vector. Mdv1 variants were expressed from the *pRS416-MET25* plasmid. Yeast cells were grown at 30°C in selective synthetic dextrose medium containing 0.1 mg/ml methionine. Overnight cultures were diluted to 0.2 OD_{600} and grown for 3–5 h (OD_{600}, 0.5–1.0). The methionine-repressible *MET25* promoter is leaky under these conditions and expresses approximately fourfold more protein at steady state than that expressed from the endogenous *DNM1* or *MDV1* promoters (Karren et al., 2005).

A microscope (Axioplan 2; Carl Zeiss) equipped with a 100x oil immersion objective was used to observe and image cells. For mitochondria and GFP-Dnm1 puncta, 0.275 µm optical sections encompassing the entire yeast cells were deconvolved and analyzed using Axiovision version 4.6 (Carl Zeiss). All slices were projected on the transparency setting and the three-dimensional projections were converted to a single image. Final images were assembled using Photoshop and Illustrator (Adobe). Linear brightness and contrast adjustments were applied to the entire image.

CoIP assays

For Dnm1–Dnm1 interaction experiments, functional HA- and Myc-tagged Dnm1 variants were expressed in *dnm1Δ* cells. CoIPs with anti–c-Myc agarose-conjugated beads (Sigma-Aldrich) were performed as described previously (Koirala et al., 2010). 30 OD_{600} cell equivalents were harvested and resuspended in 500 µl IP buffer (0.5% Triton X-100, 150 mM NaCl, 1 mM EDTA, 50 mM Tris, pH 7.4, and 1:500 protease inhibitor cocktail set III [EMD]). Cells were lysed with glass bead and cleared by centrifugation at 18,000 *g* for 10 min. 400 µl of supernatant was incubated with 40 µl of anti–c-Myc–conjugated agarose beads (Sigma-Aldrich) for 1 h at 4°C. Agarose beads were collected and washed in immunoprecipitation buffer. The bound proteins were released by incubating the beads in 60 µl SDS-PAGE sample buffer lacking β-mercaptoethanol at 60°C for 8 min. 3.2 µl β-mercaptoethanol was added to the samples before boiling. Immunoprecipitated proteins were analyzed by SDS-PAGE and Western blotting with anti-Myc (Santa Cruz Biotechnology, Inc.) and anti-HA (University of Utah Core Facility) antibodies.

Mdv1–Dnm1 interaction was analyzed by coIP after dithiobis(succinimidyl propionate) (DSP) cross-linking in *dnm1Δ* cells expressing endogenous Mdv1 and plasmid-borne Myc-tagged Dnm1 variants (Koirala et al., 2010). 50 OD_{600} cell equivalents were spheroplasted by treating with 0.2 mg/ml zymolase for 60 min at 30°C followed by treatment with 2.5 mM DSP (Thermo Fisher Scientific) at 30°C for 30 min. 50 mM glycine was added to the cell suspensions and all subsequent buffers to quench DSP. Spheroplasts disrupted using a dounce homogenizer (Wheaton) were spun at 18,000 *g* for 10 min. Pellets were solubilized for 10 min at 4°C in 500 µl of immunoprecipitation buffer (1% Triton X-100, 150 mM NaCl, 30 mM Hepes-KOH, pH 7.4, and 1:500 protease inhibitor cocktail set III) and centrifuged at 18,000 *g* for an additional 10 min. 400 µl of supernatant was incubated for 1 h at 4°C with anti-HA–conjugated agarose beads (Sigma-Aldrich). Proteins released from agarose beads were separated by SDS-PAGE and analyzed by ECL Western blotting with anti-Myc and anti-Mdv1 antibodies.

Screen for *mdv1* suppressors of the *dnm1^{F610A}* allele

The growth phenotypes of strains used for this screen are summarized in Table S1. PCR amplification with Taq DNA polymerase was used to introduce random mutations into the *MDV1* coding region. The PCR products were introduced into linearized *pRS416-MET25* using gap repair (Orr-Weaver et al., 1983) in *mdv1Δ dnm1::dnm1^{F610A} fzo1-1* cells. In temperature-sensitive *fzo1-1* cells, ongoing mitochondrial fission causes fragmentation, mitochondrial genome loss, and inability to grow on glycerol medium at 37°C (Hermann et al., 1998). Disrupting fission in this strain by introducing an *mdv1Δ* mutation and expressing *dnm1^{F610A}* from the endogenous *DNM1* locus (*dnm1::dnm1^{F610A}*) prevents mitochondrial fragmentation and genome loss, allowing *mdv1Δ dnm1::dnm1^{F610A} fzo1-1* strains to grow on glycerol at the elevated temperature. Expression of WT Mdv1 from a plasmid does not restore the temperature-sensitive glycerol growth defect in this strain. In contrast, *mdv1Δ dnm1::dnm1^{F610A} fzo1-1* cells expressing Mdv1^{suppressor} from a plasmid fail to grow on glycerol at 37°C, indicating that Mdv1^{suppressor} restores mitochondrial fission. Cells containing Mdv1^{suppressor}-expressing plasmids were identified by their ability to grow on glycerol at 25°C, but not at 37°C. Candidate clones with verified phenotypes were sequenced to identify *MDV1* mutations. In alleles with multiple amino acid changes, mutations were separated by site-directed mutagenesis. Mutations contributing to growth phenotypes were analyzed for mitochondrial morphology and GFP-Dnm1 localization.

Mdv1 β-propeller modeling

The β-propeller model shown in Fig. 4 was generated from the crystal structure of the Cdc4 WD40 repeat (PDB accession no. 1NEX) using the PHYRE Protein Fold Recognition server (Kelley and Sternberg, 2009). Residues 349–713 of Mdv1 are variably modeled as a seven- or an eight-bladed β-propeller, depending on the structures most recently deposited in the PDB. The eight-bladed β-propeller model shown in Fig. 4 includes the majority of residues identified in the second-site suppressor analysis described here.

Yeast two-hybrid analysis

Yeast two-hybrid studies to analyze Dnm1–Mdv1 and Dnm1 self-interactions were performed in the Y187 *S. cerevisiae* strain background (Takara Bio Inc.) via a growth assay as described previously (Guthrie and Fink,

2002). pGAD and pGBD plasmid expressing the indicated fusion proteins were cotransformed into the Y187 reporter strain. Interaction between two fusion proteins leads to expression of one of several reporter genes in this strain, allowing the yeast cells to grow on S-dextrose minus histidine or minus adenine. WT Dnm1–Dnm1^{InsBmut} interactions were performed in cells coexpressing GAD-Dnm1 WT and GBD-Dnm1^{InsBmut}. The Dnm1–Mdv1 interaction was tested in both directions. However, the interaction was only detected when Dnm1 and Mdv1 were fused with the GAD and GBD domains, respectively.

Online supplemental material

Table S1 shows a screen for *mdv1* suppressors of *dnm1*^{F610A}. Table S2 shows the plasmids used in this study. Fig. S1 shows expression, interaction, and assembly properties of Dnm1 and Mdv1 variants. Online supplemental material is available at http://www.jcb.org/cgi/content/full/jcb.201207079/DC1.

We thank Jane Macfarlane for expertise in mutagenesis and plasmid construction, members of the Shaw laboratory for critical discussions, and J. Nunnari for the His-Dnm1 expression plasmid.

Research support was provided by National Institutes of Health grants GM53466 and GM84970 to J.M. Shaw. Sequencing and oligonucleotide synthesis services were provided by University of Utah Core Facilities.

Submitted: 12 July 2012
Accepted: 4 October 2012

References

Arimura, S., M. Fujimoto, Y. Doniwa, N. Kadoya, M. Nakazono, W. Sakamoto, and N. Tsutsumi. 2008. Arabidopsis ELONGATED MITOCHONDRIA1 is required for localization of DYNAMIN-RELATED PROTEIN3A to mitochondrial fission sites. *Plant Cell.* 20:1555–1566. http://dx.doi.org/10.1105/tpc.108.058578

Bhar, D., M.A. Karren, M. Babst, and J.M. Shaw. 2006. Dimeric Dnm1-G385D interacts with Mdv1 on mitochondria and can be stimulated to assemble into fission complexes containing Mdv1 and Fis1. *J. Biol. Chem.* 281:17312–17320. http://dx.doi.org/10.1074/jbc.M513530200

Bleazard, W., J.M. McCaffery, E.J. King, S. Bale, A. Mozdy, Q. Tieu, J. Nunnari, and J.M. Shaw. 1999. The dynamin-related GTPase Dnm1 regulates mitochondrial fission in yeast. *Nat. Cell Biol.* 1:298–304. http://dx.doi.org/10.1038/13014

Cerveny, K.L., and R.E. Jensen. 2003. The WD-repeats of Net2p interact with Dnm1p and Fis1p to regulate division of mitochondria. *Mol. Biol. Cell.* 14:4126–4139. http://dx.doi.org/10.1091/mbc.E03-02-0092

Cerveny, K.L., J.M. McCaffery, and R.E. Jensen. 2001. Division of mitochondria requires a novel DMN1-interacting protein, Net2p. *Mol. Biol. Cell.* 12:309–321.

Chen, H., S.A. Detmer, A.J. Ewald, E.E. Griffin, S.E. Fraser, and D.C. Chan. 2003. Mitofusins Mfn1 and Mfn2 coordinately regulate mitochondrial fusion and are essential for embryonic development. *J. Cell Biol.* 160:189–200. http://dx.doi.org/10.1083/jcb.200211046

Eura, Y., N. Ishihara, S. Yokota, and K. Mihara. 2003. Two mitofusin proteins, mammalian homologues of FZO, with distinct functions are both required for mitochondrial fusion. *J. Biochem.* 134:333–344. http://dx.doi.org/10.1093/jb/mvg150

Faelber, K., Y. Posor, S. Gao, M. Held, Y. Roske, D. Schulze, V. Haucke, F. Noé, and O. Daumke. 2011. Crystal structure of nucleotide-free dynamin. *Nature.* 477:556–560. http://dx.doi.org/10.1038/nature10369

Ford, M.G., S. Jenni, and J. Nunnari. 2011. The crystal structure of dynamin. *Nature.* 477:561–566. http://dx.doi.org/10.1038/nature10441

Gandre-Babbe, S., and A.M. van der Bliek. 2008. The novel tail-anchored membrane protein Mff controls mitochondrial and peroxisomal fission in mammalian cells. *Mol. Biol. Cell.* 19:2402–2412. http://dx.doi.org/10.1091/mbc.E07-12-1287

Gao, H., D. Kadirjan-Kalbach, J.E. Froehlich, and K.W. Osteryoung. 2003. ARC5, a cytosolic dynamin-like protein from plants, is part of the chloroplast division machinery. *Proc. Natl. Acad. Sci. USA.* 100:4328–4333. http://dx.doi.org/10.1073/pnas.0530206100

Griffin, E.E., J. Graumann, and D.C. Chan. 2005. The WD40 protein Caf4p is a component of the mitochondrial fission machinery and recruits Dnm1p to mitochondria. *J. Cell Biol.* 170:237–248. http://dx.doi.org/10.1083/jcb.200503148

Guthrie, C., and G. Fink. 2002. Guide to yeast genetics and molecular biology. *Methods in enzymology series.* Vol. 350. San Diego: Academic Press, Inc.

Hales, K.G., and M.T. Fuller. 1997. Developmentally regulated mitochondrial fusion mediated by a conserved, novel, predicted GTPase. *Cell.* 90:121–129. http://dx.doi.org/10.1016/S0092-8674(00)80319-0

Hermann, G.J., J.W. Thatcher, J.P. Mills, K.G. Hales, M.T. Fuller, J. Nunnari, and J.M. Shaw. 1998. Mitochondrial fusion in yeast requires the transmembrane GTPase Fzo1p. *J. Cell Biol.* 143:359–373. http://dx.doi.org/10.1083/jcb.143.2.359

Hu, J., Y. Shibata, P.P. Zhu, C. Voss, N. Rismanchi, W.A. Prinz, T.A. Rapoport, and C. Blackstone. 2009. A class of dynamin-like GTPases involved in the generation of the tubular ER network. *Cell.* 138:549–561. http://dx.doi.org/10.1016/j.cell.2009.05.025

Karren, M.A., E.M. Coonrod, T.K. Anderson, and J.M. Shaw. 2005. The role of Fis1p–Mdv1p interactions in mitochondrial fission complex assembly. *J. Cell Biol.* 171:291–301. http://dx.doi.org/10.1083/jcb.200506158

Kelley, L.A., and M.J. Sternberg. 2009. Protein structure prediction on the Web: a case study using the Phyre server. *Nat. Protoc.* 4:363–371. http://dx.doi.org/10.1038/nprot.2009.2

Koch, A., M. Thiemann, M. Grabenbauer, Y. Yoon, M.A. McNiven, and M. Schrader. 2003. Dynamin-like protein 1 is involved in peroxisomal fission. *J. Biol. Chem.* 278:8597–8605. http://dx.doi.org/10.1074/jbc.M211761200

Koirala, S., H.T. Bui, H.L. Schubert, D.M. Eckert, C.P. Hill, M.S. Kay, and J.M. Shaw. 2010. Molecular architecture of a dynamin adaptor: implications for assembly of mitochondrial fission complexes. *J. Cell Biol.* 191:1127–1139. http://dx.doi.org/10.1083/jcb.201005046

Kuravi, K., S. Nagotu, A.M. Krikken, K. Sjollema, M. Deckers, R. Erdmann, M. Veenhuis, and I.J. van der Klei. 2006. Dynamin-related proteins Vps1p and Dnm1p control peroxisome abundance in *Saccharomyces cerevisiae*. *J. Cell Sci.* 119:3994–4001. http://dx.doi.org/10.1242/jcs.03166

Labrousse, A.M., M.D. Zappaterra, D.A. Rube, and A.M. van der Bliek. 1999. *C. elegans* dynamin-related protein DRP-1 controls severing of the mitochondrial outer membrane. *Mol. Cell.* 4:815–826. http://dx.doi.org/10.1016/S1097-2765(00)80391-3

Lackner, L.L., J.S. Horner, and J. Nunnari. 2009. Mechanistic analysis of a dynamin effector. *Science.* 325:874–877. http://dx.doi.org/10.1126/science.1176921

Li, X., and S.J. Gould. 2003. The dynamin-like GTPase DLP1 is essential for peroxisome division and is recruited to peroxisomes in part by PEX11. *J. Biol. Chem.* 278:17012–17020. http://dx.doi.org/10.1074/jbc.M212031200

Mears, J.A., P. Ray, and J.E. Hinshaw. 2007. A corkscrew model for dynamin constriction. *Structure.* 15:1190–1202. http://dx.doi.org/10.1016/j.str.2007.08.012

Mears, J.A., L.L. Lackner, S. Fang, E. Ingerman, J. Nunnari, and J.E. Hinshaw. 2011. Conformational changes in Dnm1 support a contractile mechanism for mitochondrial fission. *Nat. Struct. Mol. Biol.* 18:20–26. http://dx.doi.org/10.1038/nsmb.1949

Moss, T.J., C. Andreazza, A. Verma, A. Daga, and J.A. McNew. 2011. Membrane fusion by the GTPase atlastin requires a conserved C-terminal cytoplasmic tail and dimerization through the middle domain. *Proc. Natl. Acad. Sci. USA.* 108:11133–11138. http://dx.doi.org/10.1073/pnas.1105056108

Mozdy, A.D., J.M. McCaffery, and J.M. Shaw. 2000. Dnm1p GTPase-mediated mitochondrial fission is a multi-step process requiring the novel integral membrane component Fis1p. *J. Cell Biol.* 151:367–380. http://dx.doi.org/10.1083/jcb.151.2.367

Naylor, K., E. Ingerman, V. Okreglak, M. Marino, J.E. Hinshaw, and J. Nunnari. 2006. Mdv1 interacts with assembled dnm1 to promote mitochondrial division. *J. Biol. Chem.* 281:2177–2183. http://dx.doi.org/10.1074/jbc.M507943200

Nishida, K., F. Yagisawa, H. Kuroiwa, Y. Yoshida, and T. Kuroiwa. 2007. WD40 protein Mda1 is purified with Dnm1 and forms a dividing ring for mitochondria before Dnm1 in *Cyanidioschyzon merolae*. *Proc. Natl. Acad. Sci. USA.* 104:4736–4741. http://dx.doi.org/10.1073/pnas.0609364104

Orr-Weaver, T.L., J.W. Szostak, and R.J. Rothstein. 1983. Genetic applications of yeast transformation with linear and gapped plasmids. *Methods Enzymol.* 101:228–245. http://dx.doi.org/10.1016/0076-6879(83)01017-4

Orso, G., D. Pendin, S. Liu, J. Tosetto, T.J. Moss, J.E. Faust, M. Micaroni, A. Egorova, A. Martinuzzi, J.A. McNew, and A. Daga. 2009. Homotypic fusion of ER membranes requires the dynamin-like GTPase atlastin. *Nature.* 460:978–983. http://dx.doi.org/10.1038/nature08280

Otera, H., C. Wang, M.M. Cleland, K. Setoguchi, S. Yokota, R.J. Youle, and K. Mihara. 2010. Mff is an essential factor for mitochondrial recruitment of Drp1 during mitochondrial fission in mammalian cells. *J. Cell Biol.* 191:1141–1158. http://dx.doi.org/10.1083/jcb.201007152

Otsuga, D., B.R. Keegan, E. Brisch, J.W. Thatcher, G.J. Hermann, W. Bleazard, and J.M. Shaw. 1998. The dynamin-related GTPase, Dnm1p, controls mi-

tochondrial morphology in yeast. *J. Cell Biol.* 143:333–349. http://dx.doi.org/10.1083/jcb.143.2.333

Palmer, C.S., L.D. Osellame, D. Laine, O.S. Koutsopoulos, A.E. Frazier, and M.T. Ryan. 2011. MiD49 and MiD51, new components of the mitochondrial fission machinery. *EMBO Rep.* 12:565–573. http://dx.doi.org/10.1038/embor.2011.54

Praefcke, G.J., and H.T. McMahon. 2004. The dynamin superfamily: universal membrane tubulation and fission molecules? *Nat. Rev. Mol. Cell Biol.* 5:133–147. http://dx.doi.org/10.1038/nrm1313

Rapaport, D., M. Brunner, W. Neupert, and B. Westermann. 1998. Fzo1p is a mitochondrial outer membrane protein essential for the biogenesis of functional mitochondria in *Saccharomyces cerevisiae*. *J. Biol. Chem.* 273:20150–20155. http://dx.doi.org/10.1074/jbc.273.32.20150

Sesaki, H., and R.E. Jensen. 1999. Division versus fusion: Dnm1p and Fzo1p antagonistically regulate mitochondrial shape. *J. Cell Biol.* 147:699–706. http://dx.doi.org/10.1083/jcb.147.4.699

Strack, S., and J.T. Cribbs. 2012. Allosteric modulation of Drp1 mechanoenzyme assembly and mitochondrial fission by the variable domain. *J. Biol. Chem.* 287:10990–11001. http://dx.doi.org/10.1074/jbc.M112.342105

Tieu, Q., and J. Nunnari. 2000. Mdv1p is a WD repeat protein that interacts with the dynamin-related GTPase, Dnm1p, to trigger mitochondrial division. *J. Cell Biol.* 151:353–366. http://dx.doi.org/10.1083/jcb.151.2.353

van der Bliek, A.M. 1999. Functional diversity in the dynamin family. *Trends Cell Biol.* 9:96–102. http://dx.doi.org/10.1016/S0962-8924(98)01490-1

Zhang, Y., N.C. Chan, H.B. Ngo, H. Gristick, and D.C. Chan. 2012. Crystal structure of mitochondrial fission complex reveals scaffolding function for mitochondrial division 1 (Mdv1) coiled coil. *J. Biol. Chem.* 287:9855–9861. http://dx.doi.org/10.1074/jbc.M111.329359

Zhao, J., T. Liu, S. Jin, X. Wang, M. Qu, P. Uhlén, N. Tomilin, O. Shupliakov, U. Lendahl, and M. Nistér. 2011. Human MIEF1 recruits Drp1 to mitochondrial outer membranes and promotes mitochondrial fusion rather than fission. *EMBO J.* 30:2762–2778. http://dx.doi.org/10.1038/emboj.2011.198

Supplemental material JCB

Bui et al., http://www.jcb.org/cgi/content/full/jcb.201207079/DC1

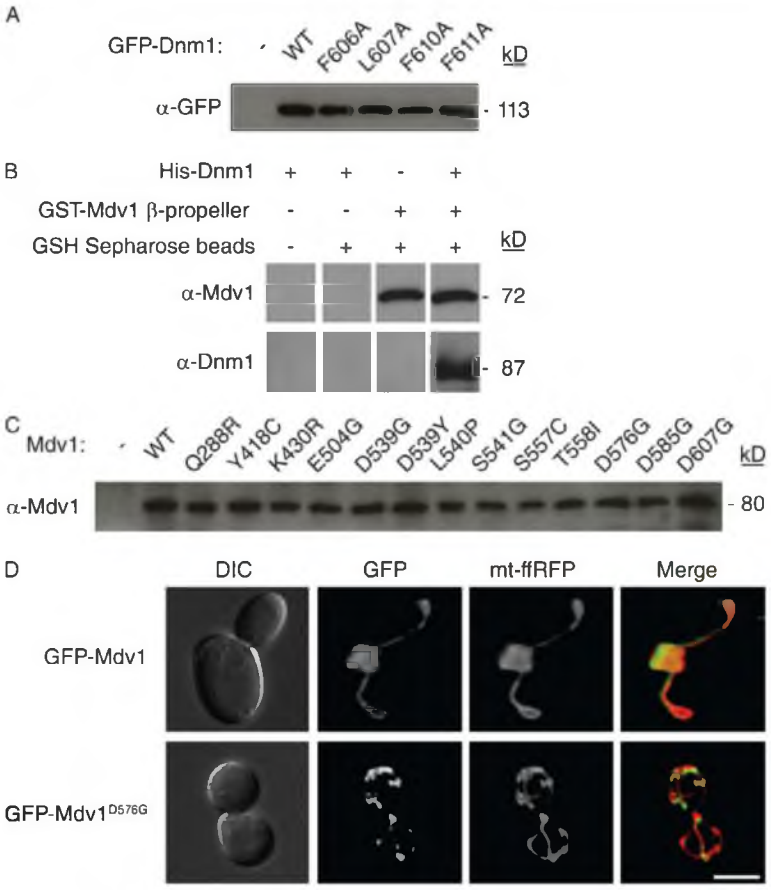

Figure S1. **Expression, interaction, and assembly properties of Dnm1 and Mdv1 variants.** (A) Steady-state abundance of N-terminal GFP-tagged WT and Dnm1^{InsBmut} proteins expressed from a plasmid in *dnm1*Δ cells. Whole cell lysates from 0.5 OD_{600} cell equivalents were separated by SDS-PAGE and immunoblotted with anti-GFP antibody. (B) In vitro GST pull-down assay. Bacterial expressed GST-Mdv1 β-propeller immobilized on glutathione resin was incubated for 2 h at 4°C with purified His-Dnm1 (expressed in insect cells using a plasmid provided by J. Nunnari; Ingerman et al., 2005). After washing, bound proteins were eluted, separated by SDS-PAGE, and immunoblotted with anti-Mdv1 and -Dnm1 antibodies. (C) Steady-state abundance of Mdv1 suppressor proteins. Whole cell lysates from 0.5 OD_{600} cell equivalents were separated by SDS-PAGE and immunoblotted with anti-Mdv1 antibody. (D) Representative images of GFP-Mdv1 and GFP-Mdv1^{D576G} localization in cells expressing Dnm1^{F610A} from the genome. Differential interference contrast microscopy (DIC), mitochondrial matrix-targeted dsRed (mt-ffRFP), GFP, and merged images are shown. Bar, 5 µm.

Table S1. **Screen for *mdv1* suppressors of *dnm1*^{F610A}**

Strain	25°C		37°C	
	Mitochondrial morphology	Glycerol growth	Mitochondrial morphology	Glycerol growth
fzo1-1 (ts) DNM1 MDV1	WT/Not fragmented	Yes	Fragmented	No
fzo1-1 mdv1Δ dnm1::dnm1^{F610A}	Nets	Yes	Not fragmented	Yes
fzo1-1 mdv1Δ dnm1::dnm1^{F610A} *expressing Mdv1*^{WT}	Nets	Yes	Not fragmented	Yes
fzo1-1 mdv1Δ dnm1::dnm1^{F610A} *expressing* ***Mdv1***^{suppressor}	WT/Not fragmented	**Yes**	Fragmented	**No**

See Materials and methods for additional description of genetic screen.

Table S2. **Plasmids used in this study**

ID number	Plasmid	Source
B363	*pRS415-DNM1*	Otsuga et al., 1998
B2901, B2902, B2940-2945	*pRS415-DNM1*$^{(F606A, L607A, N608A, Y609A, F610A, F611A, G612A or K613A)}$	This study
B2144	*pRS415-MET25-GFP-DNM1*	Karren et al., 2005
B2949, B3004-3006	*pRS415-MET25-GFP- DNM1*, *pRS426-DNM1-3xHA*	This study, Karren et al., 2005
B2947, B2973-2975	*pRS426-DNM*$^{(F606A, L607A, F610A or K611A)}$*-3xHA*	This study
B955	*pRS425-DNM1-MYC*	Karren et al., 2005
B2950, B3007-3009	*pRS425-DNM*$^{(F606A, L607A, F610A or F611A)}$*-MYC*	This study
B1642, B1643	*pRS414-GPD-mt-ffRFP, pRS416-GPD-mt-ffRFP*	Karren et al., 2005
B2053	*pRS416-MET25-MDV1*	Karren et al., 2005
B3312-B3323	*pRS416-MET25-MDV1*^{suppressor}	This study
B3324	*pGAD-C1-DNM1*	This study
B3325	*pGAD-C1-DNM1*^{F610A}	This study
B3352	*pGBD-C1-DNM1*	This study
B3353-3356	*pGBD-C1-DNM1*$^{F606A, L607A, F610A, F611A}$	This study
B3326	*pGBD-C1-MDV1*	This study
B3327-3338	*pGBD-C1-MDV1*^{suppressor}	This study
B2455, B2456	*pGAD-C, pGBD-C1*	Guthrie and Fink, 2002

References

Guthrie, C., and G. Fink. 2002. Guide to yeast genetics and molecular biology. *Methods in enzymology series*. Vol. 350. San Diego: Academic Press, Inc.

Ingerman, E., E.M. Perkins, M. Marino, J.A. Mears, J.M. McCaffery, J.E. Hinshaw, and J. Nunnari. 2005. Dnm1 forms spirals that are structurally tailored to fit mitochondria. *J. Cell Biol.* 170:1021–1027. http://dx.doi.org/10.1083/jcb.200506078

Karren, M.A., E.M. Coonrod, T.K. Anderson, and J.M. Shaw. 2005. The role of Fis1p-Mdv1p interactions in mitochondrial fission complex assembly. *J. Cell Biol.* 171:291–301. http://dx.doi.org/10.1083/jcb.200506158

Otsuga, D., B.R. Keegan, E. Brisch, J.W. Thatcher, G.J. Hermann, W. Bleazard, and J.M. Shaw. 1998. The dynamin-related GTPase, Dnm1p, controls mitochondrial morphology in yeast. *J. Cell Biol.* 143:333–349. http://dx.doi.org/10.1083/jcb.143.2.333

CHAPTER 3

MOLECULAR ARCHITECTURE OF A DYNAMIN ADAPTOR: IMPLICATIONS FOR ASSEMBLY OF MITOCHONDRIAL FISSION COMPLEXES

Authors

Sajjan Koirala, Huyen T. Bui, Heidi L. Schubert, Debra Eckert, Christopher P. Hill, Michael S. Kay, and Janet M. Shaw

Molecular architecture of a dynamin adaptor: implications for assembly of mitochondrial fission complexes

Sajjan Koirala, Huyen T. Bui, Heidi L. Schubert, Debra M. Eckert, Christopher P. Hill, Michael S. Kay, and Janet M. Shaw

Department of Biochemistry, University of Utah, Salt Lake City, UT 84112

Recruitment and assembly of some dynamin-related guanosine triphosphatases depends on adaptor proteins restricted to distinct cellular membranes. The yeast Mdv1 adaptor localizes to mitochondria by binding to the membrane protein Fis1. Subsequent Mdv1 binding to the mitochondrial dynamin Dnm1 stimulates Dnm1 assembly into spirals, which encircle and divide the mitochondrial compartment. In this study, we report that dimeric Mdv1 is joined at its center by a 92-Å antiparallel coiled coil (CC). Modeling of the Fis1–Mdv1 complex using available crystal structures suggests that the Mdv1 CC lies parallel to the bilayer with N termini at opposite ends bound to Fis1 and C-terminal β-propeller domains (Dnm1-binding sites) extending into the cytoplasm. A CC length of appropriate length and sequence is necessary for optimal Mdv1 interaction with Fis1 and Dnm1 and is important for proper Dnm1 assembly before membrane scission. Our results provide a framework for understanding how adaptors act as scaffolds to orient and stabilize the assembly of dynamins on membranes.

Introduction

In eukaryotes, mitochondrial fission regulates organelle copy number and mitochondrial function in metabolism, development, and programmed cell death (Chen and Chan, 2005; Okamoto and Shaw, 2005). Fission begins when a dynamin-related GTPase is recruited from the cytoplasm to the outer membrane, where it assembles into large polymers that hydrolyze GTP and sever the mitochondrial compartment. Protein–protein interactions between the GTPase and a membrane-anchored receptor are essential for the recruitment step and are also thought to provide a structural scaffold that promotes GTPase assembly.

The membrane receptor for yeast mitochondrial fission is a complex composed of two proteins, membrane-anchored Fis1 (Mozdy et al., 2000) and its binding partner, Mdv1 (Tieu and Nunnari, 2000; Cerveny et al., 2001; Tieu et al., 2002; Cerveny and Jensen, 2003). Mdv1 functions as an adaptor to bridge the interaction between Fis1 and the cytoplasmic Dnm1 GTPase. Binding of Dnm1 to Mdv1 nucleates the polymerization of Dnm1 dimers into spirals that encircle and constrict the membrane (Bleazard et al., 1999; Ingerman et al., 2005; Bhar et al., 2006; Lackner et al., 2009). Mdv1 coassembles with Dnm1 in these spirals to generate functional fission complexes (Shaw and Nunnari, 2002). Although fission complexes could, in principle, assemble uniformly on the mitochondrial surface, assembly usually occurs at discrete sites on tubular mitochondria in living cells.

The architectural features of the Mdv1–Fis1 receptor required for Dnm1 recruitment and assembly remain unclear. Structural analysis of the Fis1 cytoplasmic domain reveals a single tetratricopeptide repeat (TPR; Suzuki et al., 2005). The N terminus of Mdv1 contains a short, helix-loop-helix motif that surrounds and clamps the surface of the Fis1 TPR domain (Zhang and Chan, 2007). The C terminus of Mdv1, which is required for Dnm1 binding, is predicted to form a multibladed β-propeller. The N- and C-terminal domains are linked by a predicted heptad repeat (HR). Because Mdv1 acts both to recruit Dnm1 and nucleate Dnm1 assembly, defining the structure,

Correspondence to Michael S. Kay: kay@biochem.utah.edu; or Janet M. Shaw: shaw@biochem.utah.edu

Abbreviations used in this paper: CC, coiled coil; CD, circular dichroism; DIC, differential interference contrast; ES, equilibrium sedimentation; HR, heptad repeat; IP, immunoprecipitation; MBP, maltose-binding protein; NTE, N-terminal extension; TPR, tetratricopeptide repeat; WCE, whole cell extract; WT, wild type.

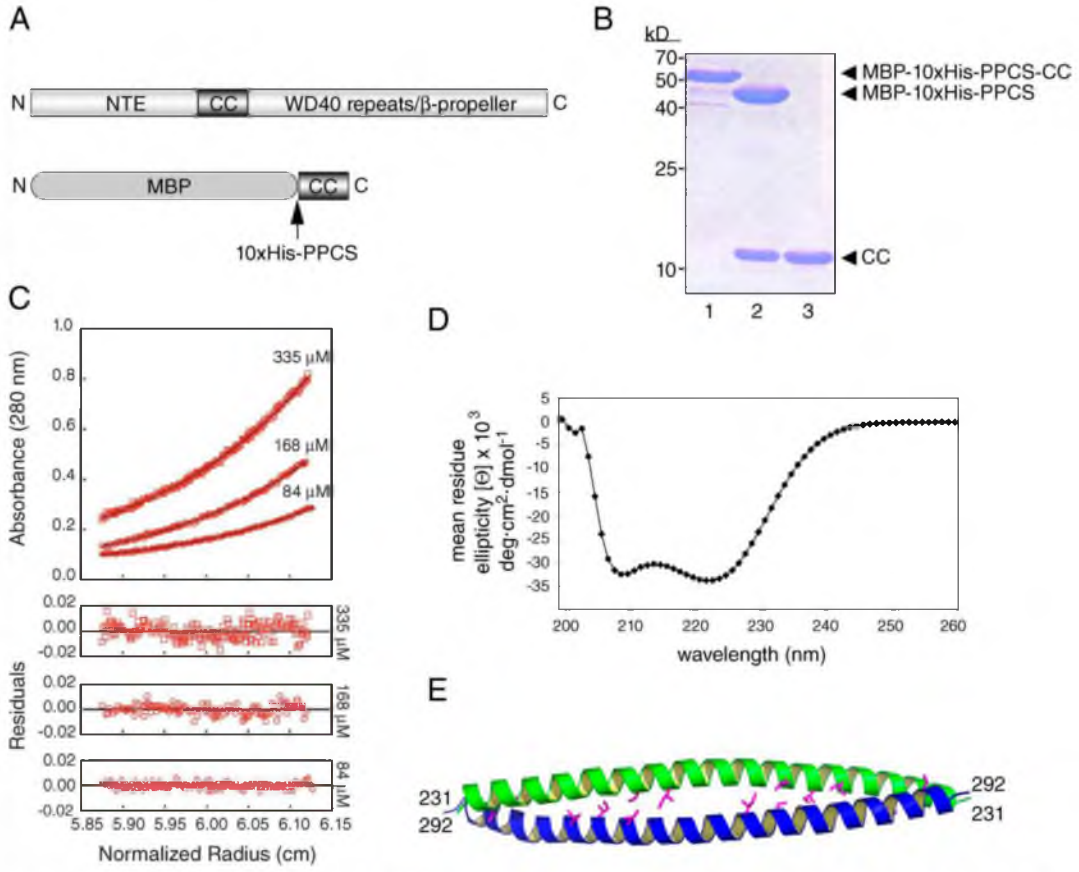

Figure 1. **Mdv1 self-assembles via a dimeric, antiparallel CC.** (A, top) Domain structure of Mdv1, including the NTE, predicted CC, and WD repeats predicted to form a β-propeller. (bottom) The construct used for purification of the Mdv1 CC domain includes the MBP fused to 10xHis, the PreScission protease cleavage site (PPCS), and Mdv1 residues 231–299 (CC; MBP-10xHis-PPCS-CC). (B) SDS-PAGE analysis of purified MBP-10xHis-PPCS-CC fusion protein stained with Coomassie brilliant blue (lane 1), PreScission protease–cleaved MBP-10xHis-PPCS + CC (lane 2), and purified CC (lane 3). (C) Sedimentation equilibrium profile of the Mdv1 CC fragment at the indicated initial loading concentrations (open symbols) with the corresponding fit of 16,263 D ($MW_{obs}/MW_{monomer}$ = 1.95). Residuals for the nonlinear least-squared fits are shown below. (D) CD wavelength scan of $CC^{231–299}$ dimer. (E) Crystal structure of $CC^{231–292}$ dimer at a 2.6-Å resolution. Hydrophobic side chains of residues L233, L237, I251, I254, L268, I272, and I275 are shown in magenta.

oligomeric state, and orientation of this domain is important to understand how Mdv1 initially interacts with the Dnm1 dimer and how this interaction positions the Dnm1 dimer for further polymerization.

In this study, we present the structure of the Mdv1 HR, which forms an unusually long (92 Å) antiparallel coiled coil (CC). We also provide a structural model of dimeric Mdv1 bound to two uncomplexed Fis1 molecules anchored at the mitochondrial membrane. This model shows how the CC positions the two β-propeller domains of Mdv1 to interact with Dnm1 as it transitions from the cytoplasm to mitochondria. In vivo experiments indicate that formation of the Mdv1 antiparallel CC and CC length are important for Fis1 binding, Dnm1 recruitment and assembly, coassembly of Mdv1 into the fission complex, and mitochondrial fission. Surprisingly, restoring Mdv1 oligomerization using a heterologous antiparallel CC rescues Dnm1, but not Fis1, interactions. Thus, the sequence of the Mdv1 CC plays an important but unanticipated role in Mdv1–Fis1 binding. Using a substitution exposed at the surface of the CC, we show that the CC sequence can function to stabilize the Mdv1–Fis1 complex. The combined data reveal new insights into the formation of functional mitochondrial fission complexes.

Results

Structure of the Mdv1 CC

The Mdv1 sequence was analyzed using the MultiCoil CC prediction program (Wolf et al., 1997). The ends (231–299) for the expression construct were chosen based on the total probability score ($P > 0.2$). Mdv1 $CC^{231–299}$ was expressed as a maltose-binding protein (MBP) fusion protein in *Escherichia coli*, released by proteolytic cleavage, and purified to homogeneity (see Materials and methods; Fig. 1, A and B). Equilibrium sedimentation (ES) centrifugation (Fig. 1 C) and circular dichroism (CD) analyses (Fig. 1 D) indicated that Mdv1 $CC^{231–299}$ is a dimer exhibiting double minima typical of a strong α-helix.

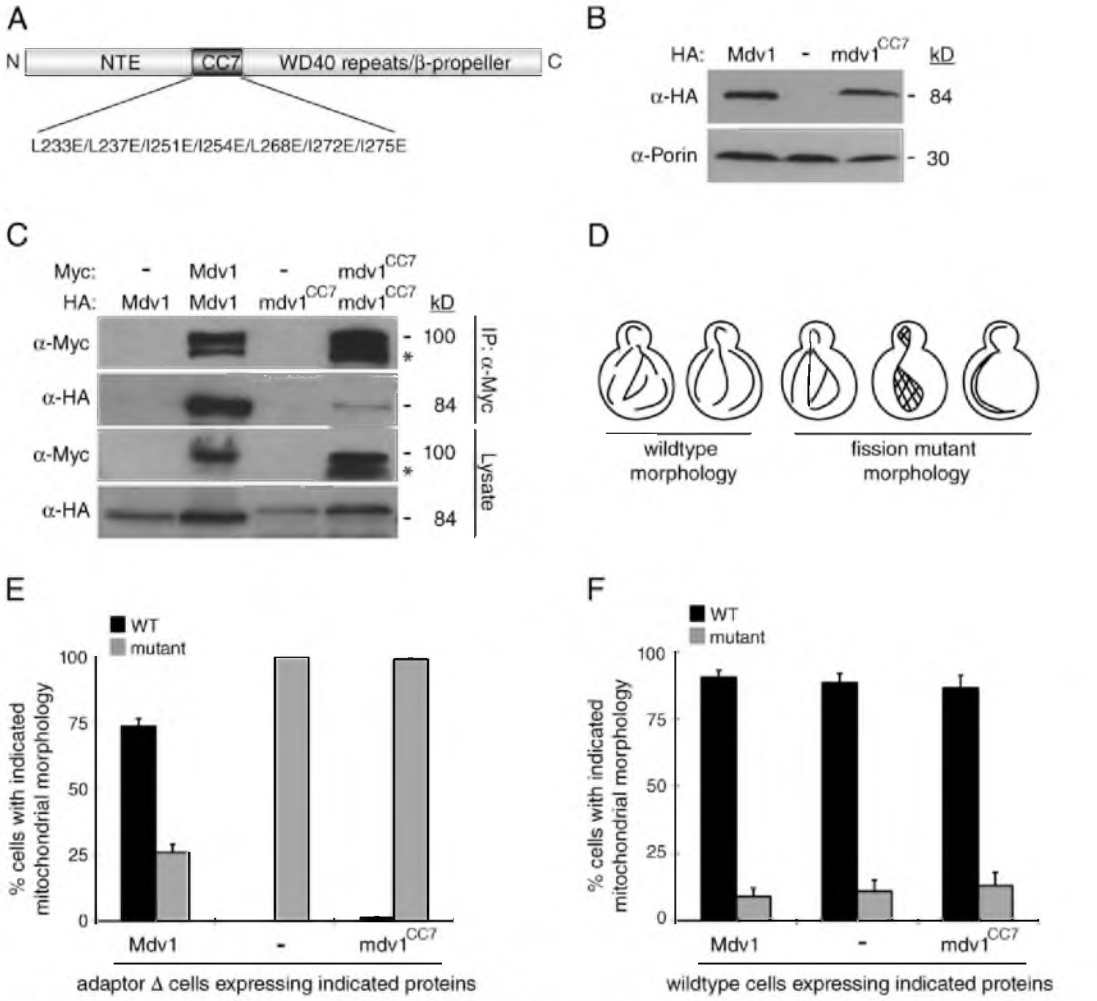

Figure 2. **Disruption of Mdv1 CC formation blocks mitochondrial fission.** (A) Schematic of the mdv1^{CC7} mutant protein. Substitutions introduced at a and d positions in the CC to generate the mdv1^{CC7} mutant protein are listed below the diagram. (B) Steady-state abundance of C-terminal HA-tagged Mdv1 and mdv1^{CC7} mutant proteins expressed in adaptor Δ cells. The mdv1^{CC7} protein sometimes migrates at a higher molecular mass than WT Mdv1 (Figs. 3 A, 4 A, and 6). WCEs separated by SDS-PAGE were immunoblotted with anti-HA and anti-porin antibodies. (C) Lysates from cells expressing the indicated C-terminal Myc- and HA-tagged Mdv1 proteins were used for IP with anti-Myc agarose beads. Lysates (bottom) and immunoprecipitated fractions (top) were analyzed by SDS-PAGE and Western blotting with anti-Myc and anti-HA antibodies. Asterisks mark protein breakdown products. (D) Cartoons depicting mitochondrial morphologies scored in quantification experiments as WT or fission mutant. (E and F) Quantification of mitochondrial morphologies in adaptor Δ (E) or WT (F) cells expressing Mdv1 and mdv1^{CC7} mutant proteins. Black and gray bars and error bars represent the mean and standard deviation of at least three independent experiments (n = 100).

The crystal structure of a selenomethionine-substituted Mdv1 CC$^{231-299}$ construct (L248M and L281M; 2.6 Å; Fig. 1 E and Table S2) revealed that residues 231–292 of this polypeptide fold into a single, 92-Å helix that forms an antiparallel homodimer. This structure is unusual, as intermolecular homodimeric CCs are predominantly parallel. To our knowledge, the structure of only one other homodimeric antiparallel CC of this length (>90 Å) has been reported, also in a protein required for mitochondrial membrane dynamics (Mfn1 HR2, 95 Å; Koshiba et al., 2004). The electrostatic surface of the structure is not highly positive (unpublished data), suggesting that Mdv1 CC$^{231-292}$ does not associate directly with negatively charged lipids exposed at the cytoplasmic face of the outer mitochondrial membrane.

The Mdv1 CC is essential for mitochondrial fission

To determine whether the antiparallel CC interaction in Mdv1 was required for mitochondrial fission, we changed isoleucine and leucine residues contributing to formation of the hydrophobic interface in this structure to glutamate in the full-length protein (Figs. 1 E and 2 A, magenta side chains). Consistent with

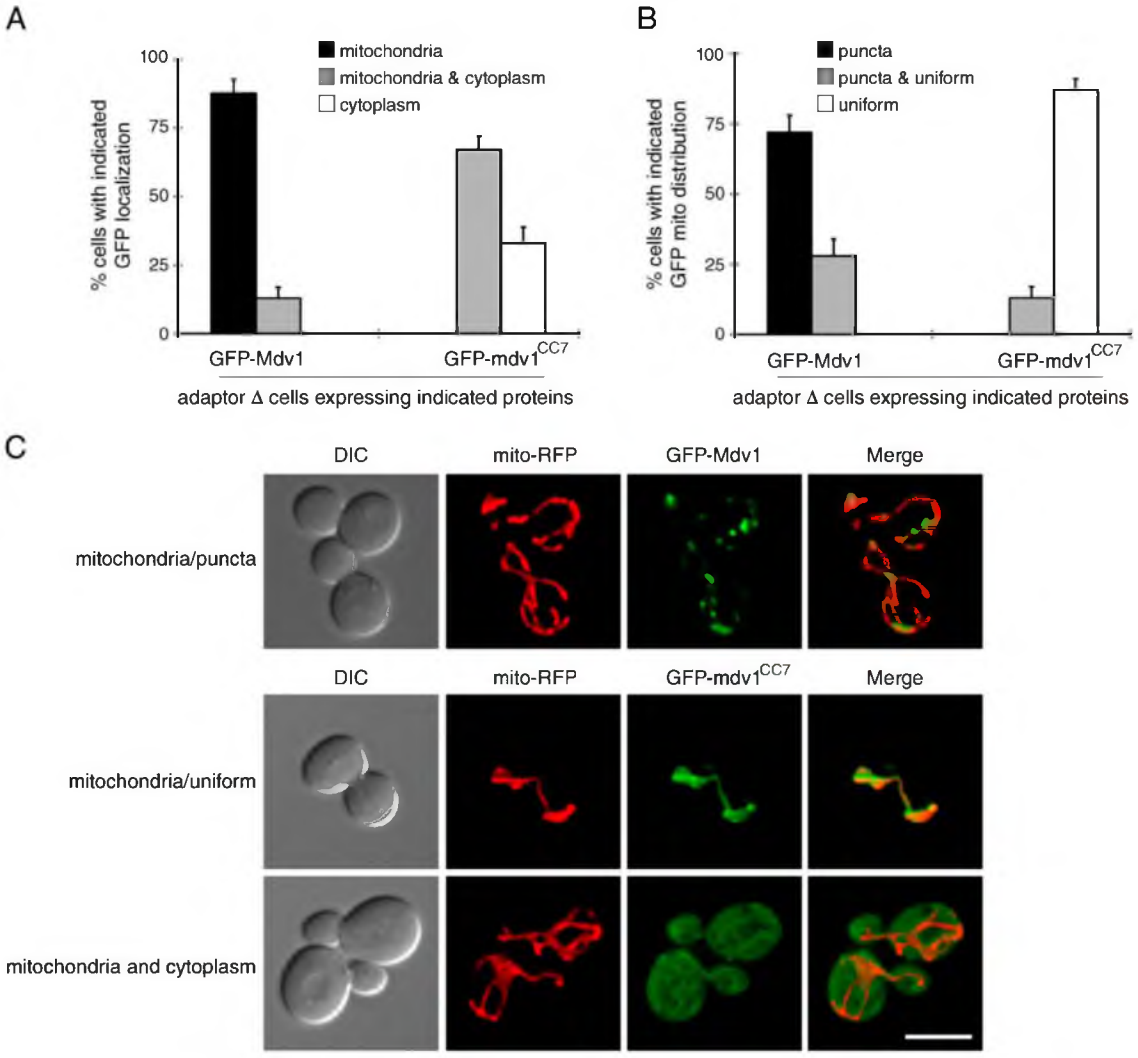

Figure 3. **CC formation promotes mitochondrial recruitment and assembly of the Mdv1 fission adaptor.** (A) Subcellular localization of N-terminal GFP-tagged Mdv1 and mdv1^{CC7} proteins imaged in adaptor Δ cells. (B) Mitochondrial distribution of GFP-tagged Mdv1 and mdv1^{CC7} proteins imaged in adaptor Δ cells. Bars and error bars represent the mean and standard deviation of at least three independent experiments (n = 100). (C) Representative images of GFP-Mdv1 and GFP-mdv1^{CC7} localization and distribution quantified in A and B. DIC, mitochondrial matrix–targeted dsRed (mito-RFP), and merged RFP and GFP images are shown. Bar, 5 μm.

the extended length of this CC, glutamate substitution of all seven isoleucine and leucine residues depicted in Fig. 2 A was necessary to disrupt Mdv1 function (unpublished data). Western blotting of yeast whole cell extracts (WCEs) indicated that the abundance of the mutant adaptor protein, hereafter referred to as mdv1^{CC7}, was similar to that of wild-type (WT) Mdv1 (Figs. 2 B and S4 A). However, these mutations nearly abolished the ability of mdv1^{CC7} to self-interact in coimmunoprecipitation (co-IP) experiments (Fig. 2 C).

We tested the ability of mdv1^{CC7} to support mitochondrial fission in adaptor-null (adaptor Δ) yeast cells lacking Mdv1 and its paralogue Caf4 (Griffin et al., 2005). Although Mdv1 is required for the majority of mitochondrial fission that occurs in vivo, deletion of both Mdv1 and Caf4 is necessary to completely abolish fission. The adaptor Δ strain exhibits severe fission defects, including interconnected, netlike, or collapsed mitochondrial tubules (Fig. 2, D and E). Although expression of Mdv1 restored WT morphology in ~75% of the population, expression of mdv1^{CC7} failed to rescue fission defects (Fig. 2, D and E). Thus, dimerization of Mdv1 via its antiparallel CC plays a critical role in mitochondrial fission. When expressed from the uninduced *MET25* promoter, steady-state abundance of Mdv1 is fourfold higher than that of Mdv1 expressed from its native promoter (Karren et al., 2005; unpublished data). Although expressing

fourfold higher levels of mdv1^{CC7} protein did not cause dominant fission defects in WT cells (Fig. 2 F), dominant-negative fission phenotypes began to appear when expression was further elevated by a 4-h induction of the *MET25* promoter (Fig. S4 C, ~16-fold overexpression). This dominant-negative effect suggests that mdv1^{CC7} continues to interact with one or more of its other two binding partners, effectively interfering with the WT fission machinery.

CC formation promotes mitochondrial recruitment and assembly of the Mdv1 fission adaptor

We used the mdv1^{CC7} mutant protein to test the importance of Mdv1 CC formation for its membrane recruitment. Experiments in intact cells expressing GFP-mdv1^{CC7} revealed that the localization of the mutant protein was compromised relative to WT. In control experiments, the majority of WT GFP-Mdv1 colocalized with RFP-labeled mitochondrial tubules (Fig. 3, A and C, top), whereas a small fraction of cells also displayed dual localization to mitochondria and the cytoplasm (Fig. 3 A). In contrast, GFP-mdv1^{CC7} did not localize exclusively with mitochondria. Instead, yeast cells expressing GFP-mdv1^{CC7} exhibited dual mitochondrial and cytoplasmic localization or exclusively cytoplasmic localization of the adaptor protein (Fig. 3, A and C, bottom). Western blotting indicated that this cytoplasmic localization was not caused by proteolysis and release of GFP from the N terminus of the fusion protein (unpublished data).

After membrane recruitment, localization of a subpopulation of Mdv1 appears punctate because of its coassembly with the Dnm1 GTPase into fission complexes (Tieu and Nunnari, 2000; Cerveny et al., 2001; Griffin et al., 2005; Karren et al., 2005; Naylor et al., 2006). Although mitochondrial localized GFP-Mdv1 was largely punctate (Fig. 3 B), GFP-mdv1^{CC7} failed to coassemble into punctate fission complexes and uniformly labeled mitochondrial membranes in the majority of cells (Fig. 3, B and C, middle). This uniform mitochondrial labeling resulted from association of Mdv1 with Fis1 and was abolished in cells lacking Fis1 (mdv1^{CC7} had no effect on Fis1 localization; unpublished data). These combined data indicate that CC formation promotes both Mdv1 recruitment to Fis1 on mitochondria and subsequent higher order assembly of Mdv1 into fission complexes.

Mitochondrial recruitment and self-assembly of the Dnm1 GTPase requires Mdv1 CC formation

The Dnm1 GTPase interacts with the C terminus of Mdv1 (Tieu et al., 2002; Cerveny and Jensen, 2003), which is predicted to form a multibladed β-propeller. This interaction promotes the self-assembly of Dnm1 into rings and spirals (Lackner et al., 2009) that are visualized as mitochondrial puncta (fission complexes) when labeled with a fluorescent marker (Otsuga et al., 1998). We tested whether Mdv1 dimerization in vivo was required for Mdv1–Dnm1 interaction and Dnm1 assembly into mitochondrial puncta. Although HA-tagged Mdv1 efficiently coprecipitated Dnm1 from cell lysates, complex formation between mdv1^{CC7}-HA and Dnm1 was significantly reduced (Fig. 4 A). This reduced interaction was also apparent in vivo. Although GFP-Dnm1 efficiently assembled into puncta on mitochondria when cells expressed WT Mdv1 (Fig. 4, B and C, top), the fraction of cytoplasmic GFP-Dnm1 increased in cells expressing mdv1^{CC7} (Fig. 4, B and C, bottom). Residual GFP-Dnm1 puncta on mitochondria in mdv1^{CC7}-expressing cells were often smaller and less-evenly distributed on the organelle tubules (Fig. 4 C, middle). This may be caused in part by the fact that mdv1^{CC7} uniformly labels mitochondrial membranes (RFP-mdv1^{CC7}; Fig. 4 D) but does not efficiently coassemble into puncta with Dnm1 (Fig. 3 C, middle and bottom). When combined with our finding that GFP-mdv1^{CC7} fails to form mitochondrial puncta and cannot support fission (Fig. 2 E; and Fig. 3 C, middle and bottom), these results provide a direct demonstration that dimeric Mdv1 must coassemble with the Dnm1 GTPase to form functional fission complexes.

Mdv1 dimerization via a heterologous antiparallel CC partially restores adaptor function

To determine whether physical CC formation was sufficient for adaptor function, we generated a chimeric protein, which replaced the Mdv1 CC with residues 674–734 of the mammalian mitofusin protein Mfn1 (mdv1^{HR2}; Fig. 5 A). In crystallographic experiments, this Mfn1 domain forms an antiparallel CC similar in length to the Mdv1 CC (95 Å; Koshiba et al., 2004). As observed for WT Mdv1, the mdv1^{HR2} chimera was stably expressed (Figs. 5 B and S4 A), localized with mitochondria in differential fractionation and fluorescence microscopy experiments (Figs. 5 C and S1 A), and was able to self-interact in co-IP experiments (Fig. 5 D). Unlike WT Mdv1, mdv1^{HR2} only partially rescued mitochondrial fission and morphology defects in the adaptor Δ strain (Figs. 5 E and S1 B). This partial rescue could not be attributed to defects in mdv1^{HR2}–Dnm1 interactions because mdv1^{HR2}-HA coimmunoprecipitated Dnm1 and the WT adaptor (Fig. 5 F), formed mitochondrial puncta in vivo when labeled with GFP (Fig. S1 C), and also promoted assembly of GFP-Dnm1 into punctate mitochondrial fission complexes (Fig. S1 D). These results were surprising because they suggested that dimerization of Mdv1 via an antiparallel CC is important but not sufficient for the adaptor's function in mitochondrial fission. Instead, the sequence of the Mdv1 CC may also contribute to adaptor function.

The sequence of the Mdv1 CC is critical for interaction with Fis1

We noticed that the mitochondrial localization of mdv1^{HR2} decreased relative to Mdv1 when Dnm1 was absent (Fig. S1 E). Under these conditions, stable mitochondrial association of mdv1^{HR2} depends entirely upon interactions with Fis1. Thus, the inability of mdv1^{HR2} to fully rescue fission defects in vivo could result from a reduced Fis1 interaction. It has been unclear whether the Mdv1 CC is necessary for interaction with Fis1. A crystal structure showed that α-helices in the N-terminal extension (NTE) of fission adaptor proteins bind directly to the cytoplasmic tetratricopeptide domain of Fis1 (Zhang and Chan, 2007). Mutations predicted to disrupt contact sites in this complex interfered with Mdv1–Fis1 interactions and reduced fission in vivo.

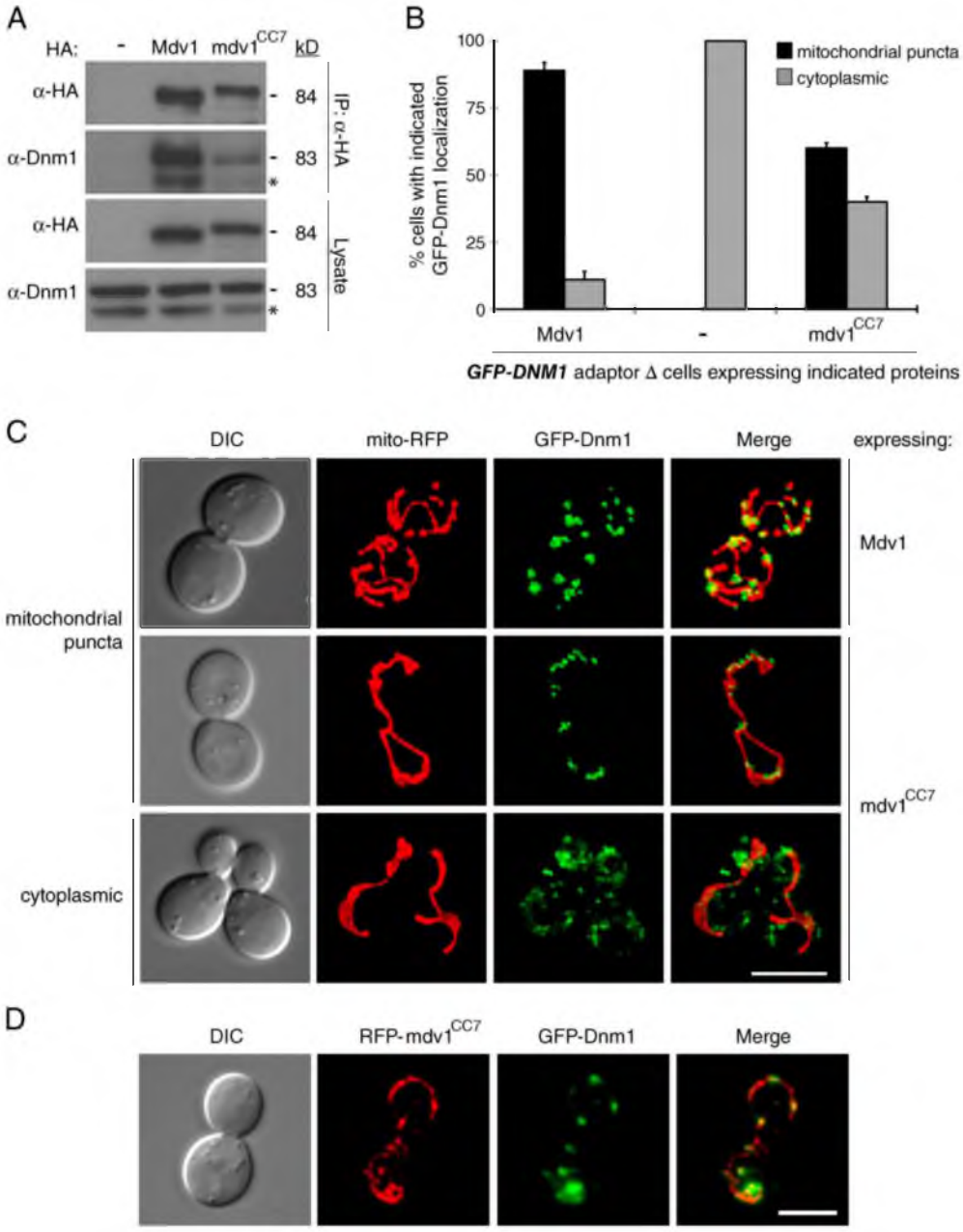

Figure 4. **Efficient Dnm1–Mdv1 interaction and Dnm1 assembly into functional mitochondrial fission complexes requires Mdv1 CC formation.** (A) Lysates from cells expressing the indicated C-terminal HA-tagged Mdv1 proteins were used for IP with anti-HA agarose beads. Lysate (bottom) and immunoprecipitated fractions (top) were analyzed by SDS-PAGE and Western blotting with anti-HA and anti-Dnm1 antibodies. Asterisks mark protein breakdown products. (B) Localization of genomically expressed GFP-Dnm1 in cells expressing Mdv1 or mdv1^{CC7}. Bars and error bars represent the mean and standard deviation of at least three independent experiments (n = 100). (C) Representative images of GFP-Dnm1 localization quantified in B. DIC, mitochondrial matrix–targeted RFP (mito-RFP), GFP-Dnm1, and merged RFP and GFP images are shown. (D) Colocalization of RFP-mdv^{CC7} and GFP-Dnm1. DIC and merged RFP with GFP images are shown. Bars, 5 μm.

However, genetic suppressor experiments from our laboratory suggested that the Mdv1 CC also contributes to the Mdv1–Fis1 interaction. We previously screened for suppressors of a Fis1 protein–destabilizing mutation (*fis1-3*; Karren et al., 2005). *fis1-3* contains E78D, I85T, and Y88H substitutions in the concave surface of the Fis1 TPR domain that destabilize the protein at an

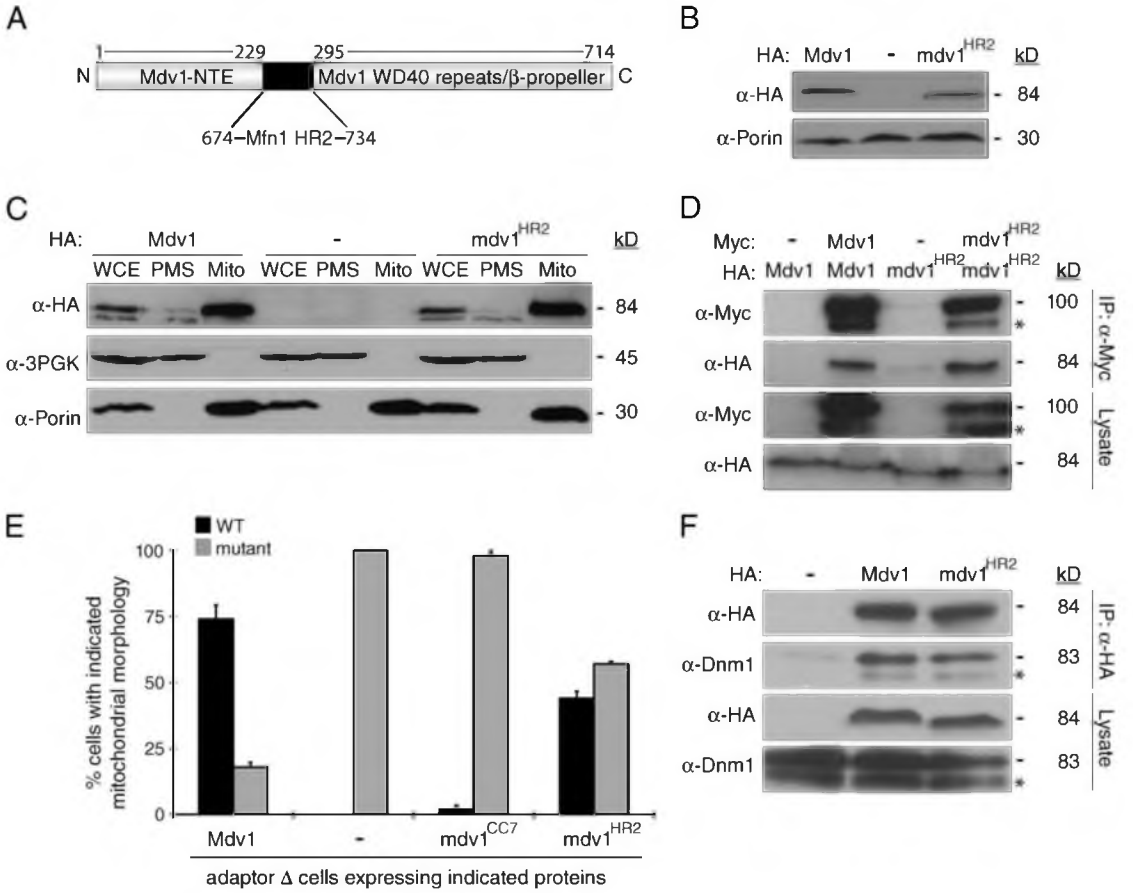

Figure 5. **Dimerization via a heterologous antiparallel CC partially restores Mdv1 adaptor function.** (A) Schematic representation of the mdv1^{HR2} chimera. Residues 230–294 encompassing the Mdv1 antiparallel CC are replaced by residues 674–734 of the Mfn1 HR2 domain. (B) Steady-state abundance of C-terminal HA-tagged Mdv1 and mdv1^{HR2} mutant proteins expressed in fission adaptor Δ cells. WCEs separated by SDS-PAGE were immunoblotted with anti-HA and anti-porin antibodies. (C) Differential sedimentation and Western blot analysis of cytoplasmic 3PGK, mitochondrial porin, and HA-tagged Mdv1 and mdv1^{HR2} proteins in WCE, postmitochondrial supernatant (PMS), and mitochondrial (Mito) fractions. (D) Lysates from cells expressing the indicated C-terminal Myc- and HA-tagged Mdv1 and mdv1^{HR2} proteins were used for IP with anti-Myc agarose beads. Lysate (bottom) and immunoprecipitated fractions (top) were analyzed by SDS-PAGE and Western blotting with anti-HA and anti-Myc antibodies. (E) Quantification of mitochondrial morphologies in adaptor Δ cells expressing Mdv1, mdv1^{CC7} mutant, or mdv1^{HR2} chimeric proteins. Bars and error bars represent the mean and standard deviation of at least three independent experiments (n = 100). (F) Lysates from cells expressing HA-tagged Mdv1 or mdv1^{HR2} were used for IP with anti-HA agarose beads. Lysates (bottom) and immunoprecipitated fractions (top) were analyzed by SDS-PAGE and Western blotting with anti-HA and anti-Dnm1 antibodies. Asterisks mark protein breakdown products.

elevated temperature (37°C). We identified an E250G substitution in the Mdv1 CC domain (at position g in the HR; Fig. S2) that stabilized Mdv1–Fis1 complex formation and restored mitochondrial fission at 37°C in the *fis1-3* strain. These findings strongly suggest that the CC sequence is important for Mdv1–Fis1 interaction. To test this idea, we examined the ability of mdv1^{HR2} to interact with Fis1. As shown in Fig. 6, Myc-tagged Fis1 efficiently coprecipitated HA-tagged Mdv1 from cell lysates, whereas coprecipitation of the CC defective mdv1^{CC7}-HA protein was reduced. Significantly, coprecipitation of mdv1^{HR2}-HA with Myc-Fis1 was also reduced despite the fact that this chimeric adaptor protein can self-interact via the heterologous Mfn1 HR2 domain. Quantification of these Fis1–Mdv1 coIP interactions confirmed that Fis1 complex formation with mdv1^{CC7} and mdv1^{HR2} proteins are reduced, whereas Fis1 interaction with the mdv1^{E250G} suppressor is enhanced relative to WT (Fig. 6 B). The straightforward interpretation of these results is that the sequence of the Mdv1 CC (and not just its dimerization capability) is critical for Mdv1 binding to Fis1 during early steps in fission complex assembly.

The length of the Mdv1 CC is optimized for mitochondrial fission

To test the influence of CC length on Mdv1 function, we generated variants lacking two (mdv1$^{\Delta 2HR}$) or four (mdv1$^{\Delta 4HR}$) HRs of the native Mdv1 CC (Fig. 7 A). Both ΔHR proteins were stably expressed at similar steady-state abundance, continued to self-interact, localized to mitochondria in a Fis1-dependent manner,

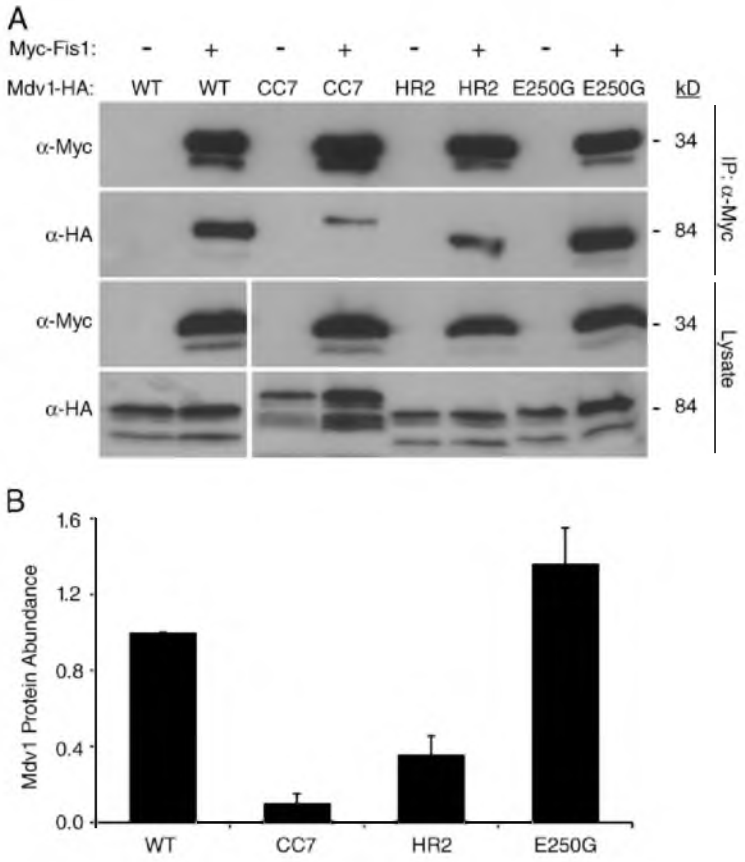

Figure 6. **The Mdv1 CC sequence contributes to efficient Fis1 binding.** (A) Lysates from cells expressing the indicated Mdv1-HA variants and Myc-Fis1 were used for coIP with anti-Myc agarose beads. Lysate (bottom) and IP fractions (top) were analyzed by SDS-PAGE and ECL Western blotting with anti-HA and anti-Myc antibodies. Lower molecular mass bands in all lanes are protein breakdown products. (B) Quantification of coIPs shown in A. Myc- and HA-tagged proteins were detected using a fluorescent secondary antibody followed by scanning on an imaging system. The mean intensity of each Mdv1-HA protein band was normalized to the Myc-Fis1 signal in the same coIP. Bars represent the abundance of Mdv1-HA signal in each coIP relative to the WT. Error bars represent the mean and standard deviation from three independent experiments.

and promoted Dnm1 assembly into mitochondrial fission complexes in vivo (Fig. S3, A, B, and D; Fig. S4, A and B; and not depicted). However, the ΔHR Mdv1 variants did not form mitochondrial puncta as efficiently as WT Mdv1 and exhibited increased uniform labeling of mitochondrial tubules (Fig. S3 C). Moreover, neither ΔHR protein rescued fission defects in the adaptor Δ strain and WT (Fig. 7 B). Thus, the ΔHR Mdv1 variants have a reduced ability to assemble and function in fission. Like the mdv1^{CC7} mutant, the ΔHR variants continued to interact with binding partners in vivo and caused dominant-negative fission defects when overexpressed in a WT strain (Fig. S4 C and not depicted). The dominant-negative defects induced by the ΔHR variants were more severe than those caused by overexpression of mdv1^{CC7} or WT Mdv1, indicating that they have greater ability to interfere with the WT fission machinery in vivo.

We also compared the ability of the ΔHR and E250G Mdv1 variants to restore mitochondrial fission at 25°C and 37°C in cells harboring the *fis1-3* allele. In the *fis1-3 mdv1Δ* strain grown at an elevated temperature, mitochondrial fission is rescued by expression of Mdv1^{E250G} but not WT Mdv1 (Fig. 7 C). The mdv1$^{\Delta 2HR}$ and mdv1$^{\Delta 4HR}$ proteins rescued mitochondrial fission defects at 37°C but less efficiently than Mdv1^{E250G}. In addition, neither mdv1$^{\Delta 2HR}$ nor mdv1$^{\Delta 4HR}$ rescued fission defects and WT or Mdv1^{E250G} at the permissive temperature (25°C).

As with mdv1^{HR2}, we observed that mitochondrial localization of mdv1$^{\Delta 2HR}$ and mdv1$^{\Delta 4HR}$ decreased relative to WT Mdv1 in cells lacking Dnm1 (unpublished data). Because Mdv1 mitochondrial localization in *dnm1Δ* is Fis1 dependent, it is likely that shortening the native Mdv1 CC domain compromises the Fis1–Mdv1 interaction. Based on these combined results, we conclude that the overall length of the native CC is optimized for Mdv1 adaptor function in mitochondrial fission complex assembly and fission.

Discussion

Mdv1 is essential for the membrane recruitment and assembly of the mitochondrial dynamin Dnm1. By combining the new structure of the Mdv1 CC domain with a previously reported Fis1–Mdv1 NTE structure (Zhang and Chan, 2007), we provide a working model for the architecture of the Fis1–Mdv1 complex on the membrane. As depicted in Fig. 8, formation of a 92-Å antiparallel CC between two Mdv1 polypeptides forms an extended dimer. The NTE of each Mdv1 subunit is bound to distinct Fis1 TPR-like domains exposed at the cytoplasmic face of the mitochondrial membrane. Cryo-EM structures suggest that dimeric Dnm1 is the basic subunit for assembly of Dnm1 spirals (Hinshaw, J., personal communication), and two-hybrid

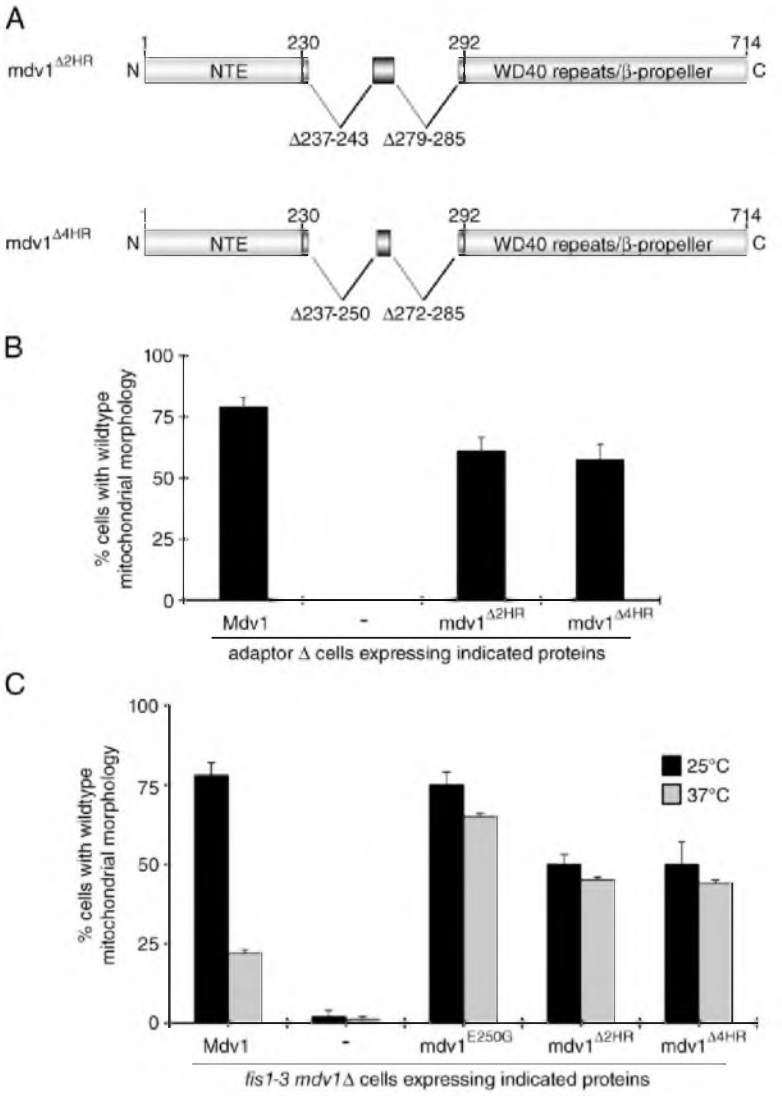

Figure 7. **Effect of CC shortening on Mdv1 function.** (A) Schematic of the mdv1$^{\Delta 2HR}$ and mdv1$^{\Delta 4HR}$ proteins. Residues corresponding to HR deletions are shown below each diagram. (B) Quantification of mitochondrial morphologies in adaptor Δ cells expressing Mdv1, mdv1$^{\Delta 2HR}$, and mdv1$^{\Delta 4HR}$ proteins. (C) Quantification of mitochondrial morphologies at 25 and 37°C in *fis1-3 mdv1Δ* cells expressing WT and mutant Mdv1 proteins. Black and gray bars and error bars represent the mean and standard deviation of at least three independent experiments (n = 100).

and co-IP analyses indicate that the predicted Mdv1 β-propeller domain is sufficient for Dnm1 interaction (Tieu et al., 2002; Cerveny and Jensen, 2003). Thus, Mdv1 β-propeller domains at each end of the CC would provide interaction sites for dimeric Dnm1 recruited from the cytoplasm. Dnm1 dimer binding could occur at the periphery or on the lateral face of one or multiple Mdv1 β-propeller domains. Alternatively, each Mdv1 dimer could bind a single Dnm1 dimer, as suggested by the ~1:1 Mdv1–Dnm1 stoichiometry of complexes assembled in vitro (Lackner et al., 2009). Previous studies identified residues in the Mdv1 β-propeller important for Dnm1 interaction (Cerveny and Jensen, 2003; Naylor et al., 2006); however, it is not known whether these residues make direct contact with Dnm1. Identification of such contact sites and/or structures of protein complexes will be necessary to model Mdv1–Dnm1 binding and determine how this interaction positions Dnm1 dimers to facilitate assembly into spirals. Although the overall length of the native Mdv1 CC is optimized for fission complex assembly and function, our experiments of the ΔHR mdv1 variants indicate that maintaining the length of this CC is not essential for Mdv1 function.

In addition to providing structural stability, Mdv1 dimerization via the CC is critical for the accurate assembly of functional Dnm1 fission complexes. The fraction of monomeric mdv1^{CC7} protein that localizes to mitochondria is sometimes sufficient to recruit and promote the assembly of Dnm1 puncta that resemble fission complexes (Fig. 4 C). However, the morphology of these structures is often qualitatively different from those observed in WT cells, as is their distribution along the mitochondrial tubule. Unlike WT Mdv1, which coassembles with Dnm1 during formation of a functional fission complex,

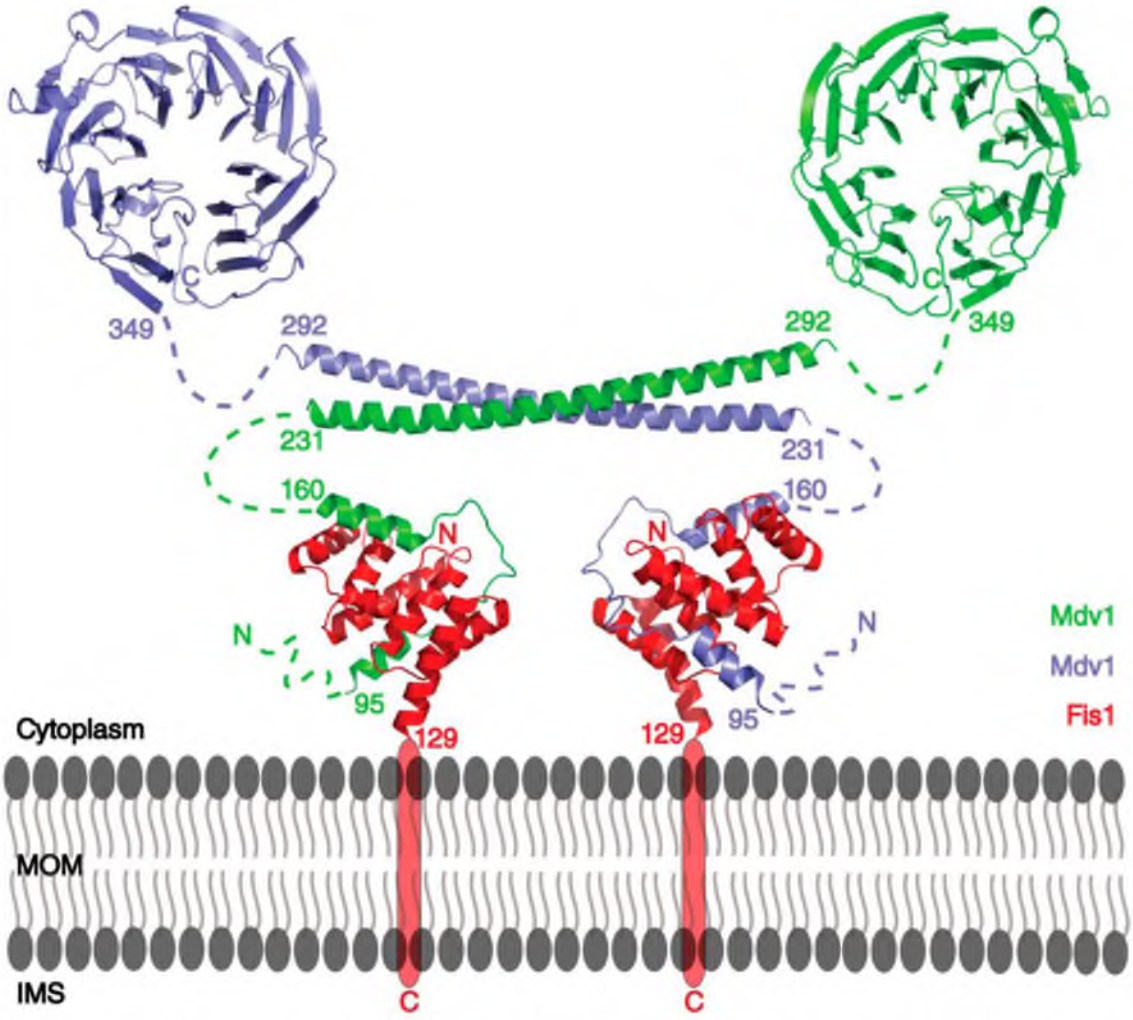

Figure 8. **Molecular architecture of the mitochondrial dynamin-related receptor.** A structural model of the Mdv1 dimer (green/purple) bound to two Fis1 cytoplasmic domains (red) anchored in the outer mitochondrial membrane (gray). The model was generated from crystal structures of the Fis1 cytoplasmic domain in complex with a fission adaptor NTE (Protein Data Bank [PDB] accession no. 2PQR) and the Mdv1 antiparallel CC (PDB accession no. 2XU6). The C-terminal WD40 domain of Mdv1 is shown as a homology model based on the known structure of the Cdc4 WD40 repeat (PDB 1NEX). Loops of variable length and unknown structure connect these two regions to the central CC dimer.

mdv1^{CC7} fails to assemble and form visible puncta in vivo (Fig. 4 D). This last observation is consistent with the idea that a scaffolding function of dimeric Mdv1 is necessary for its inclusion in the Dnm1 polymer as it assembles. The scaffolding model is also supported by our finding that restoring Mdv1 dimerization using a heterologous antiparallel CC rescues mdv1^{HR2} oligomerization and mitochondrial fission defects.

Surprisingly, the rescue provided by mdv1^{HR2} was incomplete, owing to a reduction in the interaction of the chimeric protein with Fis1 (Fig. 6). This result complements our previous finding that an E250G CC substitution stabilizes complex formation between Mdv1 and both WT and mutant Fis1 proteins (Karren et al., 2005). Glu250 lies at heptad position g in the native CC (Fig. S2) and likely participates in an electrostatic interaction that stabilizes a protein–protein interface. In additional experiments, we have shown that mdv1^{E250G} and mdv1^{E250A} substitutions suppress fission defects caused by a mutant Fis1 protein equally well (unpublished data). The E to G substitution is predicted to increase helix flexibility in addition to disrupting a side chain interaction. The E to A substitution should not increase helix flexibility but could also disrupt a side chain interaction. The simplest explanation for these combined findings is that Mdv1 Glu250 negatively regulates Fis1 binding via an Mdv1 self-interaction or interaction with another protein. According to this scenario, both the E to G and E to A substitutions would disrupt this interaction, generating a form of Mdv1 that is constitutively available for partner binding. Because the exact nature of this interaction remains to be determined, it is

not depicted in Fig. 8. A simple binding interface between Fis1 and Mdv1 seems unlikely, as the purified Fis1 cytoplasmic domain is not able to bind the purified Mdv1 CC in vitro (unpublished data).

Fis1–Mdv1 is the only membrane-anchored receptor complex known to function with a dynamin-related GTPase in a membrane fission event. Our experiments provide the first structural model for the presentation of binding sites recognized by the Dnm1 GTPase as it transitions from the cytoplasm to the mitochondrial outer membrane. Although the Fis1–Mdv1 complex is uniformly distributed on the membrane, assembly of Dnm1 and Mdv1 into fission complexes is restricted to discrete sites along the length of the mitochondrial tubule. Thus, post-translational modifications and/or induced conformation changes in the Fis1–Mdv1 complex seem essential to regulate Dnm1 access to the Mdv1 β-propellers. Alternatively, additional factors may act in vivo to stabilize Dnm1 assembly at specific locations and limit its propagation laterally on the membrane. Our results provide a framework for understanding how adaptors act as scaffolds to orient and stabilize the assembly of dynamins on membranes.

Materials and methods

Protein production

Mdv1 residues 231–299 (Mdv1-CC) were fused to the C terminus of MBP via a linker containing 10xHis and the PreScission protease cleavage site (MBP-10xHis-PPCS-CC$^{231–299}$). This construct was expressed in BL21(DE3) codon$^+$ (RIPL; Agilent Technologies) *E. coli* grown in autoinduction medium (Studier, 2005). Overnight cultures, grown in PA-0.5G, were diluted (1:1,000) in ZYP-5052 (MBP-CC) or PASM-5052 (MBP-CC^{SeMet}) and grown at 37°C for 8 h (Studier, 2005). Cultures were transferred to 23°C and grown for an additional 12–36 h before harvesting. All purification steps were performed at 4°C. Proteins were purified by affinity chromatography on amylose resin (New England Biolabs, Inc.) followed by cleavage with PreScission protease (GE Healthcare). After cleavage, Mdv1-CC contained two heterologous N-terminal residues (Gly-Pro). Protein was further purified by mono-Q anion exchange chromatography (GE Healthcare). Residual MBP and uncleaved protein were removed by additional nickel Sepharose (GE Healthcare) and amylose affinity chromatography. Purified Mdv1-CC was dialyzed in CD/ES buffer (50 mM Na-phosphate, pH 7.4, and 150 mM NaCl) or crystallization buffer (20 mM Tris-Cl, pH 7.5, and 100 mM NaCl) and concentrated to 1–10 mg/ml using Centriprep centrifugal concentrators (YM-3; 3 kD NMWL; Millipore).

CD and ES analysis

CD analysis was performed on a CD spectrometer (410; Aviv Biomedical, Inc.). Wavelength scans (200–260 nm) were performed at 23°C on 10 µM protein samples in 50 mM sodium phosphate, pH 7.4, and 150 mM NaCl using a 1-mm path length cuvette with a 5-s averaging time. ES analysis of Mdv1-CC was performed at 4°C using a centrifuge (Optima XL-A; Beckman Coulter) at initial protein subunit concentrations of 335.0, 168.0, and 84.0 µM (monomer) in a buffer containing 50 mM sodium phosphate, pH 7.4, and 150 mM NaCl. Centrifugation was performed at 20,000 rpm (Fig. 1 C) and 25,000 rpm. Resulting equilibrium datasets were globally fit to a single ideal species model with a floating molecular mass using the nonlinear least-squares algorithms in HeteroAnalysis software (Cole, 2004). Protein partial-specific volumes and solvent densities were calculated with the program SEDNTERP (version 1.09; Laue et al., 1992).

Crystallization and structure determination

The protein crystallized in several conditions of the Crystal Screen HT (Hampton Research). After optimization, Mdv1-CC^{SeMet} (10 mg/ml in 20 mM Tris-Cl, pH 7.5, and 100 mM NaCl) was crystallized in 2 µl/2 µl vapor diffusion experiments against a well solution containing 16% PEG 3350, 0.1 M Bis-Tris-Propane, pH 7.5, and 0.4 M NaCl. Flat-plate crystals were cryoprotected in 20% PEG 3350, 0.1 M BTP, pH 7.5, 0.4 M NaCl, and 25% glycerol and flash frozen in liquid nitrogen. Peak and inflection data were collected on beamline (version 7.1; SSRL) and processed with HKL2000 (Otwinowski and Minor, 1997) to a final Rmerge of 5.3% to 2.6 Å. The selenium sites were identified with SOLVE (Terwilliger and Berendzen, 1999), and solvent flattening and preliminary model building with RESOLVE (Terwilliger and Berendzen, 1999) resulted in 60% of the residues correctly positioned. Final model building and validation was performed in COOT (Emsley and Cowtan, 2004). Refinement with REFMAC5 (Murshudov et al., 1997) within the CCP4 suite (Collaborative Computational Project 4, 1994) resulted in a final R_{factor}/R_{merge} of 27.1%/31.1% and a model with good geometric statistics (Table S2).

Yeast strains and plasmids

Yeast strains used in this study include JSY5740 (*MATa leu2Δ1 his3Δ200 trp1Δ63 ura3-52 lys2Δ202*), JSY8612 (*MATa leu2Δ1 his3Δ200 trp1Δ63 ura3-52 lys2Δ202 mdv1::HIS3 caf4::KanMX*; also referred to as the adaptor Δ strain), JSY9465 (*MATa leu2Δ1 his3Δ200 trp1Δ63 ura3-52 lys2Δ202 mdv1::HIS3 caf4::KanMX dnm1::GFP-DNM1*), JSY9135 (*MATa leu2Δ1 his3Δ200 trp1Δ63 ura3-52 lys2Δ202 mdv1::HIS3 caf4::KanMX dnm1::HIS3*), JSY9541 (*MATa leu2Δ1 his3Δ200 trp1Δ63 ura3-52 lys2Δ202 mdv1::HIS3 caf4::KanMX fis1::HIS3*), and JSY7674 (*MATa leu2Δ1 his3Δ200 trp1Δ63 ura3-52 fis1-3 mdv1::HIS3*).

A list of plasmids used in this study is provided in Table S1. To construct *pMAL-c2x-mdv1-CC*, DNA sequences encoding residues 231–299 of *MDV1* were PCR amplified with a forward primer that introduced an EcoRI site, 10xHis, a PreScission Protease cleavage site, and a reverse primer that introduced three stop codons and a HindIII site. The resulting fragment was cloned into the EcoRI and HindIII sites of the *pMAL-c2x* vector (New England Biolabs, Inc.). The *pMAL-c2x-mdv1-CC^{SeMet}* construct was made by site-directed mutagenesis (QuikChange kit; Agilent Technologies) of *pMAL-c2x-mdv1-CC* to change leucine codons to methionine codons at positions encoding residues 248 and 281 in the full-length Mdv1 protein. Construction of *pRS416MET25-MDV1* was described previously (Karren et al., 2005). For *pRS416MET25-mdv1^{CC7}*, sequential site-directed mutagenesis of a *pRS416MET25-MDV1* template was used to introduce sequences encoding the substitutions L233E, L237E, I251E, I254E, L268E, I272E, and I275E. For *pRS415MET25-GFP-MDV1*, pRS415MET25-*GFP-mdv1^{CC7}*, and *pRS415MET25-GFP-mdv1^{HR2}*, PCR-amplified *MDV1*, *mdv1^{CC7}*, and *mdv1^{HR2}* sequences were cloned into the BamHI and SalI sites of *pRS415MET25-GFP*. *pRS415MET25-mdv1^{HR2}* was created using the following five steps: (1) sited-directed mutagenesis was used to introduce two silent restriction endonuclease sites into *MDV1* at nucleotides 628–633 (XmaI) and nucleotides 901–906 (XhoI) in the *pRS416MET25-MDV1* vector, (2) an existing XhoI site in the multiple-cloning site of *pRS416MET25-MDV1* was removed by site-directed mutagenesis, (3) A *$_{yeast}$MDV1-$_{mouse}$MFN1* CC chimeric sequence was synthesized by MR. GENE. The nucleotide sequence of the synthesized *MDV1-MFN1* CC chimera was *XmaI-MDV1(634–687)-MFN1(2022–2202)-MDV1 (883–900)-XhoI*, (4) the CC chimera provided in a vector was excised by XmaI and XhoI digestion and cloned into the same sites of the *pRS416MET25-MDV1* plasmid generated in step 1. To construct, *pRS416MET25-MDV1-13MYC*, *MDV1* was PCR amplified, digested with SpeI and SacII, and cloned into a vector that fused sequence encoding13MYC in frame at the C terminus of Mdv1. *pRS416MET25-mdv1^{CC7}-13MYC* and *pRS416MET25-mdv1^{HR2}-13MYC* were cloned by similar strategies. To create *pRS415MET25-MDV1-3HA*, *MDV1* was PCR amplified, digested, and cloned into the BamHI–XhoI sites of *pRS415MET25-CAF4-3HA*. In the resulting clone, the *CAF4* ORF was replaced by the *MDV1* ORF, and sequence encoding 3HA was fused in frame to the C terminus of Mdv1. A similar strategy was used to generate clones encoding C-terminal 3HA -ogged forms of mdv1^{CC7}, mdv1^{HR2}, and mdv1^{E250G}. For *pRS416MET25-9MYC-FIS1*, *9MYC-FIS1* was excised from *pRS415MET25-9MYC-FIS1* (Karren et al., 2005) using SpeI and XhoI and cloned into *pRS416MET25*. To create *pRS416MET25-mdv1^{Δ2HR}* and *pRS416MET25-mdv1^{Δ4HR}*, DNA encoding mdv1^{Δ2HR} (XmaI-634–708-ΔHR-730–836-ΔHR-855–900-XhoI) or mdv1^{Δ4HR} (XmaI-634–708-ΔΔHR-751–813-ΔΔHR-855–900-XhoI) was synthesized and cloned by Integrated DNA Technologies, Inc. After digestion of the provided plasmids with XmaI and XhoI, the cloned fragments were ligated into silent XmaI and XhoI sites engineered on either side of the encoded Mdv1 CC in *pRS416MET25-MDV1*. *pRS415MET25-mdv1^{Δ2HR}-3HA*, *pRS415MET25-mdv1^{Δ4HR}-3HA*, *pRS415MET25-GFP-mdv1^{Δ2HR}*, and *pRS415MET25-GFP-mdv1^{Δ4HR}* were generated using strategies similar to those described for WT and mutant Mdv1 variants. For *pRS416MET25-ffRFP-mdv1^{CC7}*, a PCR-amplified fragment containing mdv1^{CC7} was digested with BamHI and SalI and ligated into *pRS416MET25-ffRFP*.

Fluorescence microscopy

Mitochondrial morphologies were scored in WT, adaptor Δ, and *fis1-3 mdv1::HIS3* strains as WT (more than two free tubule ends in the mother cell) or fission mutant (less than three free tubule ends in the mother cell). Localization of GFP fusions GFP-Mdv1, GFP-mdv1^{CC7}, GFP-mdv1^{HR2}, GFP-mdv1$^{\Delta 2HR}$, and GFP-mdv1$^{\Delta 4HR}$ were scored in WT or adaptor Δ strains expressing mitochondrial-targeted fast-folding RFP (mito-RFP). GFP-Dnm1 localization/puncta formation was analyzed in the adaptor Δ strain containing genomically integrated *GFP-DNM1*. Overnight cultures grown at 30°C in appropriate synthetic dextrose dropout media containing 0.1 mg/ml methionine were diluted to ∼0.2 OD_{600} and grown for 3–5 h (OD_{600}, 0.5–1.0). Under these conditions, the *MET25* (methionine repressible) promoter is leaky. The abundance of proteins expressed from the uninduced *MET25* promoter was about fourfold greater than that of endogenously expressed Mdv1 (Karren et al., 2005). For analysis of dominant-negative phenotypes, cells were diluted in medium lacking methionine and grown for 4 h before scoring. The steady-state abundance of proteins expressed from the *MET25* promoter after a 4-h induction were ∼3–4-fold higher than that of uninduced Mdv1 expressed from the same promoter (Fig. S4, A and B; Karren et al., 2005). For analysis in the *fis1-3 mdv1::HIS3* strain, cells grown overnight at 25°C were diluted in medium lacking methionine and grown for 2 h at 25 or 37°C before scoring. Phenotypes were analyzed in 100 cells in three or more independent experiments. Data reported are the means of all experiments ($n \geq 3$) with the indicated standard deviations. Images were acquired and processed as described previously (Amiott et al., 2009). Cells were visualized on an imaging microscope (Axioplan 2; Carl Zeiss, Inc.) with a 100× NA 1.4 oil immersion objective. Digital fluorescence and differential interference contrast (DIC) images of cells were acquired using a monochrome digital camera (AxioCam MRm; Carl Zeiss, Inc.). Z stacks of 0.2-µm slices were obtained and deconvolved using AxioVision software (version 4.6; Carl Zeiss, Inc.). Three-dimensional projections of mitochondria were generated with the transparency (voxel) setting and converted to a single image. Final images were processed and assembled using Photoshop and Illustrator (CS3; Adobe). Brightness and contrast were adjusted using only linear operations applied to the entire image.

Analysis of protein expression and targeting

Protein expression was analyzed in WCEs prepared by the alkaline extraction method (Kushnirov, 2000). To analyze subcellular localization of proteins, cells grown in the appropriate synthetic galactose dropout medium were spheroplasted and homogenized to produce WCE, which was subsequently subjected to differential sedimentation to isolate postmitochondrial supernatant and mitochondrial pellet enriched fractions (Kondo-Okamoto et al., 2003). Either 0.5 OD_{600} equivalents of alkaline extract or 50 µg protein of WCE, 50 µg postmitochondrial supernatant, and 25 µg mitochondrial pellet fractions were separated by SDS-PAGE and analyzed by Western blotting using anti-HA (1:2,000; University of Utah Core Facility), anti-PGK (1:2,000; Invitrogen), anti-porin (1:2,000; Invitrogen), and HRP-conjugated secondary goat anti–mouse antibody (1:10,000; Sigma-Aldrich). Proteins were detected by ECL (GE Healthcare). Steady-state abundance of HA-tagged WT and mutant Mdv1 proteins (Fig. S4, A and B) expressed from the *MET25* promoter was determined in adaptor Δ cells grown for 4 h after dilution in selective medium containing 0.1 mg/ml methionine or lacking methionine. Alkali protein extracts (0.25 OD_{600} cell equivalents) separated by SDS-PAGE were analyzed by Western blotting with anti-HA primary antibody and fluorescent secondary antibody followed by detection using a scanner (Odyssey; LI-COR Biosciences). The mean intensity of each HA-tagged protein band was normalized to a control 3PGK protein band in each lane. To determine fold induction of *MET25*-regulated protein expression, normalized HA signals from induced and uninduced samples were compared. Bars in uninduced and induced graphs represent the abundance of HA-tagged signal in each lane relative to WT. Error bars indicate the standard deviation from three independent experiments.

Co-IP assays

For Mdv1–Mdv1 and Mdv1–Fis1 interaction experiments, functional HA- and Myc-tagged Mdv1 and Fis1 proteins and variants were expressed in adaptor Δ cells or adaptor Δ cells lacking *FIS1* (*fis1Δ* adaptor Δ). coIPs were performed with anti–c-Myc agarose-conjugated beads (Sigma-Aldrich) as described previously (Karren et al., 2005; Bhar et al., 2006). In brief, 30 OD_{600} cell equivalents were harvested and lysed with glass beads in 500 µl IP buffer (0.5% Triton X-100, 150 mM NaCl, 1 mM EDTA, 50 mM Tris, pH 7.4, and 1:500 protease inhibitor cocktail set III [EMD]). After centrifugation at 18,000 *g* for 10 min, 400 µl supernatant was incubated with 40 µl anti–c-Myc–conjugated agarose beads (Sigma-Aldrich) for 1 h at 4°C. Agarose beads were collected, washed in IP buffer, and incubated in 60 µl SDS-PAGE sample buffer lacking 2-mercaptoethanol at 60°C for 8 min to release bound proteins. After addition of 3.2 µl 2-mercaptoethanol and boiling, samples were analyzed by SDS-PAGE and Western blotting with anti-Myc (Santa Cruz Biotechnology, Inc.), and anti-HA (University of Utah Core facility) antibodies. Immunoprecipitated proteins were detected using the appropriate HRP-conjugated secondary antibodies and ECL Plus (GE Healthcare) followed by exposure to film. In Fig. 6 B, detection was accomplished using fluorescent secondary antibody (IRDye 800 anti–mouse; LI-COR Biosciences), and signals were quantified using a scanner (Odyssey) and analysis software (Odyssey version 3.0; LI-COR Biosciences).

Mdv1–Dnm1 coIPs were performed using adaptor Δ cells expressing endogenous Dnm1 and plasmid-borne HA-tagged Mdv1 variants as described previously (Karren et al., 2005). 50 OD_{600} U of cells grown at 30°C were treated with 0.2 mg/ml zymolase for 60 min at 30°C. Crosslinking was performed with 2.5 mM dithiobis(succinimidyl propionate) (DSP; Thermo Fisher Scientific) for 30 min at 30°C. DSP was quenched by addition of 50 mM glycine (also present in all subsequent buffers). After homogenization, pellets were collected by spinning at 18,000 *g* for 10 min, solubilized for 10 min at 4°C in 500 µl IP buffer (1% Triton X-100, 150 mM NaCl, 30 mM Hepes-KOH, pH 7.4, and 1:500 protease inhibitor cocktail set III), and cleared by spinning for an additional 10 min at 18,000 *g*. 400 µl cleared supernatant was incubated with 40 µl anti-HA–conjugated agarose beads (Sigma-Aldrich) for 1 h at 4°C. Agarose beads were collected, washed in IP buffer, and bound proteins were released as described in the previous paragraph. Samples were analyzed by SDS-PAGE and ECL Western blotting with anti-HA and anti-Dnm1 antibodies (Otsuga et al., 1998).

Online supplemental material

Fig. S1 shows additional analysis of mdv1^{HR2} localization and function. Fig. S2 shows that Glu250 is exposed on one face of the dimeric antiparallel CC. Fig. S3 shows an additional analysis of mdv1^{D2HR} and mdv1^{D4HR} proteins. Fig. S4 shows dominant-negative effects of WT and mutant Mdv1 proteins. Table S1 shows plasmids used in this study. Table S2 shows x-ray data and model statistics. Online supplemental material is available at http://www.jcb.org/cgi/content/full/jcb.201005046/DC1.

We thank Jane Macfarlane for expertise in mutagenesis and plasmid construction, Steve Alam for advice regarding protein purification, and members of the Shaw laboratory for critical discussions.

Research support was provided by the National Institutes of Health (grants GM53466 to J.M. Shaw, GM59135 to C.P. Hill, and GM82545 to M.S. Kay). Support for sequencing, antibody, and oligonucleotide services at the University of Utah is provided by the National Institutes of Health Center for Cancer Research Resources (grant M01RR00064). Portions of this research were carried out at the Stanford Synchrotron Radiation Light Source (SSRL) Office of Basic Energy Sciences, a national user facility operated by Stanford University on behalf of the U.S. Department of Energy. The SSRL Structural Molecular Biology Program is supported by the Department of Energy, the Office of Biological and Environmental Research, and the National Institutes of Health, National Center for Research Resources, Biomedical Technology Program, and National Institute of General Medical Sciences.

Submitted: 11 May 2010
Accepted: 8 November 2010

References

Amiott, E.A., M.M. Cohen, Y. Saint-Georges, A.M. Weissman, and J.M. Shaw. 2009. A mutation associated with CMT2A neuropathy causes defects in Fzo1 GTP hydrolysis, ubiquitylation, and protein turnover. *Mol. Biol. Cell.* 20:5026–5035. doi:10.1091/mbc.E09-07-0622

Bhar, D., M.A. Karren, M. Babst, and J.M. Shaw. 2006. Dimeric Dnm1-G385D interacts with Mdv1 on mitochondria and can be stimulated to assemble into fission complexes containing Mdv1 and Fis1. *J. Biol. Chem.* 281:17312–17320. doi:10.1074/jbc.M513530200

Bleazard, W., J.M. McCaffery, E.J. King, S. Bale, A. Mozdy, Q. Tieu, J. Nunnari, and J.M. Shaw. 1999. The dynamin-related GTPase Dnm1 regulates mitochondrial fission in yeast. *Nat. Cell Biol.* 1:298–304. doi:10.1038/13014

Collaborative Computational Project 4. 1994. The CCP4 suite: programs for protein crystallography. *Acta Crystallogr. D. Biol. Crystallogr.* D50:760–763.

Cerveny, K.L., and R.E. Jensen. 2003. The WD-repeats of Net2p interact with Dnm1p and Fis1p to regulate division of mitochondria. *Mol. Biol. Cell.* 14:4126–4139. doi:10.1091/mbc.E03-02-0092

Cerveny, K.L., J.M. McCaffery, and R.E. Jensen. 2001. Division of mitochondria requires a novel DMN1-interacting protein, Net2p. *Mol. Biol. Cell.* 12:309–321.

Chen, H., and D.C. Chan. 2005. Emerging functions of mammalian mitochondrial fusion and fission. *Hum. Mol. Genet.* 2:R283–R289. doi:10.1093/hmg/ddi270

Cole, J.L. 2004. Analysis of heterogeneous interactions. *Methods Enzymol.* 384:212–232. doi:10.1016/S0076-6879(04)84013-8

Emsley, P., and K. Cowtan. 2004. Coot: model-building tools for molecular graphics. *Acta Crystallogr. D Biol. Crystallogr.* 60:2126–2132. doi:10.1107/S0907444904019158

Griffin, E.E., J. Graumann, and D.C. Chan. 2005. The WD40 protein Caf4p is a component of the mitochondrial fission machinery and recruits Dnm1p to mitochondria. *J. Cell Biol.* 170:237–248. doi:10.1083/jcb.200503148

Ingerman, E., E.M. Perkins, M. Marino, J.A. Mears, J.M. McCaffery, J.E. Hinshaw, and J. Nunnari. 2005. Dnm1 forms spirals that are structurally tailored to fit mitochondria. *J. Cell Biol.* 170:1021–1027. doi:10.1083/jcb.200506078

Karren, M.A., E.M. Coonrod, T.K. Anderson, and J.M. Shaw. 2005. The role of Fis1p-Mdv1p interactions in mitochondrial fission complex assembly. *J. Cell Biol.* 171:291–301. doi:10.1083/jcb.200506158

Kondo-Okamoto, N., J.M. Shaw, and K. Okamoto. 2003. Mmm1p spans both the outer and inner mitochondrial membranes and contains distinct domains for targeting and foci formation. *J. Biol. Chem.* 278:48997–49005. doi:10.1074/jbc.M308436200

Koshiba, T., S.A. Detmer, J.T. Kaiser, H. Chen, J.M. McCaffery, and D.C. Chan. 2004. Structural basis of mitochondrial tethering by mitofusin complexes. *Science.* 305:858–862. doi:10.1126/science.1099793

Kushnirov, V.V. 2000. Rapid and reliable protein extraction from yeast. *Yeast.* 16:857–860. doi:10.1002/1097-0061(20000630)16:9<857::AID-YEA561>3.0.CO;2-B

Lackner, L.L., J.S. Horner, and J. Nunnari. 2009. Mechanistic analysis of a dynamin effector. *Science.* 325:874–877. doi:10.1126/science.1176921

Laue, T., B. Shah, T. Ridgeway, and S. Pelletier. 1992. Computer-aided interpretation of analytical sedimentation data for proteins. *In* Analytical Ultracentrifugation in Biochemistry and Polymer Science. Royal Society of Chemistry, Cambridge, England, UK. 90–125.

Mozdy, A.D., J.M. McCaffery, and J.M. Shaw. 2000. Dnm1p GTPase-mediated mitochondrial fission is a multi-step process requiring the novel integral membrane component Fis1p. *J. Cell Biol.* 151:367–380. doi:10.1083/jcb.151.2.367

Murshudov, G.N., A.A. Vagin, and E.J. Dodson. 1997. Refinement of macromolecular structures by the maximum-likelihood method. *Acta Crystallogr. D Biol. Crystallogr.* 53:240–255. doi:10.1107/S0907444996012255

Naylor, K., E. Ingerman, V. Okreglak, M. Marino, J.E. Hinshaw, and J. Nunnari. 2006. Mdv1 interacts with assembled dnm1 to promote mitochondrial division. *J. Biol. Chem.* 281:2177–2183. doi:10.1074/jbc.M507943200

Okamoto, K., and J.M. Shaw. 2005. Mitochondrial morphology and dynamics in yeast and multicellular eukaryotes. *Annu. Rev. Genet.* 39:503–536. doi:10.1146/annurev.genet.38.072902.093019

Otsuga, D., B.R. Keegan, E. Brisch, J.W. Thatcher, G.J. Hermann, W. Bleazard, and J.M. Shaw. 1998. The dynamin-related GTPase, Dnm1p, controls mitochondrial morphology in yeast. *J. Cell Biol.* 143:333–349. doi:10.1083/jcb.143.2.333

Otwinowski, Z., and W. Minor. 1997. Processing of x-ray diffraction data collected in oscillation mode. *In* Methods in Enzymology, Macromolecular Crystallography, part A. Vol. 276. C.W. Carter, Jr. and R.M. Sweet, editors. Academic Press, New York. 307–326.

Shaw, J.M., and J. Nunnari. 2002. Mitochondrial dynamics and division in budding yeast. *Trends Cell Biol.* 12:178–184. doi:10.1016/S0962-8924(01)02246-2

Studier, F.W. 2005. Protein production by auto-induction in high density shaking cultures. *Protein Expr. Purif.* 41:207–234. doi:10.1016/j.pep.2005.01.016

Suzuki, M., A. Neutzner, N. Tjandra, and R.J. Youle. 2005. Novel structure of the N terminus in yeast Fis1 correlates with a specialized function in mitochondrial fission. *J. Biol. Chem.* 280:21444–21452. doi:10.1074/jbc.M414092200

Terwilliger, T.C., and J. Berendzen. 1999. Automated MAD and MIR structure solution. *Acta Crystallogr. D Biol. Crystallogr.* 55:849–861. doi:10.1107/S0907444999000839

Tieu, Q., and J. Nunnari. 2000. Mdv1p is a WD repeat protein that interacts with the dynamin-related GTPase, Dnm1p, to trigger mitochondrial division. *J. Cell Biol.* 151:353–366. doi:10.1083/jcb.151.2.353

Tieu, Q., V. Okreglak, K. Naylor, and J. Nunnari. 2002. The WD repeat protein, Mdv1p, functions as a molecular adaptor by interacting with Dnm1p and Fis1p during mitochondrial fission. *J. Cell Biol.* 158:445–452. doi:10.1083/jcb.200205031

Wolf, E., P.S. Kim, and B. Berger. 1997. MultiCoil: a program for predicting two- and three-stranded coiled coils. *Protein Sci.* 6:1179–1189. doi:10.1002/pro.5560060606

Zhang, Y., and D.C. Chan. 2007. Structural basis for recruitment of mitochondrial fission complexes by Fis1. *Proc. Natl. Acad. Sci. USA.* 104:18526–18530. doi:10.1073/pnas.0706441104

Supplemental material JCB

Koirala et al., http://www.jcb.org/cgi/content/full/jcb.201005046/DC1

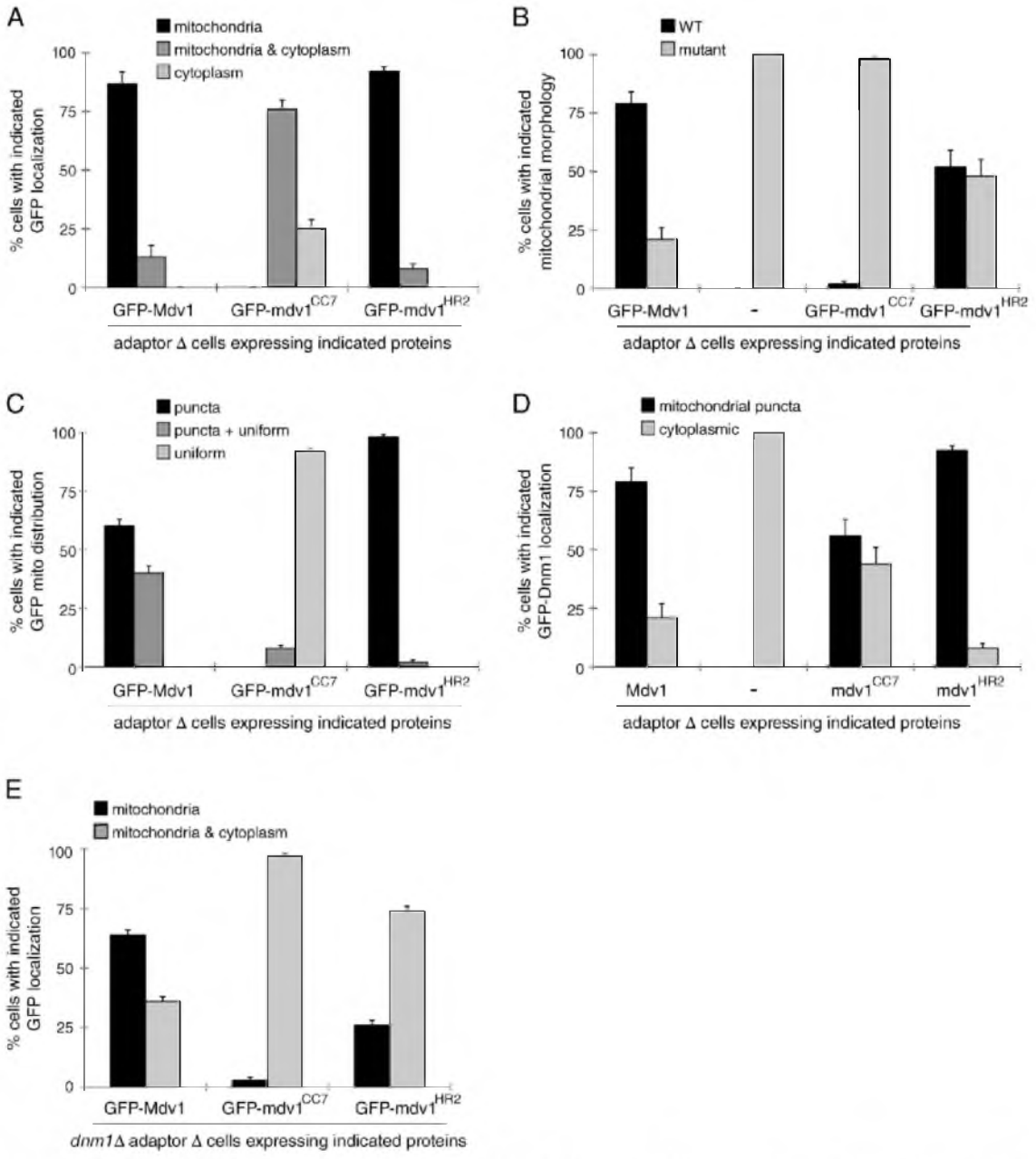

Figure S1. **Additional Analysis of mdv1^{HR2} localization and function.** (A) Subcellular localization of N-terminal GFP-tagged Mdv1, mdv1^{CC7}, and mdv1^{HR2} proteins in adaptor Δ cells. (B) Mitochondrial morphologies in adaptor Δ cells expressing GFP-tagged Mdv1, mdv1^{CC7}, and mdv1^{HR2} proteins. (C) Mitochondrial distribution of GFP-tagged Mdv1, mdv1^{CC7}, and mdv1^{HR2} proteins. (D) Localization of genomically expressed GFP-Dnm1 in cells expressing Mdv1, mdv1^{CC7}, or mdv1^{HR2}. (E) Subcellular localization of GFP-tagged Mdv1, mdv1^{CC7}, and mdv1^{HR2} proteins in *dnm1*Δ adaptor Δ cells. Error bars represent the mean and standard deviation of at least three independent experiments (n = 100).

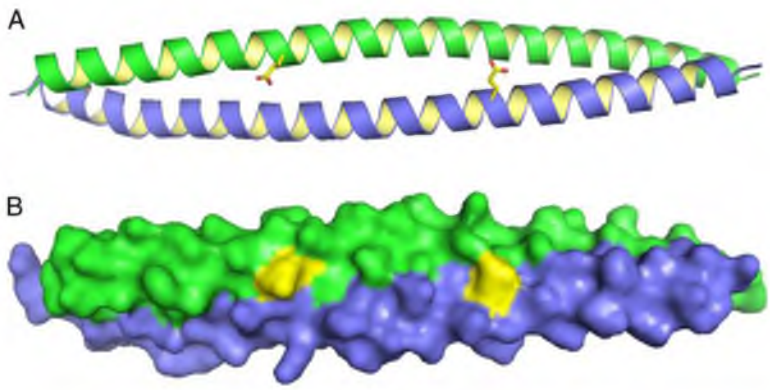

Figure S2. **Glu250 is exposed on one face of the dimeric antiparallel CC.** (A and B) Positions of E250 residues on the Mdv1 CC structure are shown as yellow side chains on the ribbon structure (A) and as yellow patches on the space-filling model (B). The different α-helices in the CC are shown in green and blue.

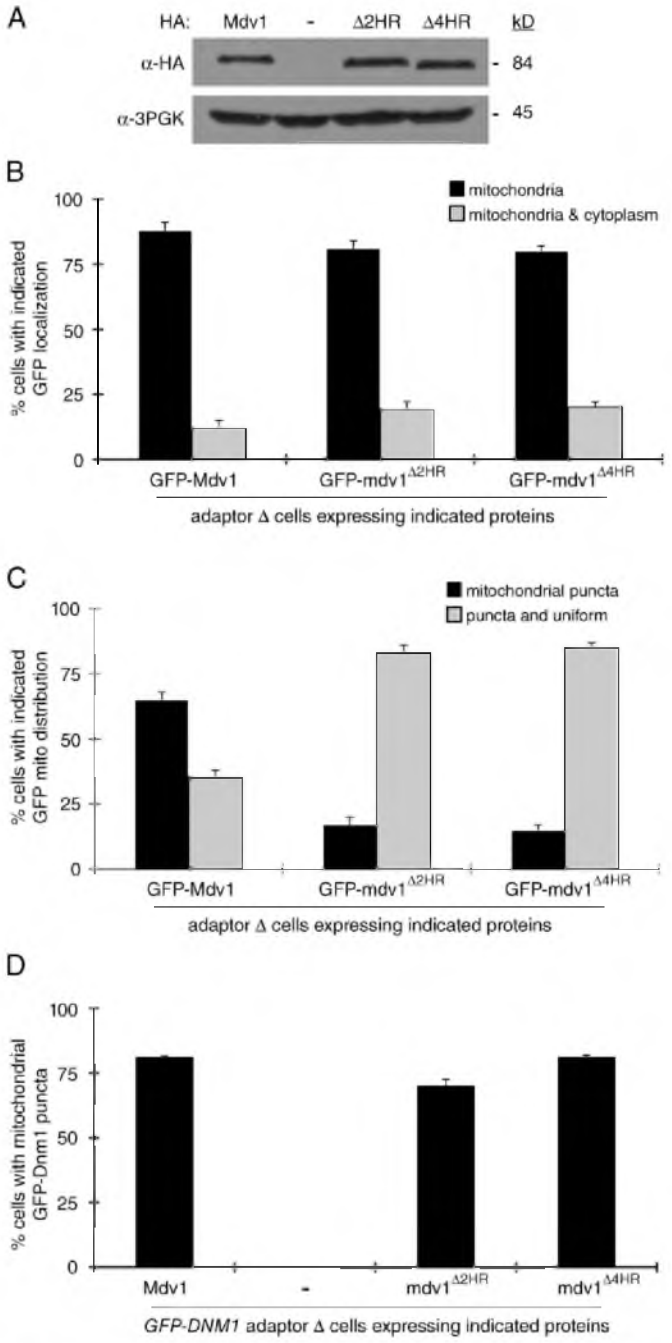

Figure S3. **Additional analysis of mdv1$^{\Delta 2HR}$ and mdv1$^{\Delta 4HR}$ proteins.** (A) Steady-state abundance of C-terminal HA-tagged Mdv1, mdv1$^{\Delta 2HR}$, and mdv1$^{\Delta 4HR}$ proteins expressed in adaptor Δ cells. WCEs separated by SDS-PAGE were immunoblotted with anti-HA and anti-3PGK antibodies. (B) Mitochondrial distribution of GFP-tagged WT and ΔHR mutant Mdv1 proteins. (C) Mitochondrial distribution of GFP-tagged Mdv1, mdv1$^{\Delta 2HR}$, and mdv1$^{\Delta 4HR}$ proteins imaged in adaptor Δ cells. (D) Localization of genomically expressed GFP-Dnm1 in cells expressing Mdv1, mdv1$^{\Delta 2HR}$, and mdv1$^{\Delta 4HR}$ proteins. Error bars represent the mean and standard deviation of at least three independent experiments (n = 100).

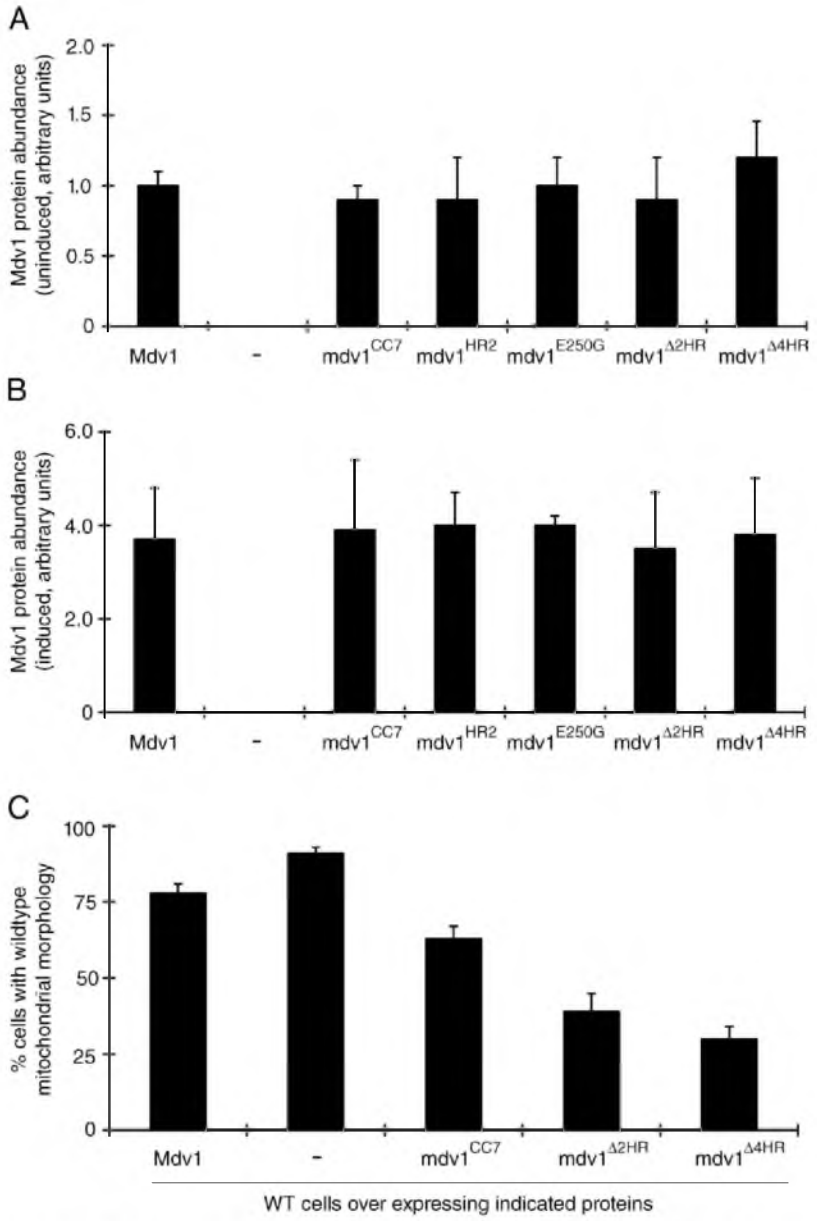

Figure S4. **Dominant-negative effects of WT and mutant Mdv1 proteins.** (A) Relative steady-state abundance of WT and mutant Mdv1 proteins expressed from the uninduced *MET25* promoter in adaptor Δ cells. (B) Relative steady-state abundance of WT and mutant proteins expressed from the induced *MET25* promoter in adaptor Δ cells. Quantification details for A and B are discussed in Materials and methods. (C) Mitochondrial morphology in WT cells expressing WT and mutant Mdv1 proteins from the *MET25* promoter after a 4-h induction. Error bars represent the mean and standard deviation of at least three independent experiments ($n = 100$).

Table S1. **Plasmids used in this study**

ID number	Plasmid	Protein expressed	Source
B493	*pRS415MET25*	None	ATCC 87322
B494	*pRS416MET25*	None	ATCC 87324
B824	*pRS415MET25-9MYC-FIS1*	9Myc-Fis1	Karren et al., 2005
B1642	*p414GPD-mt-ffRFP*	*N. crassa* ATP9(1–69) + fast-folding DsRed	Karren et al., 2005
B1808	*pRS415MET25-MDV1*	MDV1	Karren et al., 2005
B2053	*pRS416MET25-MDV1*	MDV1	Karren et al., 2005
B2054	*pRS416MET25-mdv1^{E250G}*	Mdv1^{E250G}	Karren et al., 2005
B2499	*pMAL-c2x-mdv1-CC*	10xHIS-PPCS-mdv1-CC	This study
B2620	*pRS416MET25-mdv1^{CC7}*	mdv1$^{I233E, I237E, I251E, I254E, I268E, I272E, I275E}$	This study
B2621	*pMAL-c2x-mdv1-CC^{SeMet}*	mdv1-CC$^{L248M, L281M}$	This study
B2683	*pRS415MET25-GFP-mdv1^{CC7}*	GFP-mdv1^{CC7}	This study
B2783	*pRS416MET25-mdv1^{HR2}*	Mdv1$^{1–229}$–*M. musculus* Mfn1$^{674–734}$–Mdv1$^{295–714}$	This study
B2798	*pRS416MET25-mdv1^{CC7}-13MYC*	mdv1^{CC7}-13MYC	This study
B2800	*pRS415MET25-mdv1^{HR2}-13MYC*	mdv1^{HR2}-13MYC	This study
B2821	*pRS415MET25-MDV1-3HA*	Mdv1-3HA	This study
B2832	*pRS416MET25-mdv1^{HR2}-3HA*	mdv1^{HR2}-3HA	This study
B2833	*pRS416MET25-mdv1^{HR2}-13MYC*	mdv1^{HR2}-13MYC	This study
B2837	*pRS416MET25-MDV1-13MYC*	Mdv1-13MYC	This study
B2839	*pRS415MET25-mdv1^{CC7}-3HA*	mdv1^{CC7}-3HA	This study
B2864	*pRS416MET25-9MYC-FIS1*	9MYC-Fis1	This study
B2882	*pRS415MET25-mdv1^{E250G}-3HA*	mdv1^{E250G}-3HA	This study
B2892	*pRS415MET25-GFP-mdv1^{HR2}*	GFP-mdv1^{HR2}	This study
B3003	*pRS416MET25-ffRFP-mdv1^{CC7}*	ffRFP-mdv1^{CC7}	This study
B3015	*pRS416MET25-mdv1$^{\Delta 2HR}$*	mdv1$^{\Delta 2HR}$	This study
B3016	*pRS416MET25-mdv1$^{\Delta 4HR}$*	mdv1$^{\Delta 4HR}$	This study
B3017	*pRS415MET25-mdv1$^{\Delta 2HR}$-3HA*	mdv1$^{\Delta 2HR}$-3HA	This study
B3018	*pRS415MET25-mdv1$^{\Delta 4HR}$-3HA*	mdv1$^{\Delta 4HR}$-3HA	This study
B3028	*pRS415MET25-GFP-mdv1$^{\Delta 2HR}$*	GFP-mdv1$^{\Delta 2HR}$	This study
B3029	*pRS415MET25-GFP-mdv1$^{\Delta 4HR}$*	GFP-mdv1$^{\Delta 4HR}$	This study

ATCC, American Type Culture Collection.

Table S2. **X-ray data and model statistics**

Space group $P4_12_12$	*SeMdv13* Se peak	*SeMdv13* Se inflection
Data collection		
Cell a =, c = (Å)	41.38, 227.38	41.35, 227.39
Resolution (Å) (high)	38–2.7 (2.79–2.7)	38–2.8 (2.9–2.8)
No. unique reflections	10,392	9,222
Rmerge	5.3 (27.9)	6.4 (21.1)
Completeness	99.2 (99.2)	98.8 (98.5)
I–SigI	10.0 (2.4)	10.2 (2.31)
Redundancy	1.8 (1.7)	1.8 (1.7)
Refinement		
R/Rfree	27.0/31.4	NA
No. protein atoms	1,067	NA
No. water atoms	21	NA
<B> protein	58.5	NA
<B> water	52.1	NA
Rms bond (Å)	0.014	NA
Rms angle (°)	1.5	NA

NA, not applicable.

Reference

Karren, M.A., E.M. Coonrod, T.K. Anderson, and J.M. Shaw. 2005. The role of Fis1p–Mdv1p interactions in mitochondrial fission complex assembly. *J. Cell Biol.* 171:291–301. doi:10.1083/jcb.200506158

CHAPTER 4

DISCUSSION

Biochemical properties of Dnm1 are optimized for yeast mitochondrial fission

The mitochondrial fission dynamin (Dnm1/Drp1) is predicted to have a similar structure and working mechanism as Dyn (van der Bliek, 1999). However, in structural studies, purified Dnm1 exhibits distinct characteristics that likely make it more suitable for its function in mitochondrial fission. The fundamental differences between Dnm1 and Dyn include complex architecture, GTPase kinetics, and mechanism of membrane recruitment.

In vitro, Dnm1 assembles into spirals on artificial lipid tubes similar to those formed by Dyn (Ingerman et al., 2005). However, Dnm1 tubes are different from Dyn tubes in diameter, spiral architecture, and constriction capacity (Mears et al., 2011). These differences are likely to accommodate the unique requirements of mitochondrial fission. In particular, the diameter of mitochondrial tubules is ~110 nm, twice as big as that of endocytic vesicle necks (Ingerman et al., 2005). As a consequence, mitochondrial fission requires a much more substantial constriction. The in vitro Dnm1-lipid tubes appear to fit these requirements (Mears et al., 2011). First, the average diameter of in vitro Dnm1 tubes is ~110 nm, twice as big as that of Dyn tubes. Second, in the presence of GTP, Dnm1 constricts the lipid tube by ~60 nm (from ~130 nm to ~70 nm) compared to 10 nm in the case of Dyn (from ~50 nm to ~40 nm) (Zhang and Hinshaw, 2001; Mears et al., 2011). The large difference in diameter and constriction capacity of Dnm1 and Dyn tubes suggests that DRPs can generate helical structures with a wide range of diameters, allowing them to work at different cellular membranes.

Dnm1 forms a two-start helical structure with tetramer building blocks instead of a single start helix as formed by Dyn dimers (Mears et al., 2011). Although the resolution of the cryo-EM structure is not high enough to resolve the interactions within the assembly, Dnm1 strands seem close enough together to allow Dnm1 GTPase domains dimerization both within one rung (between 2 strands) and across rungs (between second strand of rung n and the first strand of rung n+1). At this point, it is unclear why Dnm1 favors the two-start helical structure and how this structure contributes to Dnm1 activity in mitochondrial fission. These combined in vitro data indicate that although the basic protein structure and interaction interfaces are preserved among DRPs, each of them may have evolved a unique strategy to achieve the optimal complex architecture and activity for their job at a particular cellular membrane.

Adaptors are required for mitochondrial dynamin membrane recruitment

Since mitochondrial DRP Dnm1/Drp1 does not contain a PH domain, it depends on an adaptor protein for membrane association. In the cryo-EM structure, the in vitro Dnm1 tube is not tightly tethered to the lipid bilayer. Instead, there is a gap of 3-4 nm between the membrane and the inner edge of the Dnm1 tube (Mears et al., 2011). This gap may be accounted for by the Fis1-Mdv1 complexes. The anchoring molecule Fis1 has been shown to be dispensable for postrecruitment steps of mitochondrial fission (Koirala et al., submitted). The adapter protein Mdv1, on the other hand, is present in the final fission complex and is essential for Dnm1 assembly as well as the fission event (Lackner et al., 2009).

In Chapter 3, we dissect Mdv1 functions during fission complex formation in vivo, and demonstrate that Mdv1 acts as a scaffold for Dnm1 assembly. Mdv1 dimerizes via a 92Å long coiled-coil domain. The sequence and length of the Mdv1 coiled-coil seem to be optimized for Dnm1 recruitment and self-assembly on the mitochondrial membrane. In 40% of the cells expressing the coiled-coil mutants, GFP-Dnm1 is diffusely localized in the cytoplasm. This observation indicates that Mdv1 dimerization via its coiled-coil domain helps stabilize the Mdv1-Dnm1 interaction, keeping Dnm1 on the membrane. In the other 60% of coiled-coil mutant cells, GFP-Dnm1 is recruited to the mitochondrial membrane and is able to assemble into punctate structures. However, the morphology of these structures, as well as their distribution on the mitochondrial tubule, is qualitatively different from those observed in wild-type cells. These data suggest that beside its adaptor function, Mdv1 also acts as a scaffold protein for the formation of a functional fission complex. Our results are consistent with a previous study, which defined Mdv1 as a dynamin effector (Lackner et al., 2009). In that study, purified Dnm1 exhibited a kinetic lag in reaching the steady-state of assembly-stimulated GTPase activity, which was predicted to be caused by the rate-limiting self-assembly step. In the presence of Mdv1, purified Dnm1 assembled more efficiently on liposomes. As a result, the kinetic lag is significantly shortened. These combined observations strongly support both the recruitment and scaffolding functions of the dynamin adaptors. They not only help bring dynamins to the membrane, but also assure the optimal complex architecture necessary for dynamin GTPase activity stimulation and fission.

Coimmunoprecipitation (coIP) and yeast two-hybrid assays indicate that the Mdv1 β-propeller is sufficient for the interaction with Dnm1 (Chapter 2). The long coiled-coil

domain may space the β-propeller domains in an optimal manner for Dnm1 assembly. The cryo-EM reconstruction of Dnm1 assembled on liposomes showed that Dnm1 is capable of forming a double helix with two parallel strands of Dnm1 (Mears et al., 2011). While each Dnm1 strand could be constricted via stalk interactions as in the MxA ring and Dyn helix (see 1.4), it is unknown how the axial spacing between two Dnm1 strands is determined. Mdv1 scaffolding function may fit in this scenario: each Mdv1 β-propeller domain may bind to one Dnm1 molecule in each strand of the same rung. The coiled-coil domain then links two Dnm1 strands, similar to how the hydrogen bond links two strands in a DNA double helix. That way, the distance between Dnm1 strands is kept constant in the whole Dnm1 spiral. Further structural studies are required to elucidate how Mdv1 scaffolding function is carried out.

Understanding the InsB-β-propeller interaction

InsB resides between the Middle and GED domains in DRPs. In most DRPs, the structure and function of InsB domains are unknown. In Chapter 2, we found that InsB plays a role in membrane recruitment of the mitochondrial dynamin Dnm1. Dnm1 InsB contains a fungal specific motif essential for the binding of Dnm1 to the fungal mitochondrial adaptor Mdv1. Mutations in this motif dramatically reduce Dnm1-Mdv1 interaction. As a consequence, Dnm1 remains in the cytoplasm and mitochondrial fission is blocked. Suppressor mutations that rescue defects caused by InsB mutations are clustered in the Mdv1 β-propeller domain. Further analysis suggests that the suppressor mutations may have created new contacts to complement the interaction disrupted by InsB mutations. The residues identified in this suppressor screen likely represent potential binding interfaces on the Mdv1 β-propeller for InsB.

Following up on the study in Chapter 2, we characterized the biochemical properties of the purified InsB domain. Dnm1 InsB (aa 535-639) was expressed as a maltose binding protein (MBP) fusion protein in *E.coli*, released by proteolytic cleavage, and purified to homogeneity (Appendix and Fig. 4.1A). Mass spectrometry detected a single major species of 14,247 Da, which matches the calculated molecular weight (data not shown). However, on SDS-PAGE, the protein reproducibly migrated as a doublet just above the 17kDa markers (Fig. 4.1B). Equilibrium sedimentation indicated that InsB was a monomer (Fig. 4.1C). The secondary structure was analyzed by circular dichroism, which showed that InsB is mostly unstructured with 15% helical structure (Fig. 4.1D). This is consistent with the secondary structure prediction by PSIPRED v2.6, which predicted a short helix of 8-10 residues in the middle of a largely disordered loop. We were not able to resolve this small helix by nuclear magnetic resonance (NMR) using a ^{15}N-labeled protein (Fig. 4.1E). The ^{15}N-HSQC spectrum of InsB on its own shows small amide (^{1}H) chemical shift dispersion (7.9 – 8.5 ppm) in the HSQC spectrum and normal amide (^{15}N) dispersion that is consistent with an unfolded polypeptide (Cavanagh et al., 2007). Our observation may explain why InsB is missing in the Dnm1 3D cryo-EM structure (Mears et al., 2011). In the absence of Mdv1, this region is probably too disordered to be resolved. It is highly possible that InsB would adopt a stable structure in a complex with its binding partner, the Mdv1 β-propeller.

The InsB/Mdv1 β-propeller interaction was not detectable in an in vitro pull-down, which suggests that InsB is not sufficient for a stable interaction with the Mdv1 β-propeller. We proposed to study this interaction further by NMR, which is capable of detecting weak and transient bindings (Cavanagh et al., 2007). An NMR titration

Figure 4.1. **Biochemical analysis of Dnm1 InsB.** (A, top) Domain structure of Dnm1, including the GTPase, Middle, InsB, and GED domains. (bottom) The construct used for purification of the Dnm1 InsB domain includes the maltose binding protein (MBP) fused to 10xHis, the PreScission protease cleavage site (PPCS), and Dnm1 residues 535-639 (InsB, MBP-10xHis-PPCS-InsB). (B) SDS-PAGE analysis of purified MBP-10xHis-PPCS-InsB fusion protein stained with Coomassie brilliant blue (lane 1), PreScission protease-cleaved MBP-10xHis-PPCS + InsB (lane 2) and purified InsB (lane 3). (C) Sedimentation equilibrium profile of the Dnm1 InsB fragment at indicated initial loading concentrations (open symbols) with the corresponding fit of 14,418 D ($MW_{obs}/MW_{monomer}$ = 1.01). Residuals for the nonlinear least-squared fits are shown below. (D) CD wavelength scan of Dnm1 InsB fragment. MRE, mean residue ellipticity (deg cm^2 $dmol^{-1}$). The signal at 222 nm is -5667 (deg cm^2 $dmol^{-1}$), corresponding to ~15% helicity. The remainder of the signal appears to be random coil. (E) Two-dimensional [^{15}N,^{1}H] HSQC spectrum of InsB. The protein shows small amide (^{1}H) chemical shift dispersion (7.9 – 8.5 ppm) in the HSQC spectrum and normal amide (^{15}N) dispersion consistent with an unfolded polypeptide.

D

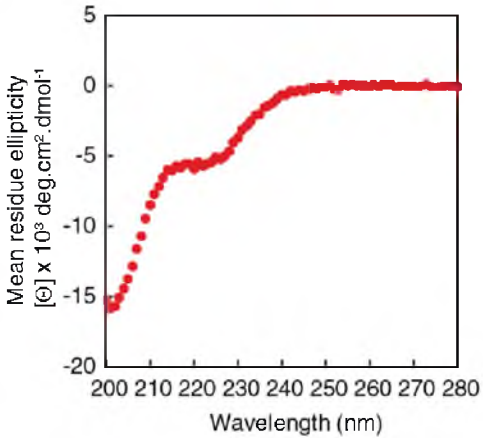
Mean residue ellipticity
[Θ] x 10³ deg.cm².dmol⁻¹
5
0
-5
-10
-15
-20
200 210 220 230 240 250 260 270 280
Wavelength (nm)

E

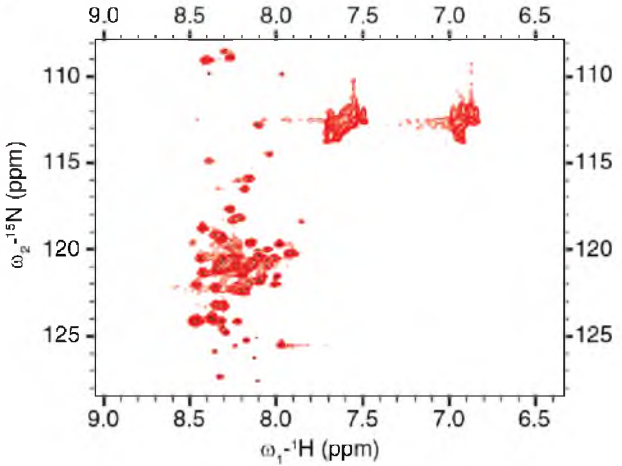
9.0 8.5 8.0 7.5 7.0 6.5
110
115
120
125
ω₂-¹⁵N (ppm)
ω₁-¹H (ppm)

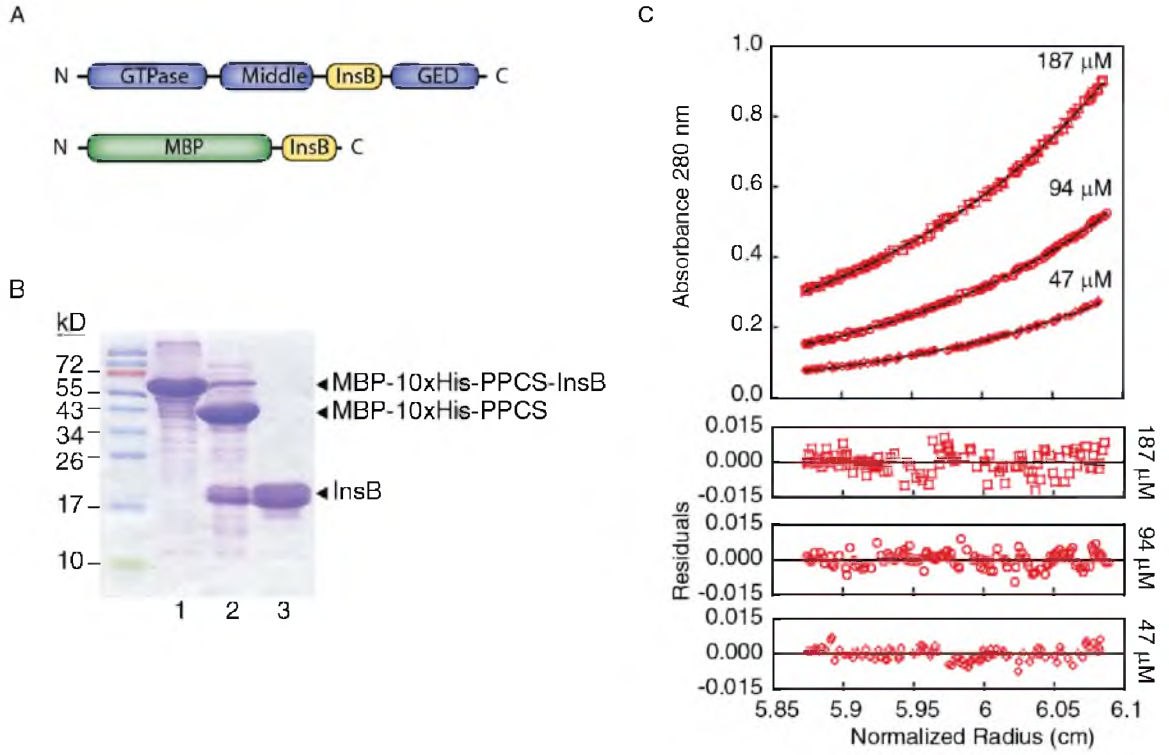
A
N
GTPase
Middle
InsB
GED
C
N
MBP
InsB
C
B
kD
72
55
43
34
26
17
10
MBP-10xHis-PPCS-InsB
MBP-10xHis-PPCS
InsB
1
2
3
C
Absorbance 280 nm
1.0
0.8
0.6
0.4
0.2
0.0
187 μM
94 μM
47 μM
Residuals
0.015
0.000
-0.015
187 μM
94 μM
47 μM
5.85
5.9
5.95
6
6.05
6.1
Normalized Radius (cm)

experiment, where purified Mdv1 β-propeller is titrated into a solution of ^{15}N-labeled InsB, would address: (1) whether InsB is sufficient for direct interaction with the Mdv1 β-propeller, and (2) whether InsB adopts a stable fold upon binding the Mdv1 β-propeller. However, there is also a good chance that other Dnm1 domains are required for the binding with Mdv1 as discussed in Chapter 2. In the latter case the Dnm1-Mdv1 interaction would need to be investigated using full-length proteins.

The Mdv1 WD40 repeat is predicted to form an eight-bladed β-propeller domain, which has been shown to be sufficient for the direct interaction with Dnm1. The β-propeller is a ubiquitous protein-protein interacting domain in eukaryotic proteins (Stirnimann et al., 2010). WD40 proteins are found in multi-subunit complexes, where they act as scaffolding factors. The barrel-like structure of the β-propeller provides three distinct surfaces for binding including the top, the bottom and the circumference (Stirnimann et al., 2010). In some cases, WD40 domains act as large interaction platforms for multiple proteins. In other cases, WD40 domains bind multiple domains in the same protein to ensure a stable interaction. The known structures of different β-propeller domains in complex with their binding partners allow us to propose possible binding modes between InsB and the Mdv1 β-propeller.

First, InsB may bind to the Mdv1 β-propeller via the short helix containing the fungal specific motif. This interaction mode has been seen in many cases (Stirnimann et al., 2010). In these examples, the short α-helices bind to the top surface of the propeller, close to the β-propeller central channel. The helices often contain specific motifs that are recognized by the corresponding WD40 proteins. The WD40-helical peptide interactions are often stabilized by a second binding of nearby domains to the same WD40.

The second possibility is that InsB forms a complete β-propeller blade and inserts into the Mdv1 β-propeller. This interesting mode of interaction was seen between Sec13 and Nup145c in the nuclear pore complex (Brohawn and Schwartz, 2009). Sec13 contains a 6-bladed β-propeller. Upon binding, the Nup145c DIM domain inserts itself between blade 1 and 6 of the Sec13 β-propeller to form the seventh blade. This interaction is further stabilized by the association of Nup145c C-terminus with the Sec13 β-propeller. In the fission complex, Dnm1 InsB is big enough to form a propeller blade. However, the molecular mechanism of the InsB-Mdv1 β-propeller interaction will remain a mystery until the crystal structure of the complex is solved.

Dynamin-adaptor interactions in the mammalian mitochondrial fission machinery

In budding yeast, mitochondrial fission is mediated by a complex of the dynamin Dnm1, the membrane adaptors Mdv1/Caf4, and the anchoring molecule Fis1. Mammalian mitochondrial dynamin Drp1 and anchoring molecule hFis are homologs of Dnm1 and Fis1, respectively. However, the mammalian adaptor proteins (Mff, MiD49 and MiD51) have no similarity with yeast Mdv1 and Caf4 (Fig. 1.3). This raises the question whether the membrane recruitment of the mammalian dynamin is regulated by the same mechanism as the yeast machinery.

Identification of mammalian adaptors

In mammalian cells, down-regulating any of the adaptor genes (Mff/MiD49/MiD51) by siRNA results in elongated, perinuclear clustering mitochondria, which is similar to those seen in Drp1 siRNA transfected cells (Gandre-Babbe and van

der Bliek, 2008; Otera et al., 2010; Palmer et al., 2011; Zhao et al., 2011). In immunostaining experiments, these proteins are found in puncta on mitochondria that colocalize with Drp1 puncta. Importantly, Drp1 association with the mitochondrial membrane is severely reduced when any of the adaptor genes is knocked down by siRNA. These combined results identify Mff, MiD49 and MiD51 as mammalian mitochondrial dynamin adaptors. Their domain structures not only differ from that of yeast adaptors Mdv1/Caf4 but also differ from each other. MiD49 and MiD51 are paralogs, and their sequences are distinct from that of Mff. Interestingly, all mammalian adaptors are anchored to mitochondrial outer membrane via a transmembrane domain, which is missing in yeast adaptors. This raised the question whether the anchoring function of Fis1 was still required for the Mff- or MiD49/51- mediated Drp1 recruitment. Indeed, a recent study showed that Fis1 is dispensable for fission in mammalianized yeast strain and each adaptor paired with Drp1 is sufficient to carry out fission (Koirala et al., submitted).

Regulation of mammalian mitochondrial dynamin recruitment

Based on the high conservation of domain structure and function between Drp1 and Dnm1, we proposed that the functional role of InsB in mitochondrial dynamin adaptor binding is conserved from yeast to human. InsB and the dynamin adaptors may have co-evolved to meet the requirements of mitochondrial fission in different organisms (see Chapter 2, Discussion). The recruitment of mammalian mitochondrial dynamin Drp1 via the InsB-adaptor interaction may be regulated by additional factors including alternative splicing, tissue-specific expression, and post-translational modification.

While yeast Dnm1 has only one isoform, mammalian Drp1 has six isoforms. Drp1 isoforms are the result of alternative splicing at exon 3, 15 and 16, in which exon 15 and 16 encode parts of the InsB region (Shin et al., 1997; Imoto et al., 1998; Yoon et al., 1998). Drp1 isoforms with InsB of differing length may be targeted to the membrane by different combinations of adaptors. One may have higher affinity for Mff while others may bind more tightly to MiDs. A certain isoform may prefer to bind a complex of two adaptors rather than a homogeneous complex composed of one adaptor.

Drp1 isoforms have been detected in variety of tissues including brain, liver, lung, heart, kidney, spleen, testis, hepatocytes and fibroblasts. Most tissues express more than one Drp1 isoform but the isoform containing the complete InsB sequence is found exclusively in brain (Yoon et al., 1998). It is still unclear if the adaptors are expressed in a tissue-specific manner, but it is possible that each tissue contains a distinct pair of a dynamin isoform and an adaptor. This may explain the conflicting reports on the effect of each adaptor on mitochondrial fission in different cell lines (Gandre-Babbe and van der Bliek, 2008; Otera et al., 2010; Palmer et al., 2011; Zhao et al., 2011).

It has been postulated that posttranslational modifications of mitochondrial DRPs influence interactions with their adaptor proteins. A variety of studies indicate that residues in and around mammalian Drp1 InsB are sumoylated (Figueroa-Romero et al., 2009), phosphorylated (Chang and Blackstone, 2007; Cribbs and Strack, 2007; Taguchi et al., 2007) and S-nitrosylated (Cho et al., 2009; Bossy et al., 2010). Some of these modifications affect mitochondrial fission (Chang and Blackstone, 2007; Cribbs and Strack, 2007; Cereghetti et al., 2008; Merrill et al., 2011), suggesting that they may modulate Drp1 binding to one or more mitochondrial adaptors.

Conclusion

Studies of the yeast mitochondrial dynamin allow us to build a more detailed working model for membrane recruitment of DRPs. We identified InsB as the "adaptor binding domain" for DRPs and the recruitment specificity is established by pairing of a certain InsB with a particular membrane adaptor. This model can now be tested as mitochondrial adaptors in different organisms are being identified.

References

Bossy, B., A. Petrilli, E. Klinglmayr, J. Chen, U. Lutz-Meindl, A.B. Knott, E. Masliah, R. Schwarzenbacher, and E. Bossy-Wetzel. 2010. S-Nitrosylation of DRP1 does not affect enzymatic activity and is not specific to Alzheimer's disease. *J Alzheimers Dis*. 20 Suppl 2:S513-526.

Brohawn, S.G., and T.U. Schwartz. 2009. Molecular architecture of the Nup84-Nup145C-Sec13 edge element in the nuclear pore complex lattice. *Nat Struct Mol Biol*. 16:1173-1177.

Cavanagh, J., W.J. Fairbrother, A.G.r. Palmer, M. Rance, and N.J. Skelton. 2007. Protein NMR Spectroscopy, Principles and Practice. Elsevier Academic Press, San Diego.

Cereghetti, G.M., A. Stangherlin, O. Martins de Brito, C.R. Chang, C. Blackstone, P. Bernardi, and L. Scorrano. 2008. Dephosphorylation by calcineurin regulates translocation of Drp1 to mitochondria. *Proc Natl Acad Sci U S A*. 105:15803-15808.

Chang, C.R., and C. Blackstone. 2007. Cyclic AMP-dependent protein kinase phosphorylation of Drp1 regulates its GTPase activity and mitochondrial morphology. *J Biol Chem*. 282:21583-21587.

Cho, D.H., T. Nakamura, J. Fang, P. Cieplak, A. Godzik, Z. Gu, and S.A. Lipton. 2009. S-nitrosylation of Drp1 mediates beta-amyloid-related mitochondrial fission and neuronal injury. *Science*. 324:102-105.

Cribbs, J.T., and S. Strack. 2007. Reversible phosphorylation of Drp1 by cyclic AMP-dependent protein kinase and calcineurin regulates mitochondrial fission and cell death. *EMBO Rep*. 8:939-944.

Figueroa-Romero, C., J.A. Iniguez-Lluhi, J. Stadler, C.R. Chang, D. Arnoult, P.J. Keller, Y. Hong, C. Blackstone, and E.L. Feldman. 2009. SUMOylation of the

mitochondrial fission protein Drp1 occurs at multiple nonconsensus sites within the B domain and is linked to its activity cycle. *FASEB J.* 23:3917-3927.

Gandre-Babbe, S., and A.M. van der Bliek. 2008. The novel tail-anchored membrane protein Mff controls mitochondrial and peroxisomal fission in mammalian cells. *Mol Biol Cell.* 19:2402-2412.

Imoto, M., I. Tachibana, and R. Urrutia. 1998. Identification and functional characterization of a novel human protein highly related to the yeast dynamin-like GTPase Vps1p. *J Cell Sci.* 111 (Pt 10):1341-1349.

Ingerman, E., E.M. Perkins, M. Marino, J.A. Mears, J.M. McCaffery, J.E. Hinshaw, and J. Nunnari. 2005. Dnm1 forms spirals that are structurally tailored to fit mitochondria. *J Cell Biol.* 170:1021-1027.

Lackner, L.L., J.S. Horner, and J. Nunnari. 2009. Mechanistic analysis of a dynamin effector. *Science.* 325:874-877.

Mears, J.A., L.L. Lackner, S. Fang, E. Ingerman, J. Nunnari, and J.E. Hinshaw. 2011. Conformational changes in Dnm1 support a contractile mechanism for mitochondrial fission. *Nat Struct Mol Biol.* 18:20-26.

Merrill, R.A., R.K. Dagda, A.S. Dickey, J.T. Cribbs, S.H. Green, Y.M. Usachev, and S. Strack. 2011. Mechanism of neuroprotective mitochondrial remodeling by PKA/AKAP1. *PLoS Biol.* 9:e1000612.

Otera, H., C. Wang, M.M. Cleland, K. Setoguchi, S. Yokota, R.J. Youle, and K. Mihara. 2010. Mff is an essential factor for mitochondrial recruitment of Drp1 during mitochondrial fission in mammalian cells. *J Cell Biol.* 191:1141-1158.

Palmer, C.S., L.D. Osellame, D. Laine, O.S. Koutsopoulos, A.E. Frazier, and M.T. Ryan. 2011. MiD49 and MiD51, new components of the mitochondrial fission machinery. *EMBO Rep.* 12:565-573.

Shin, H.W., C. Shinotsuka, S. Torii, K. Murakami, and K. Nakayama. 1997. Identification and subcellular localization of a novel mammalian dynamin-related protein homologous to yeast Vps1p and Dnm1p. *J Biochem.* 122:525-530.

Stirnimann, C.U., E. Petsalaki, R.B. Russell, and C.W. Muller. 2010. WD40 proteins propel cellular networks. *Trends Biochem Sci.* 35:565-574.

Taguchi, N., N. Ishihara, A. Jofuku, T. Oka, and K. Mihara. 2007. Mitotic phosphorylation of dynamin-related GTPase Drp1 participates in mitochondrial fission. *J Biol Chem.* 282:11521-11529.

van der Bliek, A.M. 1999. Functional diversity in the dynamin family. *Trends Cell Biol.* 9:96-102.

Yoon, Y., K.R. Pitts, S. Dahan, and M.A. McNiven. 1998. A novel dynamin-like protein associates with cytoplasmic vesicles and tubules of the endoplasmic reticulum in mammalian cells. *J Cell Biol*. 140:779-793.

Zhang, P., and J.E. Hinshaw. 2001. Three-dimensional reconstruction of dynamin in the constricted state. *Nat Cell Biol*. 3:922-926.

Zhao, J., T. Liu, S. Jin, X. Wang, M. Qu, P. Uhlen, N. Tomilin, O. Shupliakov, U. Lendahl, and M. Nister. 2011. Human MIEF1 recruits Drp1 to mitochondrial outer membranes and promotes mitochondrial fusion rather than fission. *EMBO J*. 30:2762-2778.

APPENDIX

Dnm1 InsB purification

Dnm1 residues 535-639 were fused to the C-terminus of maltose binding protein (MBP) via a linker containing 10xHis and the PreScission protease cleavage site. This construct was expressed in BL21(DE3) codon+ (RIPL; Agilent technologies) *E.coli* grown in media containing ampicillin and chloramphenicol. For circular dichroism (CD) and equilibrium sedimentation (ES) analysis, the bacteria cultures were grown in lysogeny broth (LB) at 37°C. Overnight cultures were diluted (1:1000) and grown to an OD_{600} ~ 0.5, followed by induction with 0.1mM IPTG for 4h. For nuclear magnetic resonance (NMR) experiments, overnight culture, grown in PA-0.5 at 37°C, were diluted (1:1000) in autoinduction medium containing ^{15}N and grown at 37°C for 3 h. Cultures were transferred to 18°C and grown for an additional 24h. The cultures were grown for another 8 h with 0.5mM IPTG added before harvesting. All purification steps were performed at 4°C. Proteins were purified by affinity chromatography on amylose resin (New England Biolabs, Inc.) followed by cleavage with PreScission protease (GE Healthcare). After cleavage, Dnm1 InsB contained two heterogenous N-terminal residues (Gly-Pro). The protein was further purified by mono-Q anion exchange chromatography and size-exclusion chromatography. Purified InsB was concentrated to 1-10 mg/ml using Centriprep centrifugal concentrators (YM-3; 3kD NMWL; Milipore) and dialyzed in CD/ES buffer or NMR buffer.

CD and ES analysis of InsB

CD analysis was performed on a CD spectrometer (410; Aviv Biomedical, Inc.). Wavelength scans (200-280 nm) were performed at 23°C on 9.5 μM protein samples in

50mM Na-phosphate, pH 7.4, and 150mM NaCl using a 1-mm path length cuvette with a 5 s averaging time.

ES analysis of InsB was performed at 4°C using a centrifuge (Optima XL-A; Beckman Coulter) at initial protein subunit concentration of 187, 94 and 47 μM (monomer) in a buffer containing 50mM Na-phosphate, pH 7.4, and 50mM NaCl. Centrifugation was performed at 13,000 rpm, 17,000 rpm, 21,000 rpm (Fig. 4.1) and 25,000 rpm. Resulting equilibrium datasets were globally fit into a single ideal species model with a floating molecular mass using nonlinear least-squares algorithms in HeteroAnalysis software (Cole, 2004). Protein partial-specific volumes and solvent densitites were calculated with the program SEDNTERP version 1.09, (Laue et al., 1992).

NMR Spectroscopy

For NMR experiment, the protein was dialyzed in 50mM Na-phosphate, pH 7.4, 50 NaCl, 0.1 mM DTT, 0.1 mM EDTA, 10% D_2O. A two-dimensional [15N,1H] HSQC (Cavanagh et al., 2007) was recorded using a Varian INOVA 600 MHz NMR spectrometer equipped with a cryogenic probe. The data were processed using FELIX 2007 (Felix NMR, Inc). Proton (1H) and nitrogen (15N) chemical shifts were referenced to external DSS (2,2-Dimethyl-2-silapentane-5-sulphonic acid; 0.0 ppm) and indirectly to liquid NH3 using indirect ratios, respectively (Cavanagh et al., 2007).

References

Cavanagh, J., W.J. Fairbrother, A.G.r. Palmer, M. Rance, and N.J. Skelton. 2007. Protein NMR Spectroscopy, Principles and Practice. Elsevier Academic Press, San Diego.

Cole, J.L. 2004. Analysis of heterogeneous interactions. *Methods Enzymol*. 384:212-232.

Laue, T., B. Shah, T. Ridgeway, and S. Pelletier. 1992. Computer-aided interpretation of analytical sedimentation data for proteins. *Analytical Ultracentrifugation in Biochemistry and Polymer Science. Royal Society of Chemistry, Cambridge, England, UK.*:90–125.